T.C.
ISTANBUL UNIVERSITY-CERRAHPASA
INSTITUTE OF GRADUATE STUDIES

M.Sc. THESIS

EFFECTS OF DECOMPOSITION OF NEAR-FAULT GROUND MOTIONS ON THE RESPONSE OF SDOF SYSTEMS

Mahmoud NASSAR

SUPERVISOR

Doç. Dr. Ömer Fatih YALÇIN

Department of Civil Engineering

Civil Engineering Programme

ISTANBUL April , 2022

This study was accepted on [.....] as a M. Sc. thesis in Department of Civil Engineering, Civil Engineering Programme by the following Committee.

Examining Committee Members

Doç. Dr. Ömer Fatih YALÇIN (Supervisor)
İstanbul University-Cerrahpaşa
Faculty of Engineering

[Title] [Name SURNAME]
[University]
[Faculty]

[Title] [Name SURNAME]
[University]
[Faculty]

As required by the 9/2 and 22/2 articles of the Graduate Education Regulation which was published in the Official Gazette on 20.04.2016, this graduate thesis is reported as in accordance with criteria determined by the Institute of Graduate Sttudies by using the plagiarism software to which Istanbul University-Cerrahpasa is a subscriber.

FOREWORD

I would like to give my deepest gratitude to my supervisor Dr. Fatih YALÇIN , for inspiring me with his broad view and for guiding me with his highly proficient technical knowledge.

I am also thankful to all of my teaching and research staff in the Civil Engineering department for all their help and concern

I leave to the end my persons to whom I have more to thank, my parents. Thank you for supporting me. This work, and whatever may come from it, is dedicated to you with all my heart.

Tarih girmek için burayı tıklatın. Mahmoud NASSAR

TABLE OF CONTENTS

Page

LIST OF FIGURES

Page

LIST OF TABLES

Page

LIST OF SYMBOLS AND ABBREVIATIONS

Symbol	Explanation
kr	: Effective stiffness
k1	: Elastic stiffness
k2	: Post elastic stiffness
T	: Structure fundemental period
Td	: Post elastic period
μ	: Ductility ratio
E	: Energy
RE	: Relative Energy
Fy	:Normalized yield strength
Fy	: Yield strength
ζ	: Damping ratio
c	:Damping Coefficient
ξe	: Equivalent viscous damping ratio
m	: Mass
u	: Displacement

Abbreviation	Explanation
CDS	: Constant Ductility Response Spectra
CSS	: Constant Strength Response Spectra
EEMD	: Ensemble Emprical Mode Decomposition
EMD	: Emprical Mode Decomposition
FN	: Fault Normal
FP	: Fault Parallel
GN	: Ground Motion
HHT	: Hilbert Huang transform
IMF	: Intrinsic Mode Function
NFGM	: Near Fault Ground Motion

PGA : Peak Ground Acceleration

PI :Pulse Indicator

PGV : Peak Ground Velocity

ÖZET

YÜKSEK LİSANS TEZİ

YAKIN FAY YER HAREKETLERİNİN AYRIŞTIRILMASININ TEK SERBESTLİK DERECELİ SİSTEMLERİN TEPKİLERİ ÜZERİNDEKİ ETKİLERİ

Mahmoud NASSAR

Danışman : Doç.Dr Ömer Fatih YALÇIN

Bu tezde, Hilbert-Huang Dönüşümü (HHT) yöntemi kullanılarak ayrıştırılmış yakın fay yer hareketlerine (YFYH) maruz kalan elastik ve elastik olmayan tek serbestlik dereceli sistemlerinin (TDS) davranışları incelenecektir. YFYH'lerin kendine özgü özellikleri, bir deprem sırasında önemli hasarlara neden olabilir. Çalışma, orijinal kayıtların hız kayıtlarında yüksek frekanslı veya düşük frekanslı bileşenlerin veya her ikisinin filtrelenmesinin doğrusal olmayan TDS'lerin davranışı üzerindeki etkilerini araştırmayı amaçlamaktadır. Bu amaçla, 114 YFYH ve bunların ayrıştırılmış bileşenlerine maruz kalan normal ve izolasyonlu TDS'lerin elastik ve elastik olmayan tepki spektrumları karşılaştırmalı olarak incelenmiştir. YFYH'nin iki yatay bileşeni döndürülürek en büyük hız darbelerini (pulse) içeren doğrultudaki bileşen kullanılır. Seçilen YFYH'ler, darbe periyotlarının etkilerini gözlemlemek için dalgacık (wavelet) hız darbe periyotlarına dayalı olarak altı gruba ayrılır. YFYH'ler, içsel mod fonksiyonları (IMF'ler) adı verilen tam ve yaklaşık olarak ortogonal olan fonksiyonlar kümesine ayrıştırılır. Bu işlem, HHT'nin bir parçası olan Ampirik Mod Ayrıştırma (AMA) yöntemi ile gerçekleştirilen bir eleme işlemidir. Daha sonra, bazı IMF'ler, her bir IMF'nin bağıl enerjisine göre YFYH'lerin üç önemli bileşenini çıkarmak için toplanır: (1) Darbe, (2) Darbe + Yüksek Frekans ve (3) Darbe + Düşük Frekans bileşenleri. Daha sonra, çeşitli ikili doğrusal kuvvet

deformasyon ilişkilerine, süneklik oranlarına ve akma dayanımlarına sahip çok sayıda elastik olmayan TDS, bu YFYH'ler ve bunların ayrıştırılmış bileşenleri altında analiz edilmiştir. Elastik ve elastik olmayan analizlerin sonuçları, yer hareketlerinden yüksek frekanslı içeriklerin veya düşük frekanslı içeriklerin filtrelenmesinin ve sadece darbenin uygulanmasının yapıların davranışını önemli ölçüde etkileyebileceğini ve hem kısa hem de uzun periyotlu bölgelerde ortalama spektral tepkileri azaltabileceğini ortaya koymaktadır. Yer hareketinin yüksek frekans içeriği, spektrumun kısa periyot bölgesinde önemli etkilere sahipken, düşük frekans içeriği uzun periyot bölgesinde orta derecede etkiye sahiptir.

Tarih girmek için burayı tıklatın., ... sayfa.

Anahtar kelimeler: Yakın Fay , Hilbert-Huang Dönüşümü,Ampirik Mod Ayrışımı, Hız Darbesi, Doğrusal Olmayan Spektrum

SUMMARY

M.Sc. THESIS

EFFECTS OF DECOMPOSITION OF NEAR-FAULT GROUND MOTIONS ON THE RESPONSE OF SDOF SYSTEMS

Mahmoud NASSAR

Supervisor : Assoc.Prof.Dr. Ömer Fatih YALÇIN

In this thesis, the behaviors of elastic and inelastic SDOF systems subjected to the decomposed near-fault ground motions (NFGMs) using the Hilbert-Huang Transform (HHT) method will be examined. The distinct properties of NFGMs can cause significant structural damage. The study aims to investigate the effects of filtering high-frequency or low-frequency components or both from the velocity traces of original records on the behavior of nonlinear SDOF systems. To this end, elastic and inelastic response spectra are studied for regular and isolated SDOFs subjected to 114 NFGMs and their decomposed components comparatively. The two horizontal components of NFGMs are rotated to the orientation that contains the strongest velocity pulses. The selected NFGMs are further classified into six groups, based on their wavelet velocity pulse periods to monitor the effects of pulse periods. NFGMs are decomposed into a complete and approximately orthogonal functions set called intrinsic mode functions (IMFs). This is a sifting process performed by the Empirical Mode Decomposition (EMD) method which is a procedure of Hilbert-Huang Transform. Subsequently, some IMFs are superposed to extract three components of NFGMs according to the relative energy of each IMFs as: (1) Pulse, (2) Pulse + High-Frequency components, and (3) Pulse + Low-Frequency components. Subsequently, numerous inelastic SDOF systems having various bilinear force deformation relations, ductility ratios, and yield strengths are analyzed under these NFGMs and their decomposed components. The results of elastic and inelastic analyses reveal that filtering both the high and low frequency components from the earthquake records and applying only the pulse can have a significant impact on structural behavior and reduce the mean spectral responses in both the long and short

period regions of spectra. The high-frequency content of the earthquake records has significant effects in the short period region of spectra, whereas the low-frequency content has moderate effects in the long period region.

Tarih girmek için burayı tıklatın., ... pages.

Keywords: Near-fault, Hilber-Huang Transform, Empirical Mode Decomposition, Velocity pulse, Inelastic Spectrum

1 INTRODUCTION

Earthquakes are examples of natural disasters that occur due to the earth's natural processes and whose occurrence cannot be controlled or anticipated. Earthquakes have devastating immediate impacts on human life, economic sectors, infrastructure, and their long-run effect, especially on economic sectors growth, is challenging to control.

Due to the increase of population worldwide, there is a high demand for high-rise buildings, and earthquakes cause the most damage to these buildings. Despite the fact that earthquakes cannot be prevented nor correctly predictable, the consequences of the earthquakes on the structures, people, and the economy could be minimized. In the last three decades, engineers developed many tools and analysis methods to capture the impact of earthquakes on structures accurately. Earthquake response spectra analysis is one of the first most common tools used to capture structures' behavior under seismic loads as well have a significant influence on the design of seismic structures.

The first practice of the response spectrum in seismic design was used in the 1950s by Housner and Trifunac (1967). The response spectrum is a chart plotted between the largest response of various oscillators to a given acceleration, velocity, or displacement and its periods. It describes specific ground motion at a particular location beside the actual time history record (Somerville, 2003). The use of seismic response spectrum methods to predict forces and displacements in structural systems provides analytical advantages to obtaining desired design performance for structure. Therefore, the response spectrum helps to obtain the maximum structural response in the linear range and can generate earthquake-induced shear forces in the structure, thereby facilitating the earthquake-resistant structural design (Anderson and Bertero, 1987).

Contrastingly, the properties of the earthquake records in the near-fault region are not the same as ordinary ones; they have been found to place extreme demands on designs to the extent that cannot be estimated by common approaches measurements such as response spectra (Baker, 2007). The main features in the near-fault ground motions (NFGMs) are long-period pulse and high peak ground velocity (PGV) whereas normal ground motions (GM) or far fault ground motions (FFGMs) contain low peak ground acceleration (PGA) and high-frequency pulse. The

forward directivity effect is the common reason for these large pulses, which is related to the propagation of rupture to a location (Somerville *et al.*, 1997).

Obtaining tools to identify NFGMs gives engineers the keys to improving structure design codes and evaluating seismic hazards. Various researches have been developed many tools to identify this inherent pulse. The analytical model is one of the essential tools for describing the characteristics of NFGMs by using qualitative parameters and geographic assumptions (He and Agrawal, 2008; Mavroeidis and Papageorgiu, 2003). In some conditions, due to the variety of analytical models parameters and geographical assumptions, these analytical methods have some limitations to predict the characteristic of NFGMs.

Therefore, the signal processing is more effective than analytical tools for the analysis of non-stationary and nonlinear records for example NFGMs that contain long periods and multiple pulses. This type of GM is so hard to describe completely by analytical models that have geotechnical assumptions (Chen *et. al.*, 2019a) as well signal process analysis can easily be identified and extracted the velocity pulse. It is noteworthy that the theoretical basis for most pulse extracting techniques, such as Wavelet Analysis, is the determination of the pulses containing the largest energy in the original ground motion record. It's also worth noting that, the significant damage caused by NFGMs is attributed to low frequency and significant amplitude components (Baker, 2007).

In wavelet analysis, basis functions are used to satisfy a certain set of mathematical requirements. These basis functions are also called mother wavelets. Due to these prototype functions, some characteristics may be lost during capturing the pulse from NFGMs by using Wavelet analysis. Therefore, in this study, a signal analysis procedure based on Hilbert Huang Transform (HHT) will be used (Huang *et al.*, 1998). HHT method has better performance in the separation of time and frequency contents, and it does not need any predefined basis functions, as required in wavelet and Fourier analysis, to be defined before the analysis.

The HHT methodology decomposes the NFGM records into several signals depending on their frequencies without losing any characteristic of these records, and then classification and sifting procedures are conducted on these components to classify and extract pulse-like ones.

1.1 OBJECTIVE OF STUDY

Previous studies are focused on extracting the pulse obtained from limited NFGM recordings using the HHT approach and investigating the effect of these extracted pulse components on linear SDOF systems (Chen *et al.*, 2019a; Zhang *et al.*, 2019; Xu and Agrawal, 2010). However, these studies have some lacking in capturing the effects of extracted pulses and residual low and high-frequency components on inelastic SDOF systems. Hence, this thesis aims to investigate the effects of filtering low-frequency and/or high frequency or contents from the original records on behavior of nonlinear SDOF systems. To this end, the behaviors of numerous inelastic and inelastic SDOF systems having various ductility ratios and yield strengths subjected to the decomposed NFGMs obtained by HHT method will be investigated. Consequently, inelastic and elastic spectral responses are studied comparatively for regular and isolated SDOFs subjected to 114 NFGMs and their decomposed components.

1.2 SCOPE AND STRUCTURE OF WORK

The scope of the study includes elastic and inelasticSDOF systems having bilinear force-deformation relations. For a comparative research, 114 pulse-like NFGMs and their components having different frequency contents, which are obtained by HHT, are applied to these systems as ground acceleration.

This study includes a literature review for the effects of directivity and pulse-like GMs on the response spectra in Chapter 2, as well as the methods for determining and extracting the velocity pulses. The next chapter, Chapter 3, discusses the selection of elastic and inelastic SDOF systems, selection of NFGMs, and the application of the decomposition analyses. Chapter 4 presents the linear and nonlinear spectral responses of SDOF systems having various properties. The conclusion and discussion regarding these results are provided in Chapter 5.

2 CHARACTERIZATION OF NEAR FAULT GROUND MOTIONS

The recent increase in earthquake events has highlighted the importance of predicting the seismic response of structures. Damage caused by these earthquakes on buildings, civil infrastructure, and bridges can cause significant human and property losses. Seismologists have been studying the effect of magnitude, distance, and mechanisms of ground motion to decrease the influence of earthquake impact on structures.

NFGMs are assumed to occur within 15 km of the rupture and have a magnitude greater than Mw=5.5. They have dissimilar effects on structures from ordinary far-fault ground motions. They usually contain long duration time history properties, large amplitude, and permanent ground displacements. These NFGMs are a type of Gms that are difficult to describe for seismic performance evaluation since they have the potential to cause considerable damage to a variety of structures. One of the essential characteristics of NFGMs is the directivity of the motion. The term directivity in engineering-seismology means that it considers all terms to describe the factors that cause ground motion amplitudes and directions to vary at a constant distance from an earthquake rupture.

2.1. DIRECTIVITY EFFECT

The directivity effect in NFGM is the result of the prevalence of the wave created by rupture toward the adjacent site; the wavefront is generated by superposition of the shear waves that move in front of the rupture. The directivity effect is created by an accumulation of wave energy along the fault in the rupture direction.

One of the factors that affect the formation of directivity is the alignment of direction of wave propagation between the site and hypocenter with the slip direction of the fault which is the horizontal direction of the rupture front during a quake. If the rupture occurs closer to the site, this is referred to as forward directivity; if it occurs in the opposite direction, it is termed backward directivity. Forward rupture directivity happens after two requirements are satisfied: the rupture front moves towards affected area, and the direction of slip rupture is in line with the affected area. In strike-slip faulting, the requirements for producing forward directivity features are fully achieved since the rupture propagate horizontally along the strike from one or both sides.

Backward directivity occurs while the rupture propagates off the site and causes small amplitudes and lengthy motions. Fig. 2.1 shows the effect of the direction of rupture on the behavior of velocity amplitude for 1992 Lander's event (Somerville *et al.*, 1997). However, not all NFGMs does not necessarily have directivity effect. This effect also causes azimuth variation in ground motion action, so GM is strongly influenced in fault normal direction and this causes larger GM in fault normal direction than those in fault parallel direction (Somerville *et al.*, 1997). All locations near the fault rupture, where the rupture spreads, will have significant movements in the fault normal direction, except for areas close to the epicenter. The backward directivity effect occurs because sites around the epicenter are very close to the starting rupture location for constructive interference to be substantial, and the rupture primarily moves away from them. The vertical ground motion component does not significantly change under the directivity effect. Reyes, Kalkan and Survey (2012) examined the directivity effect related to the angle of orientation and they studied the orientation of GM effects on linear and nonlinear response of structures.

To have a thorough knowledge of the orientation effect, Fig. 2.2 shows the effect of orientation on the displacement response spectra with 5% damping for two stations in Christ chord New

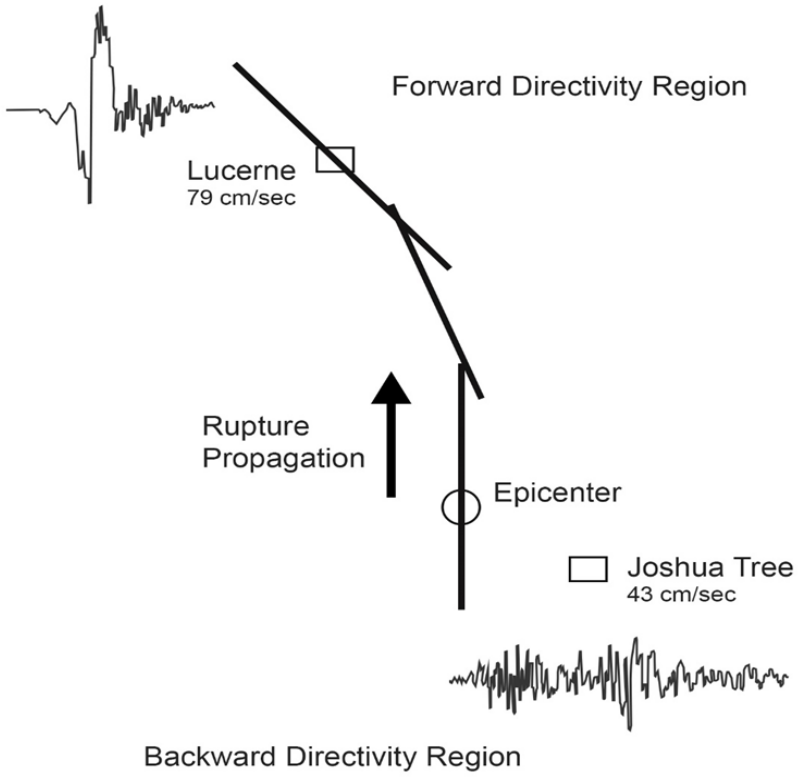

Figure 2.1 1992 Lucerne earthquake, Forward and Backward Directivity regions, (modified from Somerville *et al.*, 1995)

Zealand 2011 event, approximately 5 kilometers of the fault. The first station (SHLC) was considered not affected by the directivity, and the second station (PRPC) shows a large amplitude of motion oriented perpendicular to the fault. Due to directivity in the PRPC station, it has been observed that the strike-normal GMs are larger than the strike-parallel GMs at periods longer than about 0.8 seconds and have a significant influence on motion amplitude. On the other hand, the SHLC station shows a low ratio between fault normal and fault parallel response demand during the earthquake. As forward-directivity GMs sensitive to the rupture mechanism and slip direction, GMs near the surface rupture may additionally have a substantial permanent movement, which is called fling-step. These fling-step motions depend on the fault's tectonic displacement, which may lead to a high-intensity velocity pulse in the fault parallel direction.

One of the first studies that saw the effect of directivity is the work of Housner and Trifunac, (1967). They discovered that NFGMs have unique characteristics and significant influences on period length, velocity, displacement, and acceleration amplitudes. On the other hand, it should be noted that the acceleration amplitude does not necessarily determine the intensity of a ground motion. These ground motions that contain exceptional dynamic characteristics are described as a pulse-like ground motions that are known for putting very large demands on structures to the extent that cannot be expected by spectral responses.

The large amplitude in velocity pulse relative to a long period significantly affects the linear and non-linear dynamic behavior of structural response. However, not all NFGMs contain velocity pulses. In regard to comprehend the effects of this type of GMs on the structural response, a variety of methods were developed to evaluate outcomes of near-fault earthquakes that contain intense velocity pulses (Society *et al.*, 1974; Somerville *et al.*, 1995).

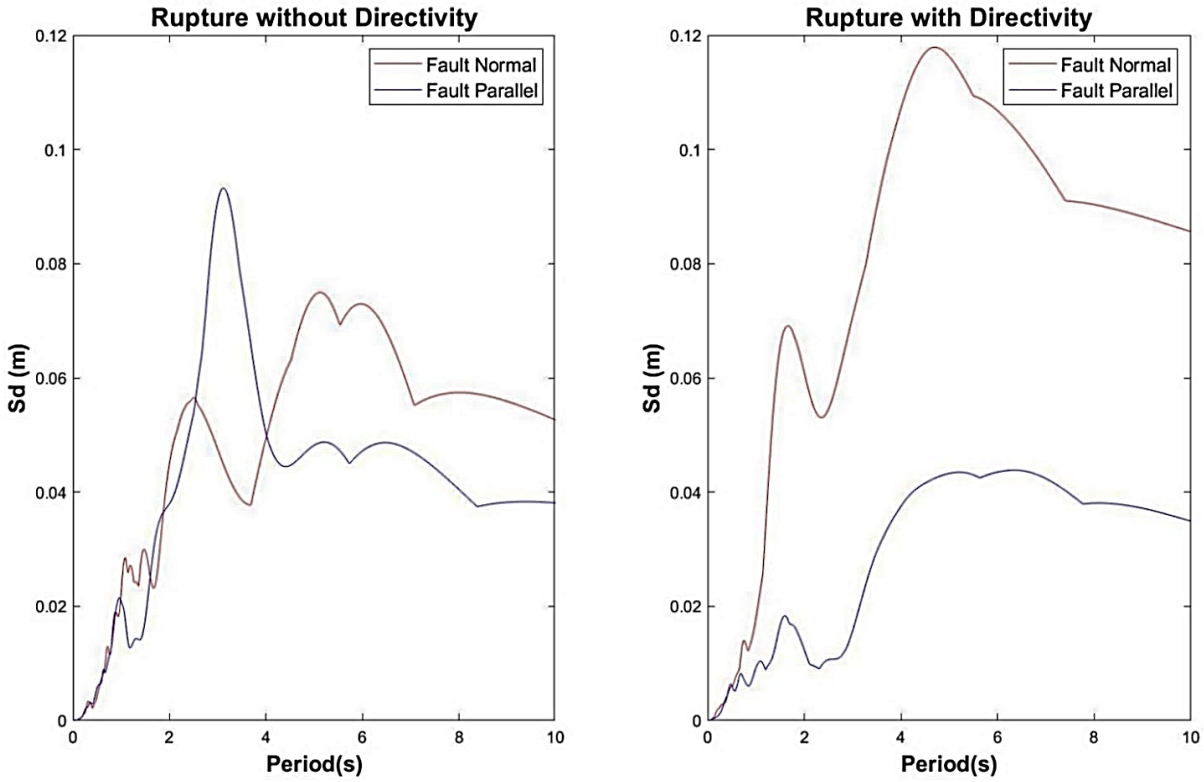

Figure 2.2 Displacement response spectra of fault-normal and fault-parallel components with 5% damping for stations within 8 km of the Christchurch, New Zealand 2011 event: Right (PRPC station) with directivity, Left (SHLC station) without directivity.

NFGMs may cause considerably larger inelastic displacement demands than far fault GMs besides large elastic displacements. Bertero *et al.*, (1978) investigated the Pacoima Dam (1971) record which is a NFGM having pulse-like characteristics and they studied whether this record could cause important structural damage related with this seismic pulse. They found that the structure subjected to a NFGM suffered extreme damage due to high amplitude pulse and large displacement cycle in structure response, which requires large ductility and/or strength demand to the structure.

In all parts of designing an earthquake resistant building, the designer faces a lot of uncertainties especially when the structure is subjected to NFGMs with high amplitude pulse similar to what happened in Italy 1979 Imperial Valley earthquake. After this event, Anderson and Bertero (1987) reported the sensitivity of linear and non-linear structural responses to NFGMs that helps the engineer to better decide the variables for design and select a proper approach. It was

observed that the structures near the fault are likely to be affected by pulse-like GMs, the deformations obtained from these pulse-like GMs are concentrated on the area of the structures that have high axial loads (lower floors).

Hall *et al.* (1995) evaluated the effect ofNFGMs on an elastic shear building and on a seismically isolated structure. Their results indicate that the 20-story steel structure show a significant impact under NFGMs more than the code design requirement. For the 3-story isolated building, the width of the isolated moat and the percent of pad damping shows a large influence on the structure response but still have immoderate yielding in the building near the fault rupture.

To understand of directivity effect on structure, Somerville et al. (1997) investigated the effect directivity on the design of structures under the influence of various ground motions. They observed that different faulting mechanisms have no significant variances in ground motion characteristics for the Kobe 1995, Northridge 1994, and Loam Prieto 1989 Earthquakes.

Bozorgnia *et al*. (1998) compared the response of 12 structure in vertical direction with UBC-97 and it was noted that real vertical response spectra can not be justified correctly by UBC-97. The high vertical acceleration records like Northridge event show that the analysis of nonstructural elements and their connection form to structural members must be considered, particularly for NFGMs.

There are many other parameters that describe the effect of NFGM such as pulse velocity, the peak ground acceleration (PGA), peak ground velocity (PGV), and peak displacement (PGD). Malhotra (1999) studied the effect of PGV / PGA ratio on elastic response spectrum for pulse like GMs and observed that these peak values are the important parameters for the structural behavior under seismic loading.

Iwan(2000) and MacRae (2001) studied the influences of directivity on the nonlinear response single or multi degree of freedom systems. The study revealed that inelastic response considering the directivity effect increases the displacement demand of structures while various structure design codes just considered the elastic demand in the design and analyses of structures. Additionally, it was reported that the ground motions causing similar elastic responses may show significant changes in inelastic displacement responses.

One of the characteristics of NFGMs that affect the behavior of long and short period structures is the high-frequency content in addition to high PGV ratio and long duration. The nonlinear static pushover analysis has been studied by Ghobarah (2004) to comprehend the structures' capacity to resist dynamic loads due to NFGMs. To correctly capture the real behavior of displacement demand of nonlinear response of a SDOF system, Zhai. et al., (2007) investigated the impact of site conditions and the ratio of PGV to PGA on nonlinear structural response. It has been reported that the inelastic displacement ratio spectra for NFGM were more affected than those for far fault GM for structural period range of 0.2-1.5 sec.

Due to the significance of this topic, a lot of research has been conducted on the impact of NFGMs on various structures. Sehhati *et al.* (2011) focused on multi-story structures; Zhang *et al.* (2013) highlighted the influence of NFGM on concrete dams; Soyluk and Karaca (2017) and Yang *et al.* (2017) presented the dynamic behavior of cable–support bridges and isolated bridges, respectively, with and without consideration of rupture directivity.

To accurately estimate the directivity effect on the dynamic structural response, the presence and parameters of velocity pulses in records should be identified and studied in detail. The following section elaborates on velocity pulses in ground motions.

2.2 PULSE LIKE GROUND MOTIONS

The directivity effect in NFGMs can cause velocity pulses to be magnified, due to the accumulation of wave energy released as a single large pulse in the direction of rupture. Essentially, defining the pulse content in ground motions may present important considerations for all aspects of structure safety, durability, and economy. Ground motions may be affected by many factors like faulting mechanisms, and the direction of rupture propagation, in addition to ground surface deformation.

The directivity effect essentially occurs in fault normal component that contains velocity pulse (high magnitude and long duration) and it has been taken into consideration for the structural analysis and design to capture the real behavior. NFGMs also show another characteristic property, besides the directivity effect, called fling step. A residual displacement together with a large magnitude velocity pulse characterizes fling-step (Kalkan *et al.*, 2006). Unlike forward directivity, in fling step the displacement step occur in the parallel direction of the strike. Contrary to expectations, some directivity effect motions show that the highest velocity

amplitude could occur on an orientation highly different from the fault normal direction (Mavroeidis and Papageorgiou, 2002; Howard *et al.* 2005). In general, the primary emphasis of research studies is on the fault normal components that contain velocity pulses (high amplitude) in GMs and their effect on response of structures.

An empirical model was established by Somerville *et al.* (1997) to predict fault normal and fault parallel spectral accelerations for long period structures. Howard, et.al., (2005) gathered near-source ground motion records that strongly reflected the directivity effect and rotated them to the angle with the highest overall spectral acceleration and compared them with the model of Somerville *et al.* (1997). It has been observed that the orientations of strong velocity pulses can extremely vary from the standard fault, and their spectral acceleration results can significantly exceed predictions in Somerville *et al.* (1997). These observations can have valuable implications for design cases in earthquake engineering, where the fault orientations of possible future earthquakes are established, and the orientations for which pulse-like ground motion could be present must be calculated (Jack W. Baker, 2007). Since pulse-like GMs have particularly destructive effects on structures, the detection and classification of velocity pulses are very crucial.

2.2.1 Identification of velocity pulse

Velocity pulses inherent in NFGMs are typically noticeable in the velocity time history. There have been many research concentrated on the classification of pulse-like GMs quantitatively and various methods have been proposed for simulating or extracting meaningful pulses. Several seismic parameters were considered relevant when determining a classification procedure such as pulse period, PGV, fault-site distance, etc.

Over the last decade, researchers have used various analyses to classify the presence of velocity pulse in GMs. Some works have been done by developing mathematical models to describe features of pulse parameters, such as velocity time history shape, magnitude, number of cycles and pulse period (Mavroeidis and Papageorgiou, 2003; Fu and Menun, 2004; He and Agrawal, 2008). One of the approaches that identify the possibility of occurrence and characteristics of pulse-like ground motions is based on the largest fractional energy contribution of any half-cycle in the velocity pulse (Mukhopadhyay and Gupta, 2013; Chang *et al.*, 2016). In addition to the previous two approaches, other helpful tools to identify the pulse velocity are signal

analysis approaches such as Wavelet analysis (Baker 2007), and Empirical mode decomposition (EMD) method (Loh et al., 2001 ;Chen et al., 2019).

2.2.1.1 Analytical Pulse Models

The analytical models are proposed for the simulation of velocity pulses inNFGMs. These models attempt to accurately characterize the impulsive essence of NFGMs, both qualitatively and quantitatively. Furthermore, they can be utilized to replicate mathematically scientific findings based on available NFGMs. Among the pulse models that we will discuss later, the pulse period and the amplitude of velocity trace are the primary pulse parameters (Mavroeidis *et al.*, 2003; He and Agrawal, 2008; Menun and Fu; 2002)

To correctly configure and evaluate the seismic effects on structures, the following features should be present in an analytical pulse model: First and foremost, it should have a meaningful mathematical description. and it should correctly simulate the attitude of all NFGMs that contain velocity pulses. Secondly, it should be capable of capturing the real behavior of SDOF systems subject to the analytical model as well as have step-space domain expression that helps in the design of seismic protective systems (He and Agrawal, 2008). Makris and Chang (2000) classified cycloidal pulses into three types of motions, depending on the number of half-cycle velocity pulses to systematically investigate the performance of different damping mechanisms. It is noted that the response of the long-period structures under cycloidal pulse is similar to structural response exposed to NFGMs. On the other side, the stiff structures are greatly affected by high-frequency components in ground motions that cycloidal pulses cannot present this effect on small period structures.

2.2.1.2 Energy Based Approach

The energy-based methodology is one of the simplest and most effective techniques to evaluate the velocity pulse in NFGMs. Mukhopadhyay and Gupta (2013) used the energy approach for identification, extraction, and modeling the velocity pulse, as it is based on the value of maximum fractional wave energy content in ground motion by dividing velocity time history into several half pulses. The cumulative squared velocity throughout the finite time interval between two consecutive zero-crossings (zero velocity times) gives the energy of each half-cycle. Eq.2.1 shows the largest energy contribution for half cycle, where *j* is the number of half-cycle depending on maximum energy contribution (when *j* increases the fractional energy for

half cycle decreases), t1 and t2 represent the border time for the half-cycle, T is the total time of velocity trace and $v(t)$ is velocity trace of the ground motion. It's clear that *fracEn*(1) have the largest fraction energy; due to that, *fracEn*(1) can detect pulse-type motion from non-pulse type motion as a predictor variable. Eq 2.2 shows the prediction equation for the pulse identifier (PI). PI takes values from 0 to 1 and it is used to characterize GM as pulse or non-pulse ground motion (PI > 0.5: pulse-like ground motion, PI<0.5: not pulse-like), and PI=0.5 implies an equivocation in this classification. One of the restrictions in the method of Mukhopadhyay and Gupta (2013) is the multiple pulses; this is because pulses contain large number of half-cycles and the PI for this case can be less than 0.5.

$$\boldsymbol{fracEn(j) = \frac{\int_{t1}^{t2} v^2(t)dt}{\int_0^T v^2(t)dt}} \tag{2.1}$$

$$\boldsymbol{PI = \frac{1}{1 + e^{7.64-27\, fracEn(1)}}} \tag{2.2}$$

Zhai (2013) proposed a technique based on energy that may be utilized to determine GMs having dominant pulses in their velocity traces and the square of velocity is utilized to reflect the energy of the motion. Afterward, the ratio of the energy of the pulse and the energy of the original GM is considered as a pulse indicator. 3600 recorded ground motions having PGVs above 30 cm/s are chosen and implemented to establish a final measure. Eq 2.3 and Eq 2.4 reflect the cumulative motion energy and relative energy stored in the pulse of the velocity time history records, respectively, where $E(t)$ represents the cumulative motion energy for velocity pulse; t_e, t_s are the end and start interval time of the velocity pulse; E_p represent the relative energy stored in the pulse. It is assumed that main velocity pulses in NFGMs having relative energy values larger than 0.3 may be described as pulse-like GMs. Zhai *et al.*, (2018) also developed an algorithm for detecting pulse-like ground motions dependent on substantial velocity half-cycles. This algorithm is based on dividing the velocity time history into several half cycles, as the time interval between two consecutive zero-crossings gives relative energy.

$$E(t) = \frac{\int_0^t v^2(t)dt}{\int_0^\infty v^2(t)dt} \tag{2.3}$$

$$E_p = E(t_e) - E(t_s) \tag{2.4}$$

The relative energy can be represented by using Eq.2.3 for each half cycle; the limit value for the energy ratio of the major half-cycle is assumed to be equal to or greater than 0.1. The pulse relative energy is based on the summation of significant velocity half-cycles. Based on the number of half-cycles, ground motions are grouped into a variety of distinctive types, from type-0, which represents no significant half cycle (no pulse) in ground motion records, to type-5, which contains many half-cycles that describe pulse characteristics. The relative energy threshold for each type of pulse-like motion is between 0.3 for type-1 and 0.73 for type-5.

2.2.1.3 Signal Analysis

On another side, analytical models may not be able to represent the pulses in GMs accurately due to apriori shape assumptions for pulses. For this reason, signal-analysis techniques could be more efficient in the study of NFGMs. The signal analysis aims to enhance extraction and representation of earthquake wave characteristics from motion records, along with other essential features such as time-frequency energy distribution, which allows to advance our understanding of the underlying physical mechanism of data exposure, as well as enhances awareness of the effect of ground motion on different engineering processes, such as the dynamic behavior of structures.

In the literature there are some effective methods that can be used in describing ground motion analysis, extracting velocity pulses, and directly computing pulse periods, which are given subsequently:

Wavelet analysis

A wavelet is a quick, short wave-like vibration with a frequency that starts at zero, rises, and then rapidly drops down to zero. Wavelets are deliberately engineered to have unique characteristics that make them more valuable for signal analysis than other types of signal analysis such as Fourier transform. Seismic signals are approximated in the Fourier transform by summing a sequence of single frequency sinusoidal signals.

Seismic signals are interpreted in the wavelet transform by superposition wavelet waveforms, each is a narrow-band signal centered at a particular time point that is widely applied to represent the seismic pulse that is nonlinear and non-stationary. The main pulse waveforms of interest may be represented succinctly by only a few wavelets using the carefully chosen mother wavelets, time, and scale parameters. Wavelets are simple oscillations that fulfill a criteria set in mathematics, to decompose a signal. For this purpose several wavelet models can be used, such as Daubechies wavelet(db), Gaussian wavelet, Morl wavelet and Harl wavelet. Fig. 2.3 shows some types of mother wavelets.

Baker (2007) extracted velocity pulses from the original NFGMs using wavelet analysis. A methodology was developed to identify the largest velocity pulses in 3500 records. Fig. 2.3 shows 4 forms of mother wavelets that are used for this approach. The properties (PGV/PGA and Relative energy) of the obtained pulse in comparison to the original GM are utilized to develop a quantitative criterion for identifying the GM as pulse-like GM. To obtain the set of GMs with the highest engineering interest in these pulse-like records, the following two conditions are applied: the pulse appears early in the GM and the PGV is high.

Baker (2007) utilized logistic regression to classify the recordings based on the ratio PGV/PGA in addition to relative energy to determine whether the given GM is pulse-like or not (see Eq. 2.5). The pulse indicator (PI) has a range of zero to one, with high values indicating that the GM is pulse-like. Records with PI values larger than 0.85 are categorized as pulse-like ground motion, and below 0.15 are defined as non-pulses.

Many other studies also used the wavelet approach to describe ground motions. Xia (2019) presented a methodology for defining and describing the multi-pulse NFGMs using adaptive wavelet transform. A new adaptive mother wavelet selection technique was presented to identify the ideal mother wavelet from fifteen mother wavelets.

$$PI = \frac{1}{1 + e^{-23.3+14.6(PGV\ ratio)+20.5(Energy\ ratio)}} \tag{2.5}$$

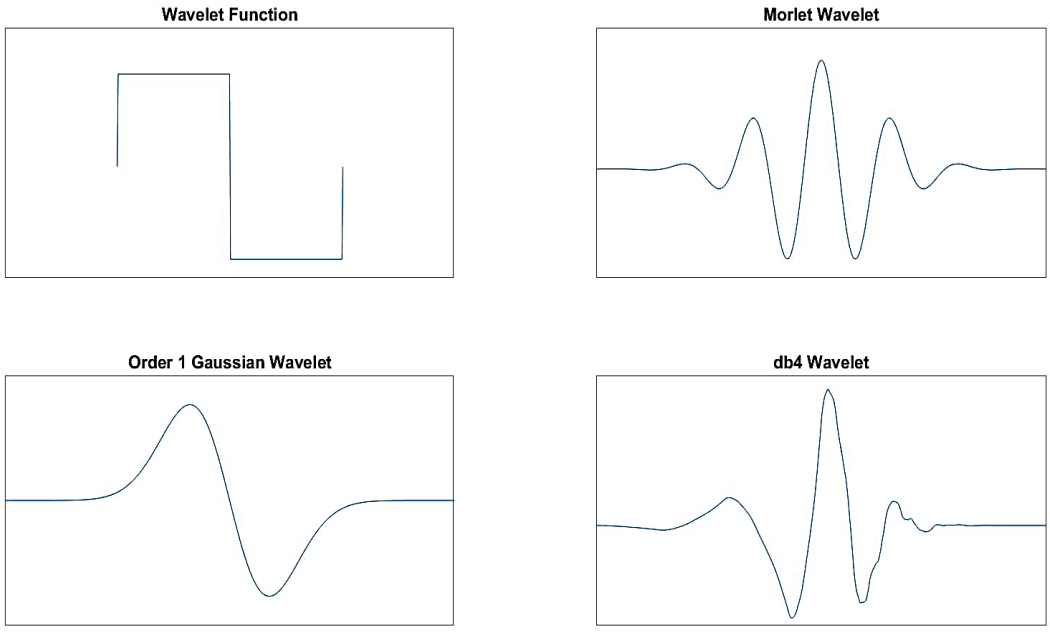

Figure 2.3 Some wavelet examples

Hilbert Huang-Transform (HHT)

This transform method was developed by Huang et al., (1998) and it is an effective technique that can show time-frequency-energy representation of signals. It has an adaptive expansion basis, so it can generate realistic representations of data from non-linear and non-stationary oscillations such as in GM records, particularly for time-frequency-energy representations, since it is affected by the local features of the original signal. Compared to wavelet analysis, HHT has enhanced time-and frequency-separation efficiency and does not require any simple functions to be defined prior to data analysis.

HHT method has two major steps namely empirical mode decomposition (EMD) and Hilbert spectral analysis (HSA). The first step (EMD) decomposes original data into several fundamental oscillations, called intrinsic mode functions (IMFs). EMD represents the basic analysis in HHT and it is a powerful tool for analyzing frequency–time domain signals, especially for nonlinear and nonstationary signals such as strong ground motions. For this study, the pulse-like waves in NFGMs are extracted using the EMD approach and the absolute input energy of the SDOF system (Loh et al., 2001). The pulse-like wave characteristics of NFGMs can be identified by evaluating the absolute input energy of each IMFs. These pulse-like waves

are captured from various frequency contents of NFGMs. The EMD method can also provide a frequency-time-amplitude range from which damage to the structural system can be detected.

Zhang *et al.* (2003) investigated the basis for Hilbert-Huang transform HHT in the analysis of ground motions used in seismology and engineering studies. They compared the results of the HHT method and Fourier analysis and concluded that the HHT method can extract some motion properties better than Fourier analysis.

Xu and Agrawal (2010a) used the EMD method to define and distinguish dominant pulses as well as long-period and high-frequency components in NFGMs, and to examine the dynamic behavior of SDOF under these components. Their results show that the characteristics and effects of the pulses developed by the analytical pulse models are close to those of the decomposed pulses by using EMD for elastic structures. In addition, the extracted pulse is the main cause for the maximum response of the elastic structures under NFGMs.

Zhang (2019b) used two factors to classify pulse-like ground-motion records, which are the PGV/PGA ratio and the energy change of each IMF. The velocity history records that contain an IMF for which the maximum energy change is greater than 0.32 and the PGV/PGA ratio larger than 0.12, are considered as pulse-like ground motion. The results of the HHT method have been verified to the result obtained by Wavelet analysis (Baker, 2007).

2.2.2 Determination of the Velocity Pulse Period (Tp)

Since the ratio of the velocity pulse period to the structure's fundamental period has a major impact on elastic and inelastic structural response, the velocity pulse period can be considered as an important parameter that must be taken into account when identifying the velocity pulse. A common technique to obtain velocity pulse period utilizes velocity response spectra, where the period at which peak velocity occurs is taken as the pulse period (Sv).

Some researchers, on the other hand, have criticized this technique (Baker, 2007; Rodriguez-Marek, 2000). Because of the presence of a high-frequency component, this approach can not represent the real PGV, which leads to incorrectly defining the period of the pulse. Other methods to calculate velocity pulse period depending on the location of PGV values to define the main pulse, as well as using nonlinear optimization to match the sine wave to the pulse

(Mavroeidis and Papageorgiou, 2003). As part of the wavelet analysis, the velocity pulse periods are conveniently calculated using the base wavelet pseudo periods. Baker (2007) used the largest wavelet and a sinusoid with a period equal to the maximum Fourier amplitude of the wavelet to define the pulse period.

Zhai *et al.* (2013) adopted a different measure known as the peak point method, which was developed originally by Ohsaki (2008). The method obtained the pulse period as one cycle time duration, which includes the PGV, between two sequential peaks or troughs.

Another suggestion to identify the pulse period is the peak of the multiplication of the spectrums as Sd*Sv, where Sd and Sv are, respectively, the displacement and velocity response spectrums (Mimoglou, 2014). This approach was also used by Kardoutsou et al. (2017). They grounded this method on the findings that the intrinsic pulse in GM influences both velocity and acceleration traces, and Tp should dominate in the convolution integral of these two traces and should be associated to the maximum of the corresponding Fourier spectrum.

3. MATERIALS AND METHODS

Within the scope of this research, numerous elastic and inelastic SDOF systems are considered to examine the effects of decomposition of NFGM records on the response of structure spectra. Furthermore, certain isolated systems and analytical pulse models will also be considered for comparing their spectra for decomposed ground motions.

3.1 SINGLE DEGREE OF FREEDOM SYSTEMS (SDOF)

The SDOF system is a simple system (contain single mass, stifnnes, and damper) that represents a complex structural systems (structures that contains various and countless variables to observe its characteristics) by using the natural frequency of the complex structure system that depends on the material, weight, shape, and other attributes of the complex systems (which is called Normal mode of the system). Figure 3.1 shows a simple oscillator is idealized as a SDOF system.

3.1.1 Linear systems

In general, linear systems in engineering means that the structure systems will return to their original phase and shape after removing the force. As well, the ratio between force and displacement is almost linear in the first stage of applying force. This section will disscuss the properties of linear SDOF systems.

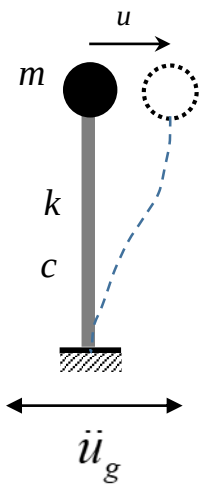

Figure 3.1 A single-degree-of-freedom oscillator

The dynamic equilibrium of the SDOF system under ground acceleration can be expressed as Eq 3.1.

$$\boldsymbol{m\,\ddot{u} + c\,\dot{u} + k\,u = -m\,\ddot{u}_g} \tag{3.1}$$

In which *k*, *c* and *m* represent the main parameters of SDOF, so that *m* represents the lumped mass of the SDOF system supported on a member having stiffness of *k*, *c* represents viscous damping coefficient, $u, \dot{u}, \ddot{u}$ and $\ddot{u}_g$ are relative displacement, velocity, acceleration, and ground acceleration, sequentially. Consequently, $m\ddot{u}, c\dot{u}, ku$ terms represent the inertia force, damping force, and inelastic forces, respectively. As it is seen in the equation, ground acceleration $\ddot{u}_g$ creates a force on the system in opposite direction of the ground acceleration.

By dividing Eq. 3.1 by mass (*m*), the equation becomes

$$\boldsymbol{\ddot{u} + 2\zeta\omega\,\dot{u} + \omega^2 u = -\ddot{u}_g} \tag{3.2}$$

where ω is the natural frequency of the SDOF system that depends on m and the stiffness k. The natural frequency increases as the structural stiffness to mass ratio rises, conversely the decrease of stiffnes in relation to mass lead to an increase the natural frequency of SDOF systems.

$$\boldsymbol{\omega = \sqrt{\frac{k}{m}}} \tag{3.3}$$

The period of the structure (T) and angular frequency ω has the following relation

$$\boldsymbol{T = \frac{2\pi}{\omega}} \tag{3.4}$$

ξ in Eq 3.2 represents the damping ratio of the system, which is a dimensionless measure that count on the type of the materialsof the structure. The ξ is calculated as a relation between the damping coefficient and the critical damping. The ξ describes decay in structural response after a disturbance.

$$\boldsymbol{\xi = \frac{c}{c_{cr}} = \frac{c}{2m\omega}} \tag{3.5}$$

3.1.2 Non-linear systems

Current performance design approaches require ways to evaluate the realistic behavior of systems under NFGMs. Nonlinear analyses provide the means to calculate structural responses beyond the elastic spectrum, including degradation in strength and stiffness associated with inelastic material behavior and significant displacements. Therefore, comparisons of the inelastic response of the structures subjected to NFGMs and their components having various frequencies are important for the design purposes.

In order to understand the non-linear structural behavior in this study, the effect of decomposition of NFGMs by using HHT on the dynamic behavior of inelastic structures is studied using constant-ductility spectra (CDS) and constant-strength spectra (CSS). These spectra are obtained for a SDOF system having bi-linear material behavior depicted in Fig. 3.2, where f_y yield strength obtained from f_0 which is the maximum value of the earthquake-induced resistive force in the equivalent linear system, and $\bar{f}_y$ is normalized yield strength.

$$\boldsymbol{f_y = \bar{f}_y f_0} \tag{3.6}$$

k_1 and k_2 represent the elastic stiffness and post-elastic stiffness of the systems, respectively. u_m express the absolute peak deformation of the inelastic structure caused by the GM. It is important to normalize u_m with the system's yield deformation which gives ductility factor. Thus when u_m exceeds u_y by definition ($\mu \geq 1$), the system deforms into the inelastic range.

$$\boldsymbol{\mu = \frac{u_m}{u_y}} \tag{3.7}$$

To have a more comprehensive comparison, different ductility ratios (2, 4, 6, and 8) were chosen for CDS and various strength ratios (F_y/W =0.02, 0.06, 0.1, 0.2) for CSS are considered in this study, where W is the weight. The system refers to an elastoplastic system when there is no post elastic stiffness (k_2=0). Additionally various ratios of post elastic stiffness to elastic stiffness ($k_r = k_2/k_1$) are taken into account such as 0.02, 0.05, 0.1, 0.2.

Constant-Ductility Response Spectra (CDS)

Constant-ductility spectra is one of the means to capture the non-linear response of structures, which the structures have been designed to reach target ductity by calculate the lateral strength

of that systems. The development of a CDS necessitates iterations that determines the ratio of elastic to inelastic strength for which the the target ductility is obtained for a specified GM (Veletsos AS, 1960). To obtain the yield strength of an elastoplastic system for a given ductility factor, an interpolative technique is needed since the response of a system with arbitrarily chosen yield strength rarely corresponds to the desired ductility value (Chopra, 2000). For a detailed analysis, four ductility ratios (2, 4, 6, and 8) have been selected for CDS analysis.

Constant-Yield Strength Response Spectra (CSS)

The yield strength F_y needed in an SDOF system that can undergo inelastic deformation is lower than the minimum strength required to keep the structure elastic. In this thesis, CSS are expressed as displacement demand spectra (Sd) as a function of the system period (T). Various Fy/w ratios (0.02, 0.06, 0.10, 0.20) for regular structures are taken for more representative results.

3.1.3 Seismic isolated structures

The aim of seismic isolation is to minimize the effect of seismic force demand on the structures rather than increasing the strength of the structures. Seismic isolation system is a technique used to minimize the effect of GMs on structure by modify the response of that structure. In the

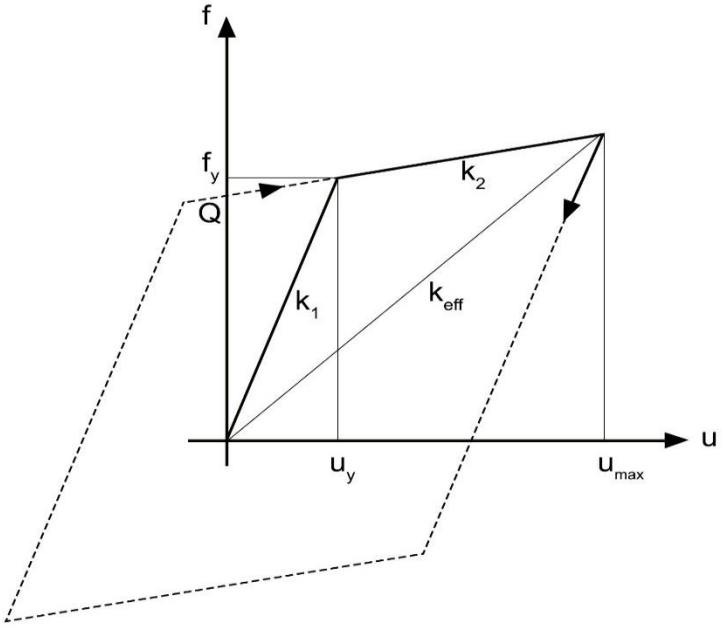

Figure 3.2 Idealized bilinear behaviour of an nonlinear material and hysteresis loop of an system

isolated structure, the structure is seperated from the GMs by using malleable layer between the structure and foundation (Dicleli *et al.*, 2006).

The flexible layer provides the structure with a longer natural period (T) than its original period. Therefore, the energy of GM is absorbed by the isolation system and the seismic forces are reduced. The effect of the seismic isolation system of a bridge on acceleration spectra is shown in Fig. 3.3 (AASHTO, 1999). The fundemental period shift from short to long periods due to the flexibility of the seismic isolation system, causes a reduction of up to 60% in seismic forces (Dicleli *et al.*, 2006).

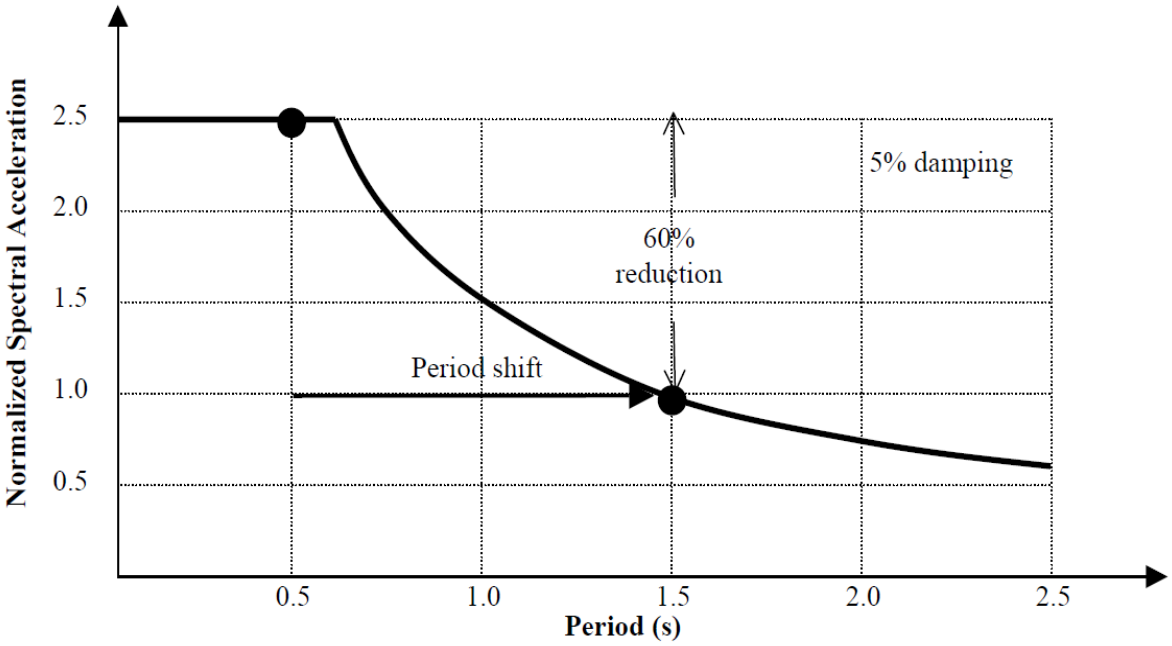

Figure 3.3 Effect of period shift in isolated system on spectral accelerations

Nonlinear force-deformation characteristics of the SDOF seismic isolator system can be substituted with a relationship between force and displacement as shown in Fig. 3.2 (bi-linear relationship). *Td,* is the post elastic period of the isolated structures that its much longer than the elastic period. In this research approach, T*d* is calculated using the post-elastic stiffness (k_2) of the seismic isolation system, which is calculated as $Td = 2\pi\sqrt{m/k_2}$. The post elastic periods change between 1 to 5 to satisfy design practices, and Table 3.1 shows the post elastic period and elastic period for $k_r = 0.01$.

The calculation steps of effective post elastic stiffness values corresponding to various elastic stiffness periods are given below:

The elastic period is:

$$T = 2\pi\sqrt{m/k_1} \tag{3.8}$$

$$0.1s = 2\pi\sqrt{1/k_1}.$$

$$k_1 = 3943.84\ kN$$

$$k_2 = k_1/k_r$$

$$k_2 = k_1 x\ k_r = 3943.84\ x\ 0.01 = 39.4384$$

The effective post elastic period is:

$$\boldsymbol{Td = 2\pi\sqrt{m/k_2}.} \tag{3.9}$$

$$Td = 2\pi\sqrt{1/39.4384} = 1\text{s}.$$

Table 3-1 Various post elastic periods for $k_r = 0.01$, and m = 1 (kN.s^2/m).

Td(s)	k_2(kN)	k_1(kN)	*T*(s)
1	39.4384	3943.84	0.1
1.5	17.52818	1752.818	0.15
2	9.8596	985.96	0.2
2.5	6.310144	631.0144	0.25
3	4.382044	438.2044	0.3
3.5	3.219461	321.9461	0.35
4	2.4649	246.49	0.4
4.5	1.947575	194.7575	0.45
5	1.577536	157.7536	0.5

The equivalent (or effective) viscous damping ratio (EVDR) of the seismically isolated systems ξ_e, is expressed as follows;

$$\xi_e = \frac{\textbf{Hysteretic Energy Dissipated}}{2\pi k_e u_{max}^2} \tag{3.10}$$

The EVDR of the isolated structure is directly related to hysteretic dissipated energy. The expression hysteretic indicate the offset during one cycle of the loading and unloading curves as described in Fig. 3.2. The energy that is consumed during the unloading process, is usually dissipated from structure by introducing a mechanism that produces friction as the isolation bearing moves. The area under force-displacement relationship curve for single cycle of the isolated system is reffered to Hysteretic energy dissipated. The slope of the line formed between the origin and the point of maximum force of a bilinear curve is defined as the effective stiffness (*ke*) of the isolation system (Buckle *et.al.* 2006). The above equation is described as;

$$\xi_e = \frac{2Q(u_m - u_y)}{2u_m\,(k_e u_m + Q)} \tag{3.11}$$

Where Q is the characteristic strength defined as;

$$Q = u_y(k_1 - k_2) \tag{3.12}$$

as well $u_m = \mu * u_y$.

EVDR is calculated as functions of ductility (μ) and effective stiffness (*ke*) :

$$\xi_e = \frac{2(1-k_e)(\mu-1)}{\mu\,\pi(1-k_e+\pi\,k_e)} \tag{3.13}$$

3.2GROUND MOTION SELECTION

A set of 114 NFGM records that strongly reflect the forward directivity was utilized in this analysis approach from the Pacific Earthquake Engineering Research Center database ("PEER" https://peer.berkeley.edu/). A similar set was also previously considered by (Shahi and Baker, 2014). To generate the extreme effects of NFGMs, two horizontal components of the records are rotated from 0° to 90° so that one of the components provides the highest amplitude value for velocity time history (highest PGV) (Shahi and Baker, 2014).

Moreover, these GMs were previously studied by wavelet analysis and categorized as pulse-like GM with directivity effect according to the classification method established by (Baker, 2007). In this study, records at stations at rupture distance less than or equals to15 km (closest distance to fault rupture) having moment magnitude (M_w) between 5.5 and 7.9 with PGV of greater than 30 cm/sec are considered. Velocity time histories containing velocity pulses have been taken into account for many studies to capture the actual dynamic behavior of the structures (Somerville, 2003; Baker, 2007; Yalcin and Dicleli, 2020). In this study, by considering the near-fault records having velocity pulses with large magnitudes, the effects of decomposition of these NFGMs by using the EMD approach are studied to evaluate the elastic and inelastic structural behavior. To achieve this aim in a thorough manner, chosen GM records are further divided into multiple groups (6 groups), based on their velocity wavelet periods; the chosen GM records have an average group wavelet periods (Tp wavelet) 0.73s, 1.4s, 2.9s, 4.8s, 7.9s, and 11.1s. A similar approach was also used earlier by Yalcin and Dicleli (2020). Table 3.2 shows the main features and categories of the chosen GMs and their grouping.

The first column in Table 3-2 contain record sequence number (RSN) as in PEER database. The other columns represent the basic characteristics of NFGMs, where Tp represents wavelet period obtained from (Baker, 2007) analysis, Sv is the SDOF system period at which the absolute maximum of the velocity spectrum is obtained (Alavi and Krawinkler, 2004), and PGV is the peak GM velocity for original records

Table 3-2 NFGMs that strongly reflect directivity effect sorted and classified according to the wavelet pulse periods

RSN	Year	Mw	Closest Dist. (km)	(Group No) Mean Tp	Tp wavelet (sec.)	Tp(Sv)	PGV (cm/s)
4211	2004	6.6	11.3		0.32	0.25	66.9
4101	2004	6	5.5		0.52	0.42	31
4126	2004	6	3.8		0.57	0.43	43.4
1050	1994	6.7	7		0.59	0.43	50.2
4103	2004	6	4.2		0.7	0.59	38.3
1052	1994	6.7	7.3	(1) 0.73	0.73	0.89	56.8
568	1986	5.8	6.3		0.81	0.65	68.3
1051	1994	6.7	7		0.84	0.73	106.1
4097	2004	6	3		0.85	0.71	53.2
1602	1999	7.1	12		0.88	0.91	65.8
1004	1994	6.7	8.4		0.93	0.78	77.9
3475	1999	6.3	10.2		1.02	0.83	39.3
4102	2004	6	3.6		1.02	0.68	43.5
451	1984	6.2	0.5		1.07	0.73	76.8
4480	2009	6.3	6.3		1.07	0.41	42.1
4100	2004	6	3		1.08	0.85	57.9
1106	1995	6.9	1		1.09	0.86	105.6
569	1986	5.8	7		1.13	0.83	92.2
148	1979	5.7	7.4		1.16	1.01	30.8
4482	2009	6.3	6.5		1.18	0.82	31.6
4107	2004	6	2.5		1.19	1	81.9
4115	2004	6	2.6		1.19	0.93	56.5
4065	2004	6	2.9		1.22	0.9	35.8
150	1979	5.7	3.1		1.23	0.83	49.6
459	1984	6.2	9.9		1.23	1.16	37.3
1054	1994	6.7	7.5	(2) 1.4	1.23	1.18	76.3
1063	1994	6.7	6.5		1.25	1.1	149.1
4098	2004	6	3		1.33	1.08	51.6
149	1979	5.7	5.7		1.35	0.95	32.1
1044	1994	6.7	5.9		1.37	0.71	116.1
4847	2007	6.8	11.9		1.4	1.33	91.1
4451	1979	7.1	7		1.44	1.48	62.7
147	1979	5.7	9		1.46	1.24	32
3965	2000	6.6	6.9		1.54	1.2	53.2
1120	1995	6.9	1.5		1.55	1.26	153.2
8123	2011	6.1	5.1		1.55	1.16	97.5
3548	1989	6.9	5		1.57	1.05	121.3
1013	1994	6.7	5.9		1.62	1.29	86.3
77	1971	6.6	1.8		1.6	1.2	121.9
764	1989	6.9	11		1.64	1.44	43.6
285	1980	6.9	8.2		1.71	1.28	38.1
766	1989	6.9	11.1		1.73	1.46	46.2

Table 3-2 NFGMs that strongly reflect directivity effect sorted and classified according to the wavelet pulse periods (Continued)

RSN	Year	Mw	Closest Dist. (km)		Tp wavelet (s)	Tp(Sv)	PGV (cm/s)
4228	2004	6.6	8.9		1.8	1.34	65.6
1119	1995	6.9	0.3		1.81	1.38	95.6
4458	1979	7.1	5.8		1.97	1.48	62.8
4483	2009	6.3	5.4		1.98	1.56	46.3
4040	2003	6.6	1.7		2.02	1.53	124.2
159	1979	6.5	0.7		2.34	1.88	53.5
723	1987	6.5	0.9		2.39	1.83	143.9
1086	1994	6.7	5.3		2.44	2.44	130.6
2734	1999	6.2	6.2		2.44	0.51	44
1182	1999	7.6	9.8		2.57	1.84	58.3
767	1989	6.9	12.8		2.64	1.97	44.8
1114	1995	6.9	3.3		2.83	1.34	103
1045	1994	6.7	5.5	(3) 2.8	2.98	2.37	118.3
1084	1994	6.7	5.3		2.98	2.64	106.3
828	1992	7	8.2		3	0.71	96.7
982	1994	6.7	5.4		3.16	2.76	101.5
2114	2002	7.9	2.7		3.16	1.83	121.4
292	1980	6.9	10.8		3.27	3.04	71.1
171	1979	6.5	0.1		3.42	2.87	116.4
1085	1994	6.7	5.2		3.53	2.92	114
983	1994	6.7	5.4		3.54	2.65	66.1
181	1979	6.5	1.4		3.77	3.36	121.6
180	1979	6.5	4		4.13	3.6	96.5
3473	1999	6.3	11.5		4.15	0.9	38.4
182	1979	6.5	0.6		4.38	3.33	111.9
161	1979	6.5	10.4		4.4	3.12	36.7
170	1979	6.5	7.3		4.42	3.5	70.8
178	1979	6.5	12.9		4.5	3.48	55.8
173	1979	6.5	8.6		4.52	3.81	55.2
802	1989	6.9	8.5		4.57	3.94	53.5
1511	1999	7.6	2.7		4.73	0.87	71.2
179	1979	6.5	7		4.79	4.03	80.8
185	1979	6.5	7.5	(4) 4.8	4.82	4.16	73.4
8119	2011	6.1	2		4.82	1.52	123.1
1176	1999	7.5	4.8		4.95	3.68	90.6
1510	1999	7.6	0.9		5	4.56	104.9
879	1992	7.3	2.2		5.12	4.4	132.3
1244	1999	7.6	9.9		5.34	4.66	108.9
3744	1992	7	12.2		5.36	2.43	80.6
1165	1999	7.5	7.2		5.37	2.92	38.1
803	1989	6.9	9.3		5.65	1.22	62
1503	1999	7.6	0.6		5.74	4.79	136.5
1161	1999	7.5	10.9		5.99	5.17	53

Table 3-2 NFGMs that strongly reflect directivity effect sorted and classified according to the wavelet pulse periods (Continued)

143	1978	7.3	2	(5) 7.9	6.19	4.88	129.7
6906	2010	7	1.2		6.23	2.34	128.5
184	1979	6.5	5.1		6.27	2.99	73.5
1501	1999	7.6	9.8		6.55	3.35	78.9
1193	1999	7.6	9.6		6.65	4.93	61.6
8606	2010	7.2	11.4		7.08	5.37	60.7
6962	2010	7	1.5		7.14	5.56	85.7
1531	1999	7.6	12.9		7.19	5.5	56.1
6927	2010	7	7.1		7.37	5.29	116.5
1148	1999	7.5	13.5		7.79	5.5	40.3
6897	2010	7	8.5		7.83	6.49	65.9
1515	1999	7.6	5.2		8.1	6.14	56.2
1530	1999	7.6	6.1		8.69	7.22	67.1
8161	2010	7.2	11.3		8.72	6.59	72.6
1550	1999	7.6	8.3		8.88	7.57	61.5
6975	2010	7	6.1		8.93	6.47	74.1
1496	1999	7.6	10.5		8.94	7.56	45.3
1548	1999	7.6	13.1		9.02	7.98	60.7
6960	2010	7	13.6		9.39	7.2	63.8
1529	1999	7.6	1.5		9.63	2.45	104.8
6911	2010	7	7.3		9.92	2.18	106.1
8164	1999	7.1	2.6	(6) 11.1	10.05	0.4	39.2
1489	1999	7.6	3.8		10.22	8.76	56.5
1528	1999	7.6	2.1		10.32	8.26	76.7
1491	1999	7.6	7.6		10.38	6.77	52.8
1519	1999	7.6	7		10.4	8.73	45.5
1492	1999	7.6	0.7		11.96	9.22	209.1
1505	1999	7.6	0.3		12.29	8.53	342.1
1493	1999	7.6	6		13.12	9.59	37.1

3.3 DECOMPOSITION OF A PULSE-LIKE GROUND MOTION USING EMD

3.3.1 Empirical mode decomposition method (EMD)

Generally, an original signal contains multiple sets of finite signals, that are simple and different in character from one to another. The EMD is an approach to decompose original data into several fundamental oscillations, called intrinsic mode functions (IMFs). These functions form a complete and nearly orthogonal basis functions. Each IMFs represent different simple oscillations as an equivalent of a basic harmonic function in the Fourier series, except that IMFs can have adjustable amplitude and frequency as a function of time, in contrast to harmonic functions built from constant amplitude and frequency. All IMFs have different frequency components and can be useful for earthquake analysis. To make sure that each IMF has a localized frequency content by avoiding the distribution of frequency due to asymmetric waveforms, IMFs should have two important properties: first, in the entire set of data both the numbers of zero crossing point and extreme point should be equal or/and different at most by one; second, at every single point the average value of the local minima and maxima (the envelope) must be equal zero (Huang *et al.*, 1998). The EMD approach uses upper and lower envelopes that are defined by designating local minima and maxima of the data sequence. Consequently, all local maxima and minima have been linked by using cubic spline data interpolation. The upper and lower envelopes should contain all the data between them.

The average of envelopes is defined as m_1, and the variation between the original data [$X(t)$] and m_1 is the first component h_1 (see Eq 3.14). The construction of h_1 through achieving all the requirements of the IMF that is described above is called the Sifting process. If h_1 does not meet all the criteria of the IMFs, the sifting procedure must be repeated k times to reach all IMFs' criteria. The next sifting process product, h_{1k} , is treated as the new original data. Last h_{1k} represent the first IMF (IMF_1), as well as indicates c_1. In order to guarantee that the IMF contents maintain an adequate physical modulation of amplitude and frequency, a criterion for stopping the sifting operation need to be provided (Huang et al., 1998). This can be achieved by minimizing the values of the standard deviation, SD, calculated from the two successive sifting outcomes.

$$\boldsymbol{X(t) - m_1 = h_1} \tag{3.14}$$

$$\boldsymbol{h_{1(k-1)} - m_{1k} = h_{1k}} \tag{3.15}$$

$$\boldsymbol{SD = \sum_{t=0}^{T} \left[\frac{\left| (h_{1(k-1)}(t) - h_{1(k)}(t)) \right|^2}{h^2{}_{1(k-1)}(t)} \right]} \tag{3.16}$$

The value for SD can be placed around 0.25 for the sifting procedure which is a very delicate limitation for the difference between siftings. As a whole, IMF_1 (c_1) should contain the highest frequency component of the signal. $c_1$can be parted from the original signal by

$$\boldsymbol{X(t) - c_1 = r_1} \tag{3.17}$$

While r_1 is a residue containing information for larger periods contents and it is considered as new data and exposed to the exact sifting process as mentioned above. This technique can be repeated for each consecutive r_j, while j is the number of IMFs.

$$\boldsymbol{r_1 - c_1 = r_2}$$

$$\boldsymbol{for\ j\ times} \tag{3.18}$$

$$\boldsymbol{r_{j-1} - c_{j-1} = r_j}$$

Eventually, the sifting process can be ended by by any of the specified conditions listed below: either when the c_j portion or the r_j residue becomes so small that it is less than the predetermined value of substantial consequence, or when the r_j residue becomes a monotonous function from which no further IMFs can be removed. So, the data ($X(t)$) have been decomposed into *n*-numbers of finite signals (empirical modes or IMF), and the residual r_n , which may be either a mean or a constant pattern (Eq 3.18). Fig. 3.4 shows EMD decomposition of signal for Iran, Tabas 1978 event.

Since the EMD method has attracted increasing attention due to its widespread applications, EMD built-in functions become available in programming languages such as Matlab (Matlab 2021) and Python.

$$\boldsymbol{X(t)} = \sum_{\boldsymbol{j=1}}^{\boldsymbol{n}} \boldsymbol{c_j} + \boldsymbol{r_n} \tag{3.19}$$

As seen in Fig. 3.4, these IMFs are arranged from high to low frequency, in addition, each IMFs contain a different special amplitude. Furthermore, one mode of IMF may contain oscillations with very different scales (frequency and amplitude), or oscillations with similar scales in different modes. However, choosing similar scales for each mode is unacceptable and this generates a problem called "mode mixing".

To mitigate mode mixing, Wu and Huang, 2009 propose a new approch called the Ensemble EMD (EEMD) to solve the scale separation issue without adding a subjective intermittent test. The application of the EEMD is achieved by adding white Guasian noise that will fill the entire time-frequency space evenly with components of various scales. Since a main signal is applied to this uniformly distributed white Guasian noise, the signal bits of varying scales are immediately mapped onto the relevant reference scales determined by the white noise. Besides, each single trial can generate very noisy effects, since each of the noise-added decompositions consists of the signal and the white noise added. Because the noise in each iteration differs in each step, the mean of sufficient trails is canceled in the ensemble. Eq 3.20 represents the different white noise W(t) to be added to the original signal, the added Gaussian white noise having a specific amplitude of noise standard deviation (NSD) of the original data. Fig. 2.5 shows the decomposition of ground motion signal by using the EEMD method which proficiently solves the mode mixing problem and for one mode of IMF, it contains uniform oscillations with a constant scale of frequency.

$$\boldsymbol{S_i(t)} = \boldsymbol{X(t)} + \boldsymbol{W(t)} \tag{3.20}$$

$$c_J = \sum_{z=1}^{N} c_{J,z}/N \tag{3.21}$$

The procedure to extract IMFs by using EEMD is described below:

1) Combine a white noise ratio to the original records, Eq 3.20. The noise ratio in this study is taken as 0.2.
2) Utilizing EEMD, sift the original signal with white noise into IMFs..
3) Repeat steps 1 and 2 continuously (for an N-th time), but with a new white noise ratio each time.
4) Obtain the corresponding IMF components of the decompositions and as the final result assume the average of ensemble corresponding to the IMFs of the decompositions.

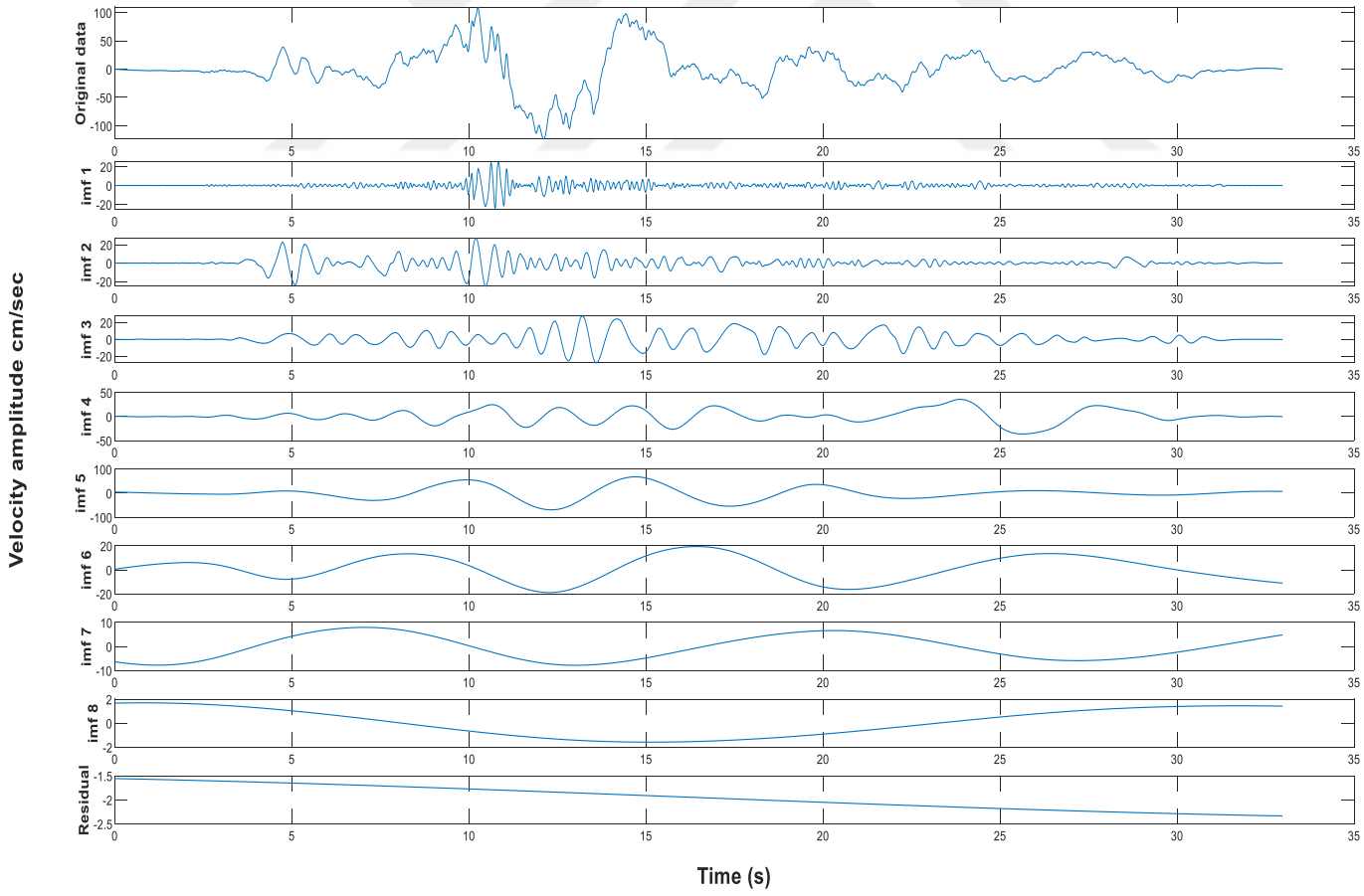

Figure 3.4 Decomposition into IMFs for the 1978 Iran, Tabas station, ground motion by using EMD.

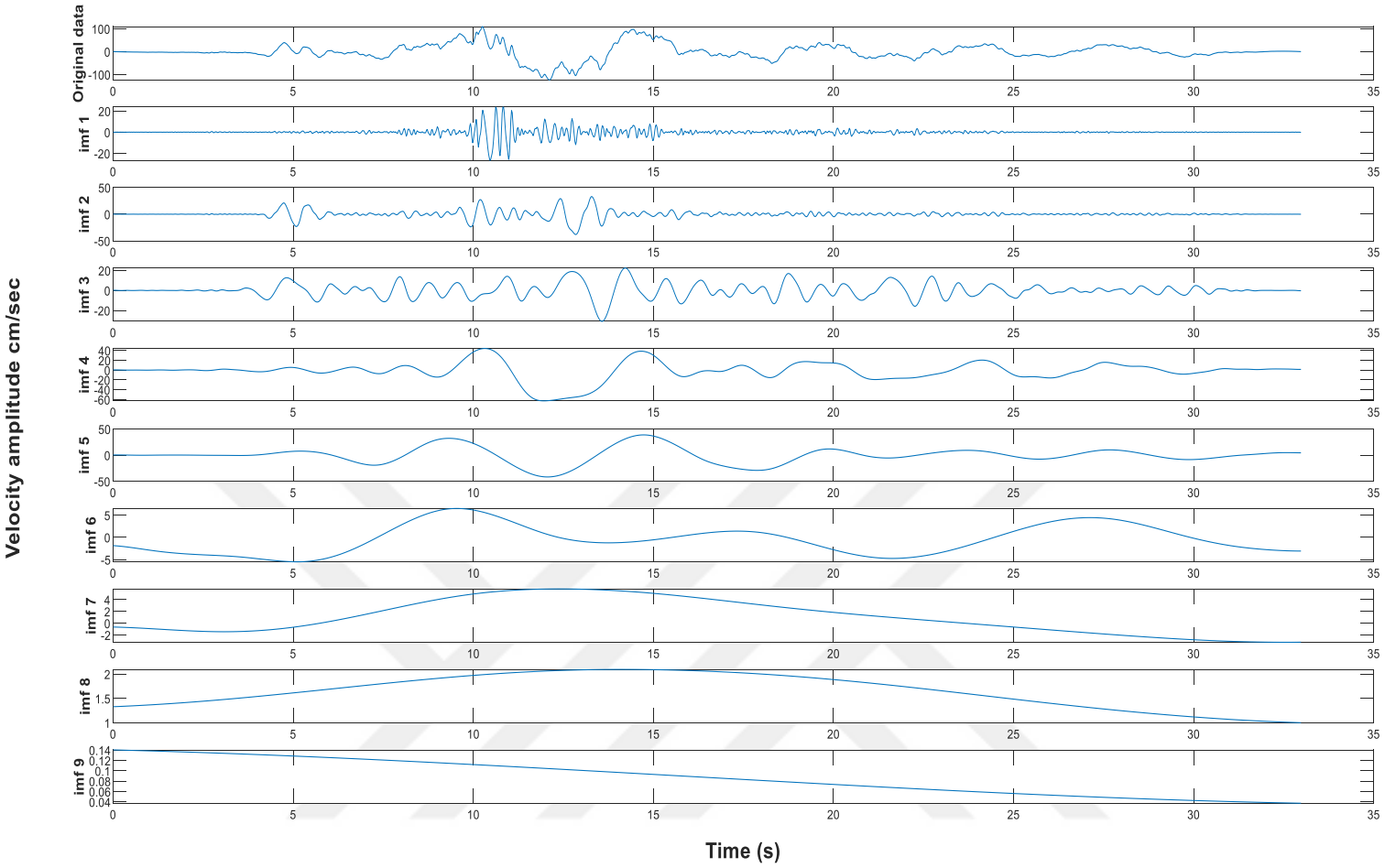

Figure 3.5 Decomposition into IMFs for the 1978 Iran, Tabas station, ground motion by using EEMD.

3.3.2 Pulse Extraction Using EEMD and Relative Energy

The inherent pulses could be found in low-frequency components that cause great changes in the energy of original records (Loh et al., 2001). To determine whether the pulses exist or not, it is necessary to identify whether a significant energy change is caused by a low-frequency IMF. A high PGV/PGA ratio in the velocity time history indicates a broad acceleration-sensitive region in the elastic spactra. Malhotra, (1999b) classified ground motion records as low-frequency ones when this ratio is more than 0.12.

In addition, (Chen et al., 2019b) calculated the PGV/PGA ratio for each IMF in the original signal, and the IMF's having a PGV ratio of more than 0.12 classified as a low-frequency component. The other important parameter is the maximum energy transition of every IMFs since it indicates the contribution of each IMF to the original GM record (Loh et al., 2001). The total energy of GM can be described as the cumulative squared root of velocity and shown in Eq. 3.22, where $\boldsymbol{v}$ is the velocity of the ground motion.

$$\boldsymbol{E} = \int_{\boldsymbol{0}}^{\boldsymbol{t}} \boldsymbol{v^2(t)dt} \tag{3.22}$$

Relative energy (RE) which shows the process of energy growth for each IMF is described as

$$\boldsymbol{RE_N} = \frac{\boldsymbol{E_N}}{\boldsymbol{E}} \tag{3.23}$$

Where $\boldsymbol{E_N}$ is the cumulative energy starting from high-frequency component to low-frequency component,

$$\boldsymbol{E_N} = \int_{\boldsymbol{0}}^{\boldsymbol{t}} \boldsymbol{IMF_1 + IMF_2 \ldots\ldots IMF_N\,(t)\,dt} \tag{3.24}$$

Here $\boldsymbol{N}$ denotes the nth number of IMF. The cumulative energy $\boldsymbol{E_N}$ will be equal to the total energy of the original GM in the last Nth number of IMFs, which means total energy is conserved.

To determine the IMFs that make a major contribution to the original records, the energy change of the IMFs, $\Delta\boldsymbol{E_N}$, can be calculated as

$$\Delta \boldsymbol{E_N} = \boldsymbol{Max(RE_N)} - \boldsymbol{Max(\ RE_{N-1})} \quad (3.25)$$

Sudden change in energy may be found in one or more low-frequency component of IMFs, which mean the original record can comprise an inherent pulse.

The values of $\Delta \boldsymbol{E_N}$ that can be an indicator of the IMFs that produce the most fundamental change in energy**.** Chen et al. (2019a) studied the relation between Baker's pulse indicators and the maximum energy changes of IMFs. It was concluded that if the ground velocity record has an IMF for which the maximum energy change is greater than 0.32 and the PGV to PGA ratio is more than or equal 0.12, this record is very likely to carry a velocity pulse and can be categorized as a pulse-like GM (Beresik, 2016).

The maximum energy change in one IMF is an indicator of the chance that the record will carry a velocity pulse. Chen et al. (2019b) established a rule that the low-frequency IMFs for which the energy change is larger than 10% could be classified as contributing parts of the pulse, and among them if there is one IMF for which the energy change must be larger than 0.32, the record may be labeled as pulse-like GMs. In this study, this methodology will be used to find the IMFs that contribute to the pulse content and consequently, the pulse will be extracted from the NFGMs by summing up these components.

Fig. 3.6 shows the cumulative energy change for each IMF from the Iran earthquake, Tabas station velocity record after decomposed into 9 IMFs by using EEMD method. As it could be easily notice that the 5th IMF contains the maximum value of energy change which is 0.55, that means 55% of the total energy is produced by IMF 5 only. In addition, the 5th IMF is considered as a low-frequency component due to the value of the PGV/PGA ratio being more than 0.12. Based on the combination of maximum energy change is more than 0.32 and PGV ratio value of the 5th IMF greater than 0.12, the 1978 Tabas earthquake can be classified as a pulse-like GM.

As noted before, one IMF may not be able to represent the entire pulse of NFGM. The maximum value of energy change in the 4th IMF from the 1978 Tabas–Iran earthquake is 0.34, which means 34% of the energy of the Tabas earthquake record is contained in IMF4, so it can be classified as a significant contributor to the pulse. As well, IMF4 is also considered a low-frequency component with a PGV/PGA ratio of 0.53. Thus this component satisfies both criteria to be selected as high-contributing IMF. After deciding IMF5 and IMF4 as the parts of the

pulse, the pulse can be extracted by superposing the IMF4 and IMF5. In Fig. 3.7 original ground motion and extracted pulse are compared.

In this research approach, different frequency contents will be considered to understand the effect of decomposition of NFGMs on the dynamic structural response. To this end, elastic and inelastic spectra of SDOF systems having numerous properties will be subjected to original GMs and their decomposed components. The velocity traces of NFGMs are decomposed into three components depending on the frequency content of IMFs: 1) pulse signal extracted by using HHT methods, 2) the superposition of extracted pulse and all IMFs that have lower frequencies than the IMFs included in the pulse (pulse+low-frequency component) and 3) the superposition of extracted pulse and all IMFs that have higher frequencies than the IMFs included in the pulse (pulse+high-frequency component). For example in Tabas-Iran earthquake, the pulse includes IMF4 and IMF5; low-frequency components include IMFs with smaller numbers than those in the pulse (IMF1,2,3) and high-frequency components include IMFs with larger numbers than those in the pulse (IMF6,7,8,9). Figure 3.8 displays these Pulse only, Pulse+Low-frequency components, and Pulse+High-frequency components for the Iran-Tabas earthquake.

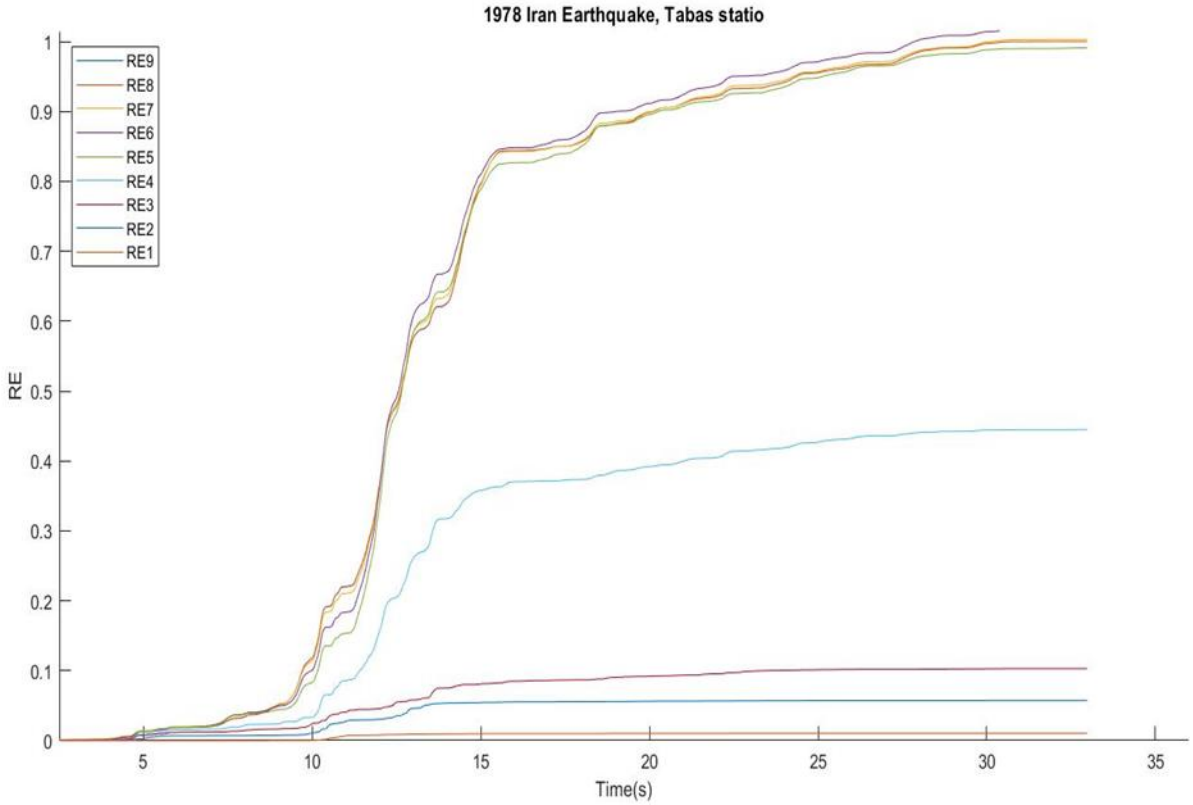

Figure 3.6 Cumulative relative energy curves for each IMFs for the 1978 Tabas–Iran earthquake

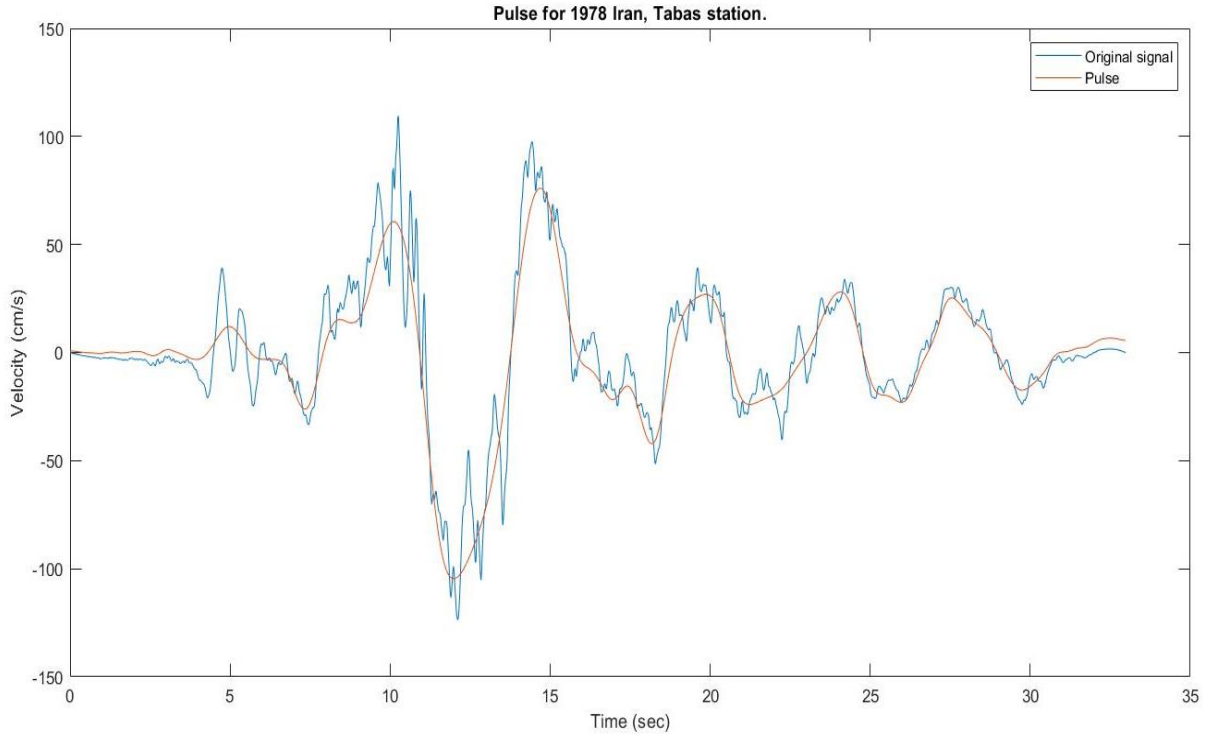

Figure 3.7 Original ground motion and extracted pulse for the 1978 Tabas–Iran earthquake

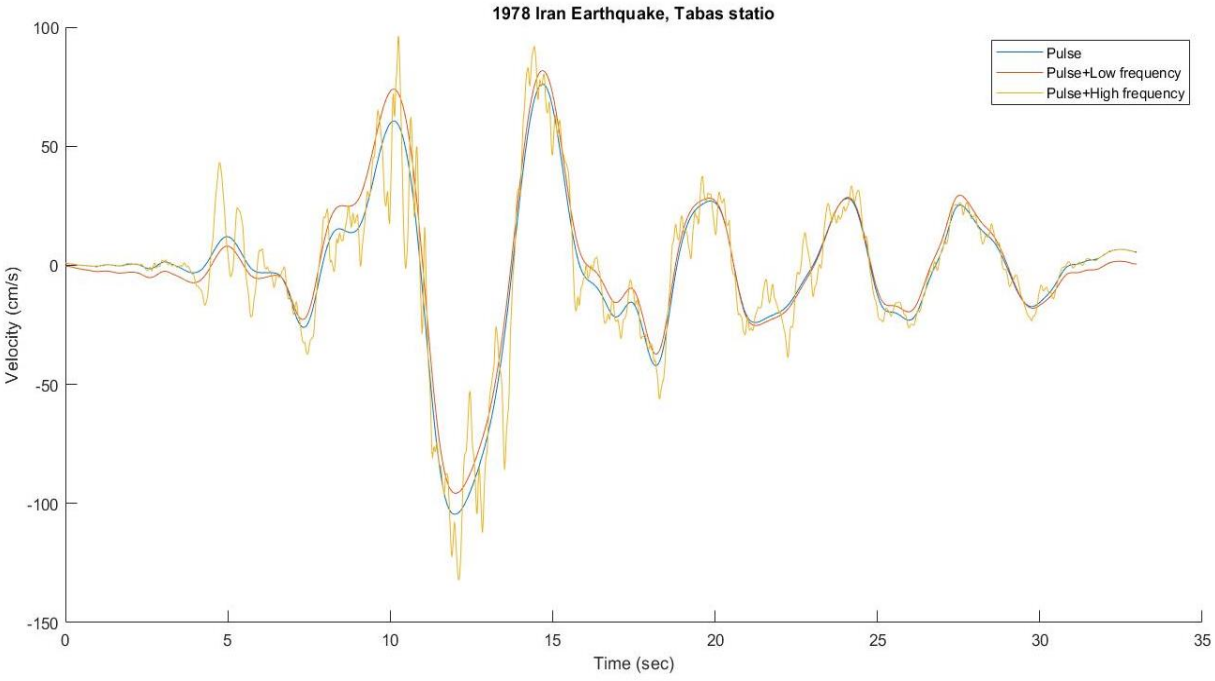

Figure 3.8 Extracted three component signals from original records for 1978 Tabas–Iran earthquake.

3.4 ANALYTICAL PULSE MODELS

In this section, some mathematical velocity pulse functions will be compared with the pulses obtained by HHT method for their appropriateness to represent NFGMs with directivity effect. For this purpose, three different pulse models (He and Agrawal, 2008; Mavroeidis and Papageorgiou, 2003; Menun and Fu, 2002) are used to observe the behavior of the SDOF systems under four NFGMs with several pulse periods calculated by Wavelet analysis (between 1 s and 13 s) chosen from groups 2–6 (Parkfield-02, CA 2004; Denali, Alaska,2002; Tabas, Iran 1978; Chi-Chi, Taiwan, 1999). In these pulse models, the important properties that define velocity pulses are the pulse period, pulse amplitude, the number of half-cycles, and the phase. The dynamic responses of linear and nonlinear SDOF systems subjected to these pulse models will be compared with the response from the pulses obtained from HHT analysis.

3.4.1 Mavroeidis & Papageorgiou

Mavroeidis and Papageorgiou (2003) new proposed a new an analytical pulse model for GM which depends on the Gabor wavelet (Gabor, 1946). This model is basically an amplitude modulated sinusoid. Due to difficulties inderivation produced by the exponential function employed in the analytical formulation of the Gabor wavelet, the Gaussian envelope was replaced with another symmetric bell-shaped function with a simpler mathematical term.(i.e., an elevated cosine function is used to replace the Gaussian envelope). Eq 3.26 shows the main Gabor Wavelet function and Eq 3.27 shows derived velocity pulse model ($v(t)$) from Gabor Wavelet.

In this pulse model, the amplitude of the signal is represented by *A*; f_p represents the frequency; v represent the phase angle of the model; γ is the variable that defines the vibration characteristics (i.e. as γ increases so does the number of zero crossings); and t_0 determines the time of pulse start. It should be noted that although the pulse model may effectively capture displacement and velocity-time history in NFGMs, it can't describe all characteristics of acceleration time history records correctly.

$$\boldsymbol{f(t) = Ae^{-(\frac{2\pi f_p}{\gamma})^2 t^2}\cos(2\pi f_p t + v)} \tag{3.26}$$

$$v(t) = \begin{cases} A\frac{1}{2}[1 + COS(\frac{2\pi f_p}{\gamma}(t - t_0))]\cos[2\pi f_p(t - t_0) + v], & t_0 - \frac{\gamma}{2f_p} \le t \le t_0 + \frac{\gamma}{2f_p} \\ 0, & otherwise \end{cases} \quad (3.27)$$

3.4.2 Menun and Fu

Another mathematical model was proposed by Menun & Fu (2002) which is defined by five parameters. θ in Eq. 3.28 is the vector containing the pulse parameters: V_P characterize the amplitude velocity pulse; t_0 and T_p defines the starting time of the pulse and the period of pulse, respectively; n_1 and n_2 are shape specifications. The adequacy of this GM model will be evaluated by comparing the linear and nonlinear dynamic responses of the SDOF systems.

$$v(t;\theta) = \begin{cases} V_P\, exp\left[-n_1\left(\frac{3}{4}T_p - t + t_0\right)\right] sin\left[\frac{2\pi}{T_p}(t - t_0)\right], & t_0 < t \le t_0 + \frac{3}{4}T_p \\ V_P\, exp\left[-n_2\left(t - t_0 - \frac{3}{4}T_p\right)\right] sin\left[\frac{2\pi}{T_p}(t - t_0)\right], & t_0 + \frac{3}{4}T_p < t \le t_0 + 2\,T_p \\ 0, & otherwise \end{cases} \quad (3.28)$$

3.4.3 He & Agrawal

The last analytical pulse that is considered in this work have been developed by He and Agrawal (2008). This model is based on Belarge wavelet (Aldridge, 1990), which was originated to simulate wave propagation. This pulse model given in Eq 3.29 contains, similar to previous models, five main parameters that describe the quantity and quality of the pulse model: ω_p is the frequency of the pulse; T_p is the period of the pulse; C represents the amplitude factor; v and a are characterize phase angle and decay factor, respectively. Additionally, n describes the integer parameter controlling the skewness of the pulse envelope with respect to time; and t_0 is the starting time of the pulse.

$$v(t) = Ct^n e^{-at}\sin(\omega_p t + v), \quad t \ge t_0 \quad (3.29)$$

He and Agrawal (2008) reported that the consider pulse model can effectively replicate GM pulses both analytically and graphically and good correlations are observed between elastic response reaction spectra for the proposed model and original GM.

As it can be noticed from the definitions of the pulse models (Eqs. 3.26-3.29), many pulse parameters need to be defined for each considered NFGM. These parameters may be obtained by the nonlinear least square method, but this procedure may be quite difficult, besides it does not provide considerable advantages (Yalcin and Dicleli, 2020). Therefore in this study analytical pulse parameters are obtained by trial and error procedures to ensure a perfect visual fit. Table 2 shows the analytical pulse model parameters for chosen pulse-like GM records.

The velocity time histories of picked four NFGMs and the fitted analytical models with the properties given in Table 3.3 are compared in Fig. 3.9.

Table 3.3 Chosen earthquake records and parameters of selected pulse models.

Pulse Models	**GMs**	Parkfield-02	Denali, Alaska	Tabas, Iran	Chi-Chi, Taiwan
	RSN	4107	2114	143	1505
	Tp wavelet (s)	1.15	3.16	5.7	10
Mavroeidis & Papageorgiou	**A**	-75	132.2	92.2	345
	γ	56	16.5	166	54
	v	1.82	1.35	2.94	1.17
	f_p	1.08	0.462	0.204	0.098
	t_0	3.35	27.2	12	37
Menun & Fu	V_P	82	125	98	330
	T_p	0.95	2.3	5.26	10.4
	n_1	1.44	2.4	0.16	0.4
	n_2	2.4	0.54	0.14	0.23
	t_0	2.73	25.15	8.3	28.2
He & Agrawel	**C**	-5000	-1110	-4.05	-200
	n	2.88	1.56	3.87	2.65
	a	4.5	2.3	0.634	0.8

T_p	1	2.1	5.1	10.2
t_0	2.65	26.4	5.95	33.3
v	2.84	0	6.32	6.2

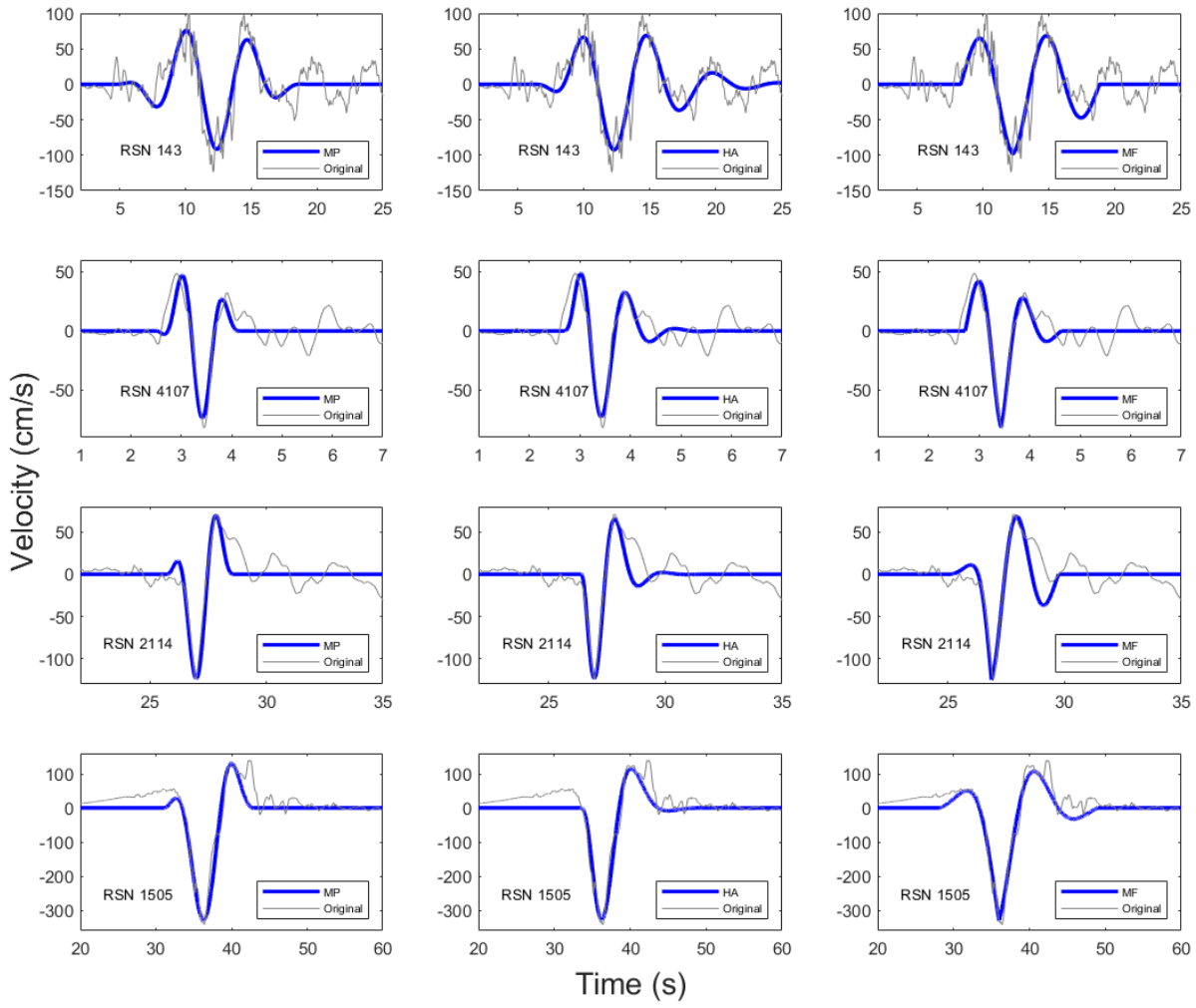

Figure 3.9 Comparison between the original velocity record and extracted pulse by using models of MP (Mavroeidis et al.,2003), HA (He et al., 2008) and MF (Menun et al., 2002) for the NFGMs with RSN 143, 4107, 2114 and 1505.

4 RESULTS

In the following sections spectral responses of SDOF systems to original GM, pulse extracted using the EEMD method, pulse + high-frequency content, and pulse + low-frequency content will be compared. It should be re-emphasized here that the GMs under consideration in this work are pulse-like NFGMs with the directivity effect. High frequency and low-frequency contents contain the IMFs filtered out from the pulse having higher frequencies and lower frequencies, respectively. Considering superpositions of high and low-frequency contents with the pulse will provide us insights into the structural response to these contents. In the comparisons, mean linear elastic and nonlinear spectra (Constant Ductility and Constant Strength spectra) will be used. Furthermore, seismic isolated structures and analytical pulse model comparisons will also be discussed. Mean spectra are calculated for each group of NFGMs, which are gathered according to their pulse periods (Tp) (see Table 3.2).

4.1 ELASTIC RESPONSE SPECTRA

The maximum elastic response of SDOF systems to original and decomposed GMs is depicted in Fig. 4.1(a) as mean spectral accelerations for different Tp groups of GMs.

The figure shows the mean spectral accelerations for groups (Gr) 1, 2, 3, 4, 5 and 6 for the original GM and for the decomposed signals from the HHT method, which are extracted pulse, pulse plus high-frequency component of IMF signals (HF+Pulse) and pulse plus low-frequency component of IMF signals (LF+Pulse). The percent differences between the original and decomposed signals for all groups are shown in Fig. 4.1(b).

The average velocity mean pulse period for groups 1 to 6 are 0.73 s, 1.4 s, 2.87 s, 4.8 s, 7.9 s, and 11.1 s, respectively. As observed from Fig. 4.1(a), the mean peak ground acceleration for original signals in groups 1 to 6 are 1.5, 1.2, 1,05, 0.8, 0.6 and 0.5*g*, respectively. The mean amplitude of elastic acceleration response drops in short period areas and increases in low-frequency regions when the mean velocity pulse periods of NFGMs' groups increases. This is anticipated because when Tp of NFGMs increases, structures having a short period stay away from the resonant response. However long period structure response comes close to resonance response because structure periods become closer to the Tp of NFGMs. When the Tp of NFGM

coincides with the natural period of a building, it will undergo very large oscillations due to resonance and suffer the greatest damage.

Fig. 4.1(a) also displays the effect of decomposed ground motions on elastic mean acceleration response spectra. The responses of the original signal and HF+pulse content are very close to each other, and in a parallel manner, pulse and LF+pulse responses are also very close. The process of removing low-frequency content from the NFGM has little effect on the spectra in the short period range, however, removal of high-frequency component has a significant impact in the short period range. The responses of extracted pulses differ from the original records as high as 75%, which is more profound for the shorter period range. Meanwhile, as the mean pulse period increases (group number increases) this difference also propagates to longer period region.

Fig. 4.1(b) shows the mean percent difference (reduction) in elastic acceleration spectra between the original signal and pulse, LF+pulse, HF+pulse as a function of Tp of each group. This figure is very suitable to observe precisely the differences between spectra of decomposed signals and the original signal.

As can be seen in the figure, the maximum differences up to 75% occur in the short period region for the pulse and LF+pulse signals. As Tp increases, this maximum value also increases and the differences propagate to higher period regions. Although for the short period range of the spectra the curves for the pulse and LF+pulse signal are very close, for the long period region, pulse and HF+pulse signals become similar. Additionally, in the short period region, the percent difference of HF+pulse signal is very low; conversely, in the long period region, the percent difference of LF+pulse decays as the period increases. It should also be noted that, the crossing point of LF+pulse and HF+pulse curves increases as the mean velocity pulse period increases.

Fig. 4.1(b) also demonstrates that removing high-frequency content from the original GM for structures having a short period may have significant effect on the response of the structure. This effect increases with the pulse period of the GM. Similarly, filtering the low-frequency content from the GM may affect the response by up to 30%, especially for GMs with lower Tp.

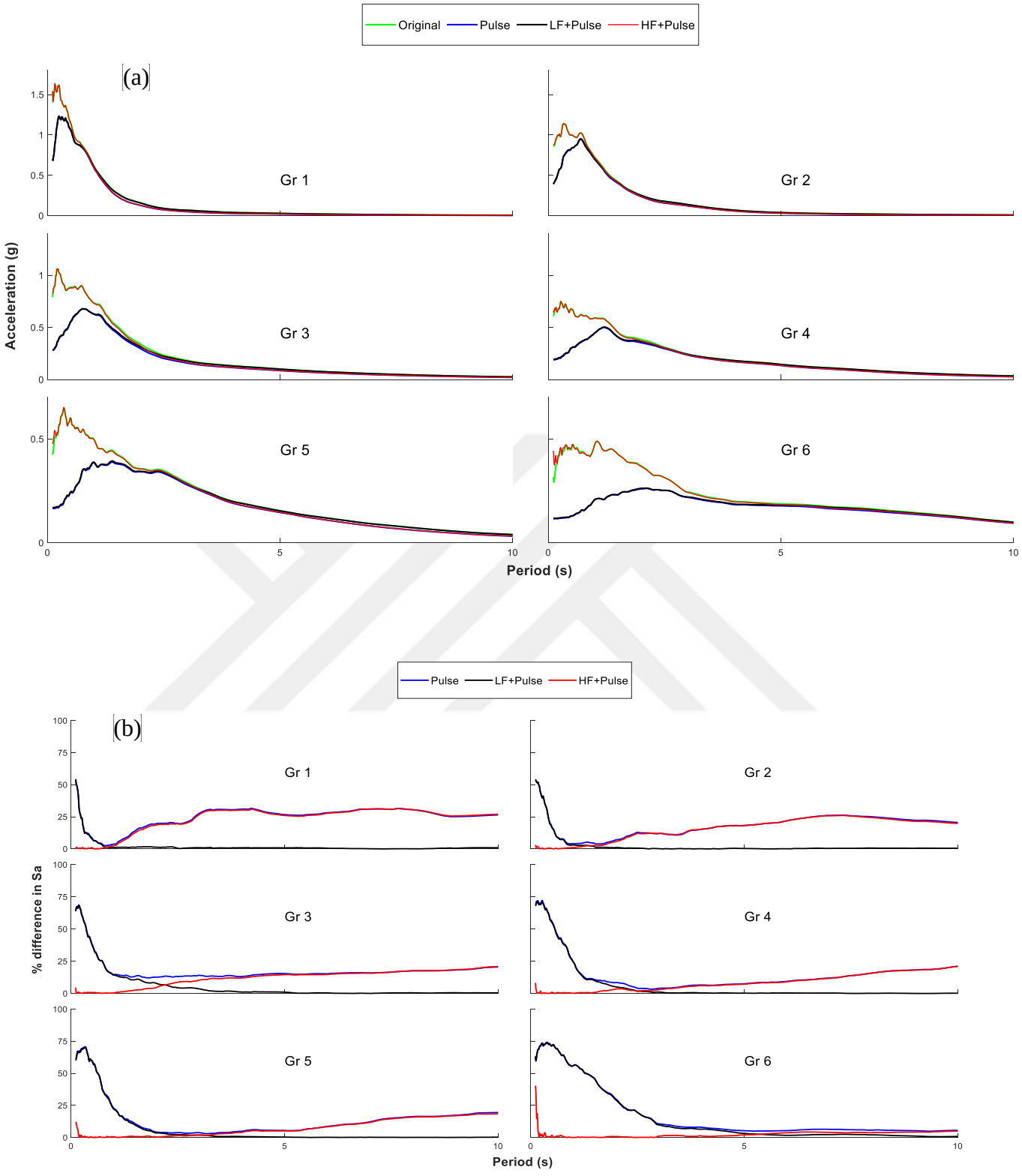

Figure 4.1. (a)Mean acceleration elastic response spectra for Groups 1 to 6, and (b)Percent differences between original signal and decomposed signals

4.2 CONSTANT DUCTILITY RESPONSE SPECTRA

Understanding the effects of yielding on the behavior of inelastic structures during a strong earthquake is crucial in earthquake engineering. Therefore it is important to examine inelastic response spectra for specified values of the ductility factor (Chopra, 2000). Ductility (μ) of a nonlinear SDOF system is defined as the ratio of absolute maximum nonlinear displacement (u_{max}) to yield displacement (u_y) of the system (see Fig. 3.2) under a ground motion. Constant Ductility Response Spectra (CDS) is the plot of maximum response quantities against the elastic period of the structure for a target ductility factor. To achieve the required constant ductility for each period an interpolative procedure between the strength and ductility must be utilized.

In this study, CDS are given for displacement responses (Sd) which is essentially the maximum displacement (u_m). The following equation may be used to calculate the yield displacement (u_y) for the inelastic system, where μ is the ductility ratio for the SDOF system.

$$u_y = \frac{u_m}{\mu}$$

Fig. 4.3(a), demonstrates mean CDS for original ground motion and decomposed signals by using the EEMD (Pulse, LF+Pulse, and HF+Pulse), for the case the system is elastic-perfectly plastic (k_r=0). The CDS are plotted for various ductility ratios such as μ=1 (elastic case),2, 4, 6, and 8. In these spectra, mean values of the displacements for each group (Gr1 to 6) are plotted. It should be reminded that as the group number increases the mean velocity pulse period and of these NFGMs also increases.

To precisely observe the changes in the CDS between the mean original signals and the decomposed signals, the percent differences are shown in Fig.4.4(b). It can be seen that displacement demand rises as the pulse periods of ground motions increase for all ductility ratios, as expected.

Removing high-frequency content from the ground motion (LF+pulse) has a great impact on the spectra in the short period region. This influence increases as To of GM (equivalent to Group number) increases. For instance, for Gr1 (mean Tp=0.71s) the reduction of spectral value is about 20%, however, for Gr6 (mean Tp=11.1s) this reduction is about 50%, and the affected period range extends from (0 - 0.5s) to (0 – 2 s). These findings are consistent with the

work of Yalcin and Dicleli (2020). On the contrary, removing low-frequency content has an insignificant effect for the short period region and a great effect on long period regions, which may lead up to a 40% reduction. However, the effects of removing low-frequency content decrease as Tp of GM increases. The effect of the ductility ratio is negligible for GMs with a small Tp and somewhat significant for those with a large pulse period.

Thus, we can conclude that for flexible structures removing high-frequency content from the GM has negligible effects on the spectra but removing high-frequency content has significant effects; on the other hand for structures having short periods, high-frequency content has considerable effects and low-frequency content has negligible effects. Furthermore, removing both high-frequency and low-frequency components from the original ground motion to extract a pulse, may cause significant reductions in spectral displacements for the entire period range of the spectra. This reduction is more pronounced, particularly for NFGMs with small Tp.

For a more comprehensive analysis, the effect of decomposition of NFGMs using the EEMD method on the inelastic response spectra of SDOF systems having several bilinear force-deformation behaviors was also studied. Fig.4.4(a) shows the mean CDS for structures with various post-elastic stiffness ratios (k_r=0.02, 0.05, 0.1 and 0.2) and the same ductility ratio of 4 (μ=4). For the same systems, Fig. 4.4 (b) shows the percent differences between the original ground motion and decomposed ones. The effect of removing high-frequency content on CDS may slightly decrease as the post elastic stiffness ratio increases for Gr1 and Gr2. Other than that, the effects of the post elastic stiffness ratio look negligible.

For many reasons, earthquake engineers want to extract the velocity pulses from NFGMs with forward directivity and apply these pulses instead of the original GM. But as it can be seen from Figs 4.3 and 4.4, removing both the high-frequency content and low-frequency content using the decomposition by EEMD method, to obtain the pulse, may considerably affect the inelastic behavior of structures and reduce the spectral displacements.

(a)

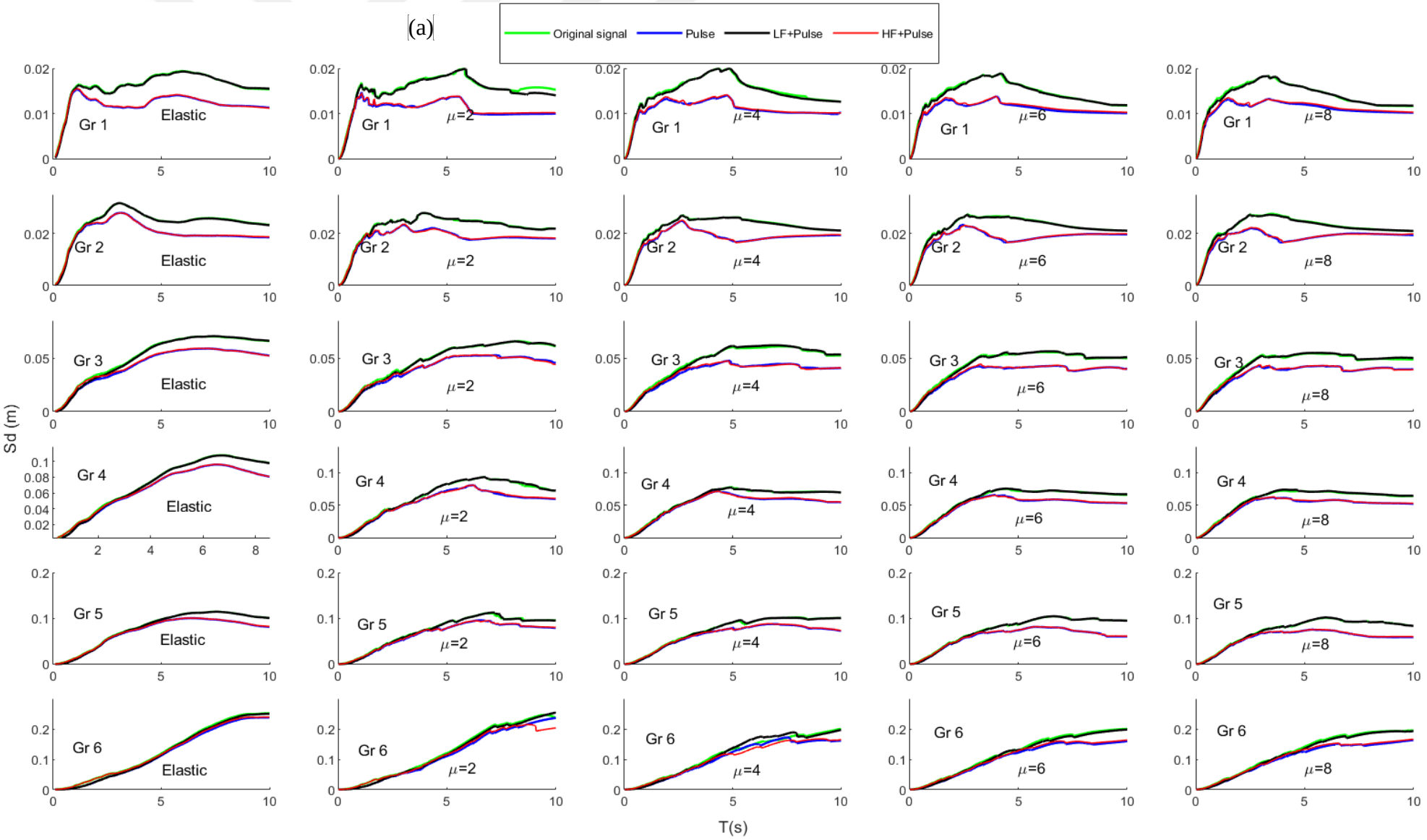
Original signal
Pulse
LF+Pulse
HF+Pulse
Gr 1
Gr 2
Gr 3
Gr 4
Gr 5
Gr 6
Elastic
μ=2
μ=4
μ=6
μ=8
Sd (m)
T(s)

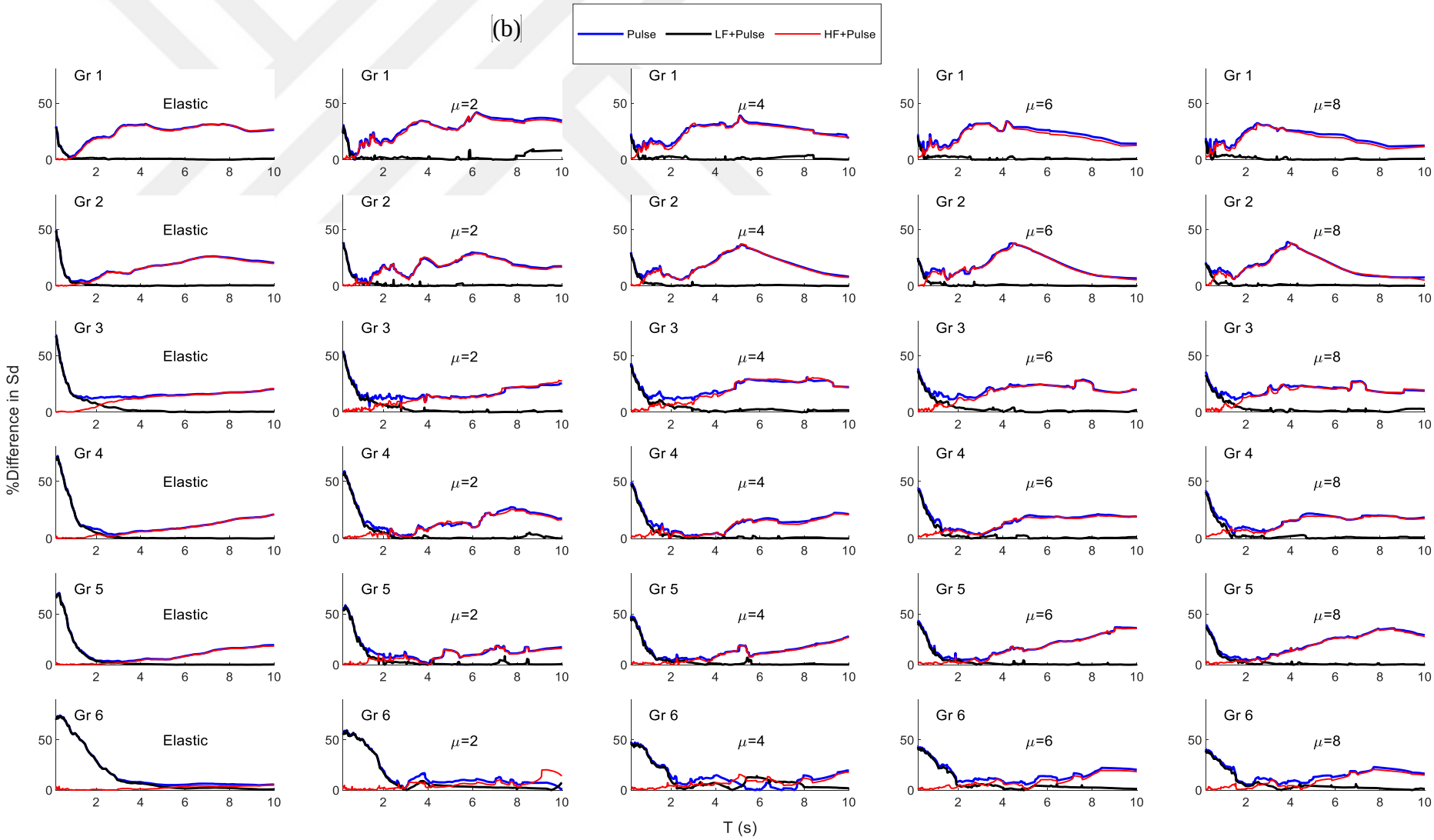

Figure 4.2 a) Mean displacement demand CDS for k_r=0 and for various dutility ratios (1 (elastic), 2, 4, 6, and 8)

b) Percent differences between original signal and decomposed signals

(a)

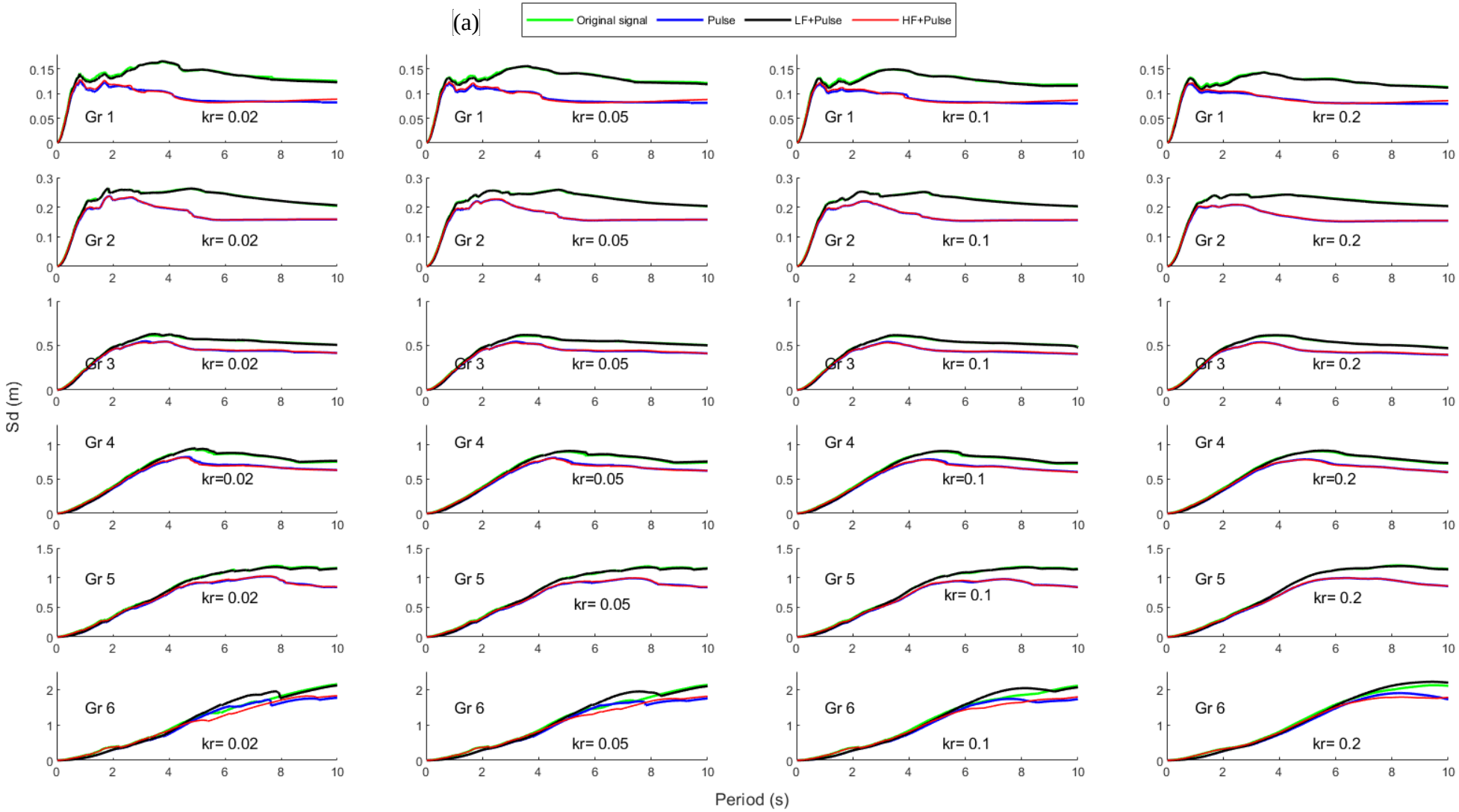
Original signal
Pulse
LF+Pulse
HF+Pulse
Gr 1
kr= 0.02
Gr 1
kr= 0.05
Gr 1
kr= 0.1
Gr 1
kr= 0.2
Gr 2
kr= 0.02
Gr 2
kr= 0.05
Gr 2
kr= 0.1
Gr 2
kr= 0.2
Gr 3
kr= 0.02
Gr 3
kr= 0.05
Gr 3
kr= 0.1
Gr 3
kr= 0.2
Gr 4
kr=0.02
Gr 4
kr=0.05
Gr 4
kr=0.1
Gr 4
kr=0.2
Gr 5
kr= 0.02
Gr 5
kr= 0.05
Gr 5
kr= 0.1
Gr 5
kr= 0.2
Gr 6
kr= 0.02
Gr 6
kr= 0.05
Gr 6
kr= 0.1
Gr 6
kr= 0.2
Sd (m)
Period (s)

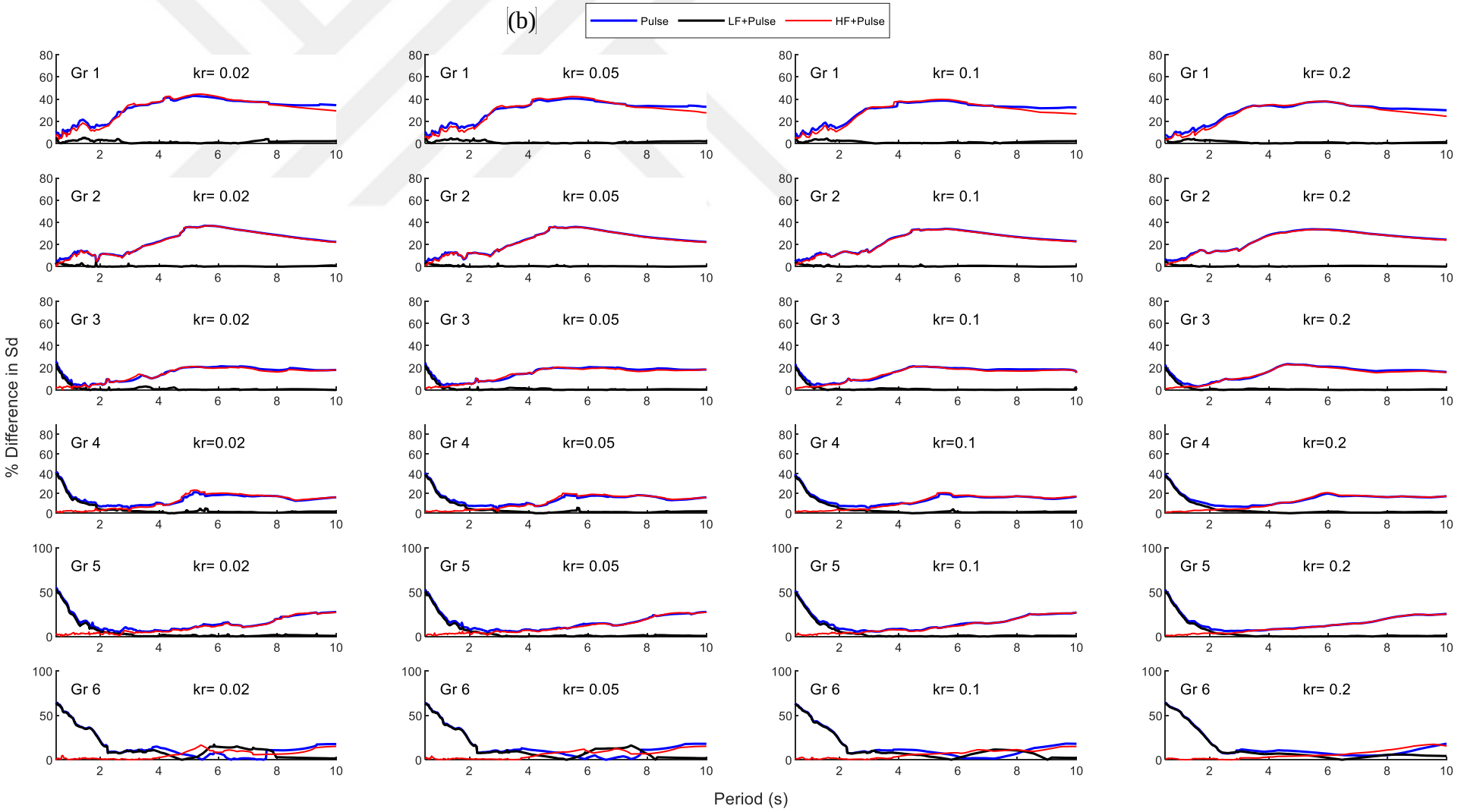

Figure 4.3 a) Mean displacement demand CDS for various post-elastic stiffnesses (k_r=0.02, 0.05, 0.1, 0.2) and for dutility ratio μ=4,

b) Percent differences between original signal and decomposed signals

4.3 CONSTANT STRENGTH RESPONSE SPECTRA

Constant Strength Response Spectra (CSS) is the plot of peak response quantities against the elastic period of the structure having a particular strength. Since there is no target ductility, during obtaining CSS, an interpolative procedure is not required. In this study, CSS is given for displacement responses (Sd) which is simply the maximum displacement (u_m).

Fig. 4.5(a) shows the CSS curves for original ground motion records and decomposed signals by using the EEMD method (Pulse, LF+Pulse, and HF+Pulse), where the SDOF systems are elastic-perfectly plastic (k_r=0) and have various yield strengths (F_y/w =0.02, 0.06, 0.08, 0.1; where W is the weight of the system). The spectral values are the mean of the maximum displacements within each group. It should be reminded that as the group number increases mean velocity pulse period within the group also increases. As it can be easily seen that there are noticeable differences between the spectral curves with and without high-frequency content, especially for groups 1 to 3.

The percent differences between the original ground motion and decomposed signals (Pulse, HF+Pulse and LF+Pulse) are shown in Fig.4.6(b). For GMs with smaller Tp (group 1 to 3) removing the high-frequency content does not significantly affect the CSS independent of the strength of the systems. Similar observations are also obtained by Yalcin and Dicleli 2020. However, for these groups removing low-frequency content significantly affect the CSS for structures with periods larger than 2 seconds and this reduction may be as high as 40%.

On the other hand, for GMs with larger pulse periods (group 4 to 6) removing the high-frequency content significantly affects the CSS for smaller periods of less than 2 seconds and this becomes more pronounced as the strength of the systems increases. For instance, for group 5 and Fy/W=0.1 case, this reduction is about 60%. Conversely, for these large pulse period groups (4 to 6) the effect of low-frequency content on CSS becomes insignificant as the Tp increases and the strength decreases.

As observed for CDS, extracting the pulse from the ground motion by removing high-frequency and low-frequency contents may reduce significantly the response values in CSS as well.

It should also be noted that the effect of decomposition NFGMs by using the EEMD approach on the displacement demand inelastic SDOF system with various bilinear force deformation

properties is almost negligible for post elastic stiffness ratio values k_r=0.02, 0.05, 0.1, and 0.2 in CSS as shown in Fig.4.6.

(a)

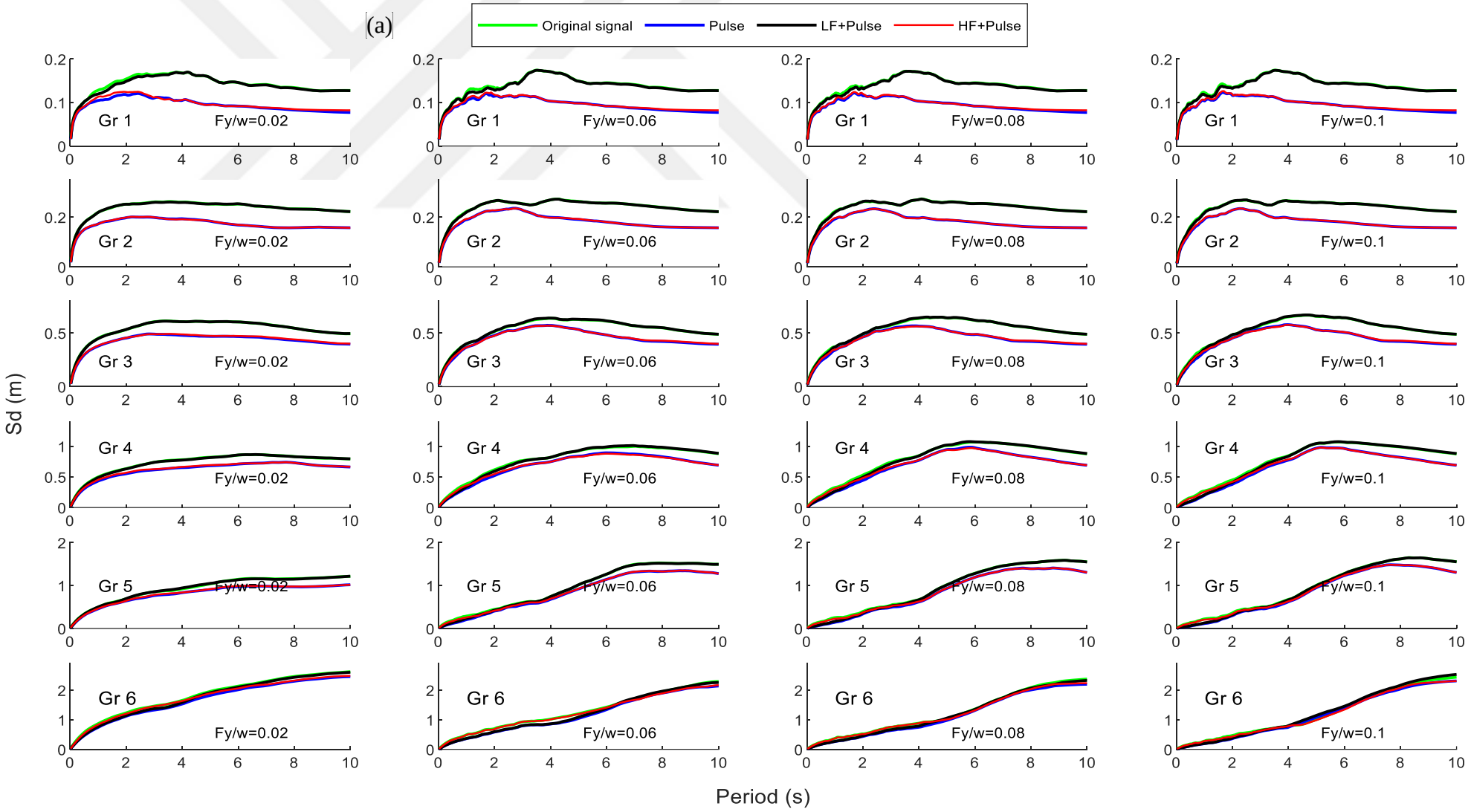
Original signal
Pulse
LF+Pulse
HF+Pulse
Gr 1 Fy/w=0.02
Gr 1 Fy/w=0.06
Gr 1 Fy/w=0.08
Gr 1 Fy/w=0.1
Gr 2 Fy/w=0.02
Gr 2 Fy/w=0.06
Gr 2 Fy/w=0.08
Gr 2 Fy/w=0.1
Gr 3 Fy/w=0.02
Gr 3 Fy/w=0.06
Gr 3 Fy/w=0.08
Gr 3 Fy/w=0.1
Gr 4 Fy/w=0.02
Gr 4 Fy/w=0.06
Gr 4 Fy/w=0.08
Gr 4 Fy/w=0.1
Gr 5 Fy/w=0.02
Gr 5 Fy/w=0.06
Gr 5 Fy/w=0.08
Gr 5 Fy/w=0.1
Gr 6 Fy/w=0.02
Gr 6 Fy/w=0.06
Gr 6 Fy/w=0.08
Gr 6 Fy/w=0.1
Sd (m)
Period (s)

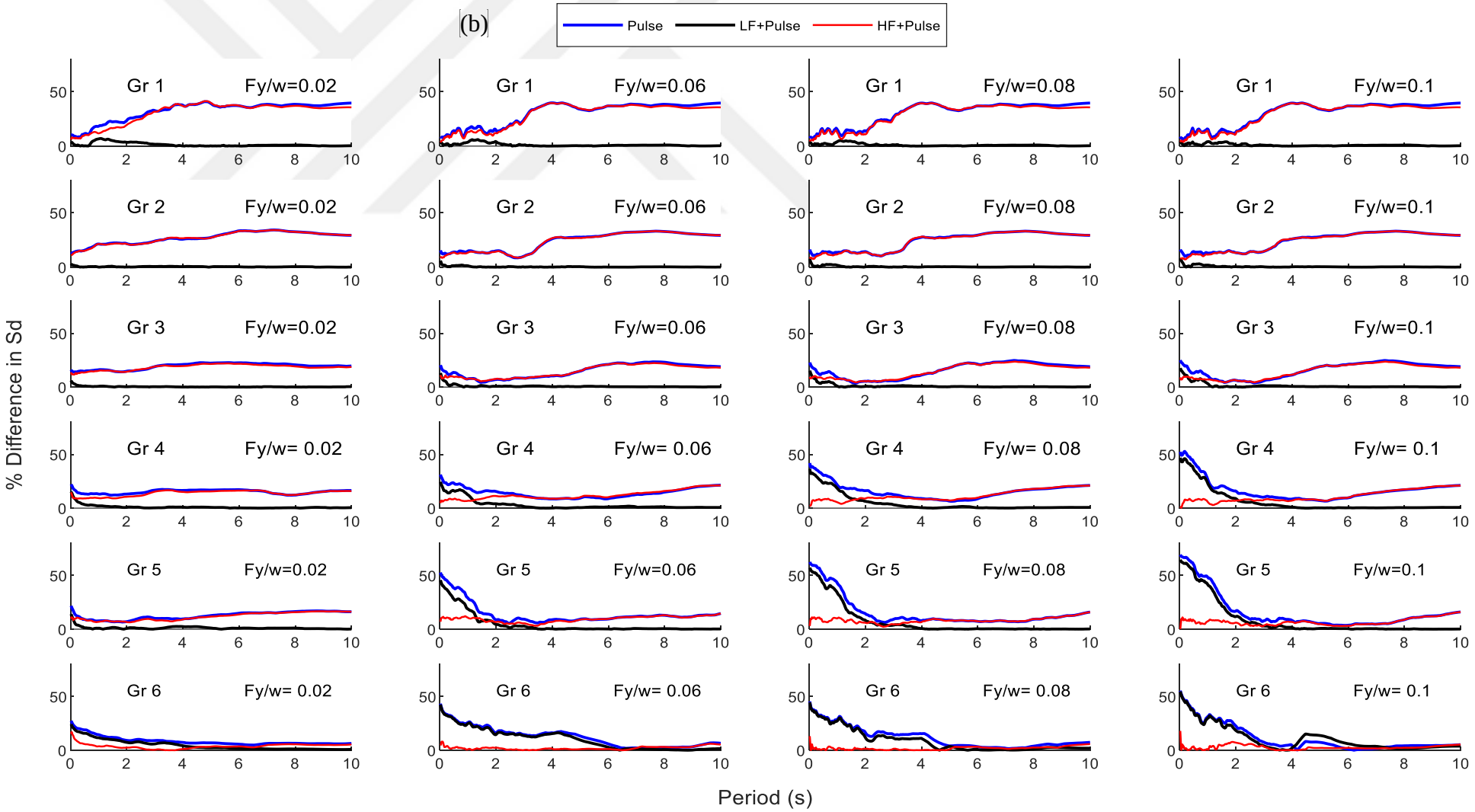

Figure 4.4 a) Mean displacement demand CSS for k_r=0 and for various yield strengths (Fy/w=0.02, 0.06, 0.08, and 0.1)

b) Percent differences between original signal and decomposet signals for mean CSS

(a)

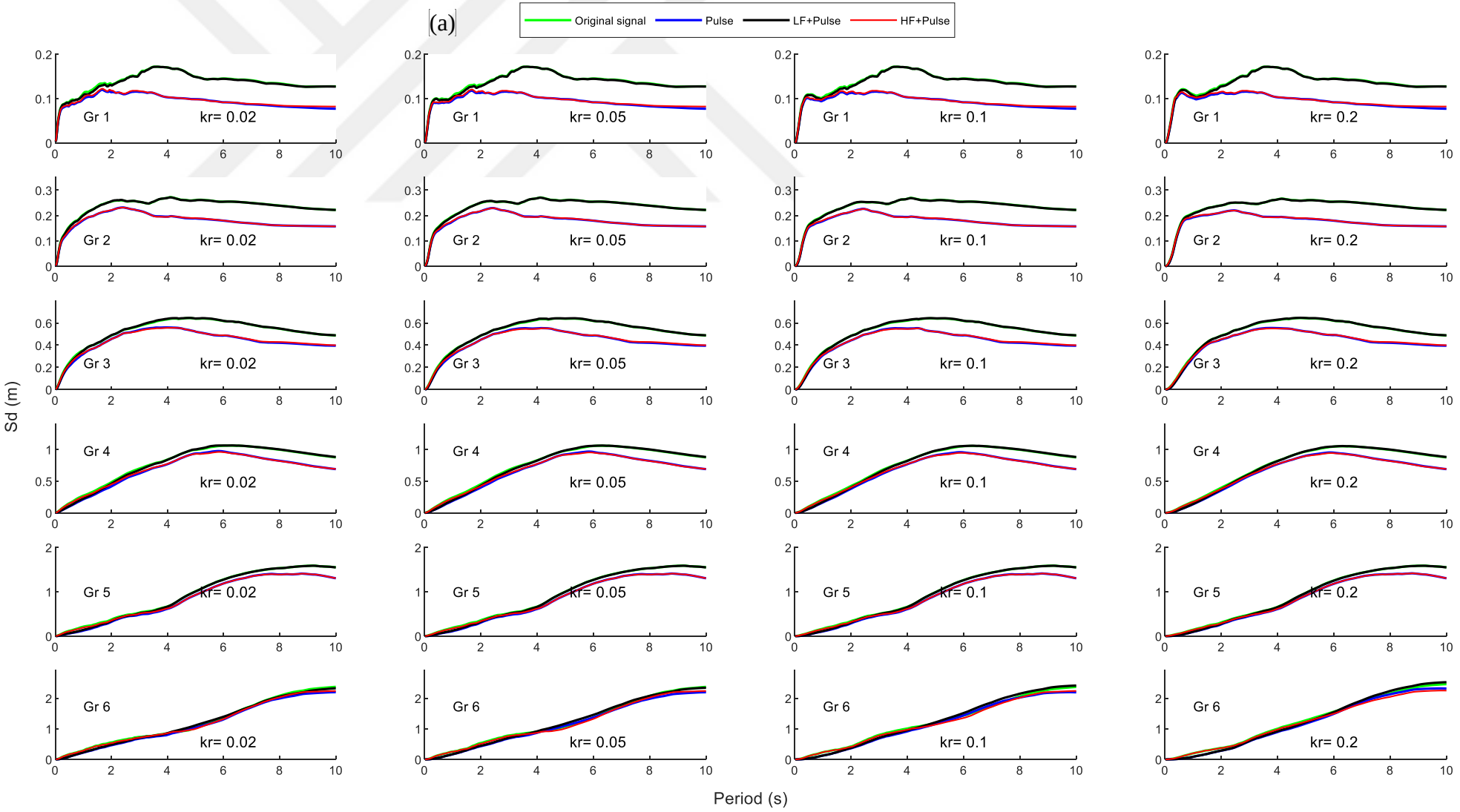
Original signal
Pulse
LF+Pulse
HF+Pulse
Gr 1
Gr 2
Gr 3
Gr 4
Gr 5
Gr 6
kr= 0.02
kr= 0.05
kr= 0.1
kr= 0.2
Sd (m)
Period (s)

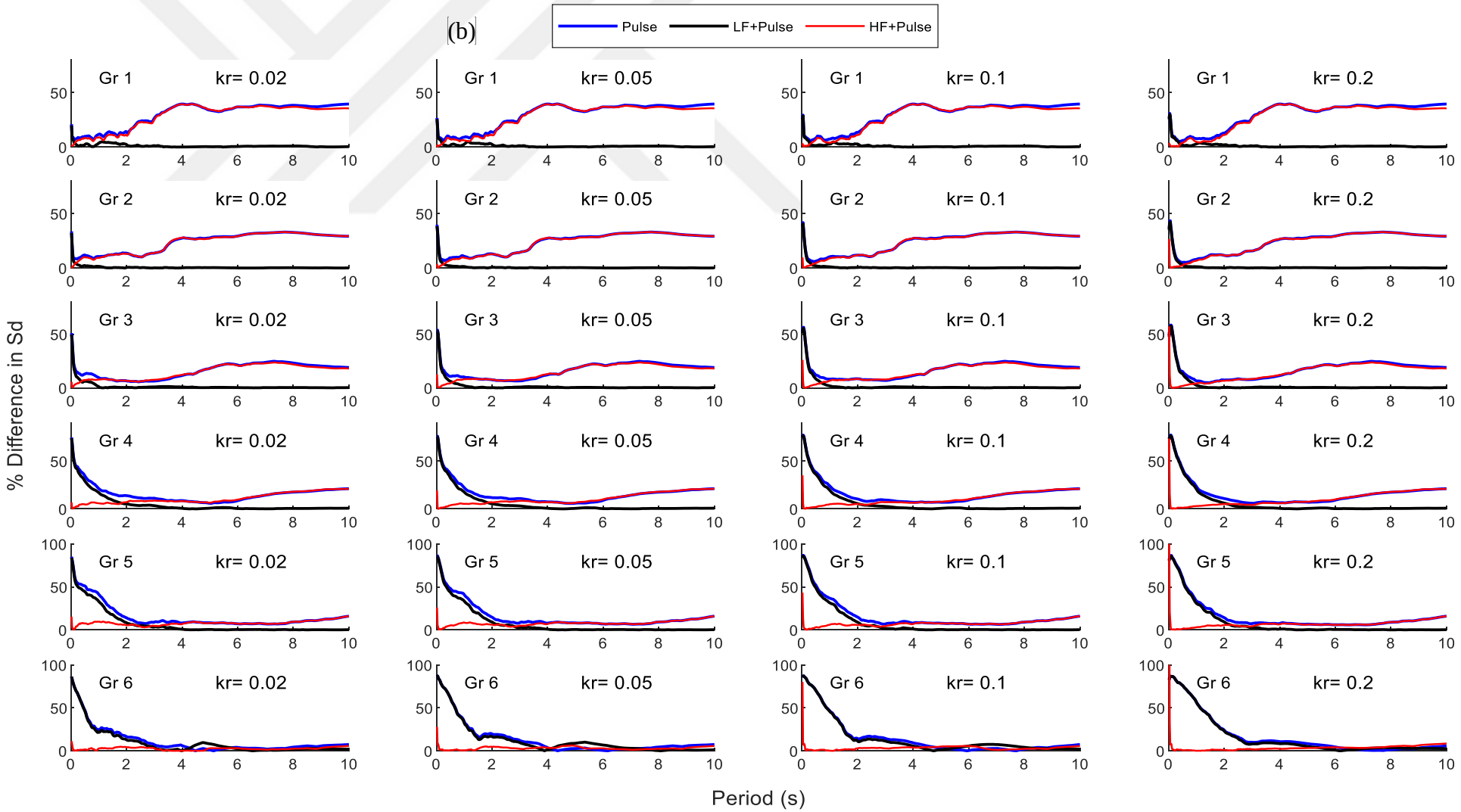

Figure 4.5 a) Mean displacement demand CSS for various post-elastic stiffnes (k_r=0.02, 0.05, 0.1, 0.2) and for yield strength Fy= 0.1w

b) Percent differences between original signal and decomposed signals

4.4 SEISMIC ISOLATED STRUCTURES

Seismically isolated structures subjected to NFGMs with forward directivity may undergo very large displacements which may be beyond the manageable ranges (Dicleli, 2007). Hence, it is important to understand the effects of pulse, high-frequency and low-frequency components in NFGMs. To this end, SDOF seismically isolated systems having bilinear force-deformation with post elastic stiffness ratio of k_r=0.05 as shown in the previous section (Fig.3.2) are considered. Various isolator yield strengths are assigned to this SDOF system like F_y =0.02W, 0.08W, 0.15W, and 0.2W. For an isolated system subjected NFGMs, displacements pass from elastic to inelastic range quickly and the system vibrates like an elastic system with a stiffness equal to post-elastic stiffness. Consequently, the vibration period of the isolated system can be taken as post elastic period so that $Td = 2\pi\sqrt{m/k_2}$. The range of Td is taken as 2 to 5 seconds to satisfy design practices.

The displacement response demands for seismic isolated structures are established for original NFGMs in groups 1 to 5, as well the extracted components that are decomposed from original signals by using the EEMD method. Fig. 4.7(a) shows the CSS curves for original ground motion records and decomposed components (Pulse, LF+Pulse, and HF+Pulse). The figure reveals that as the yield strength of the isolation system increases the maximum isolator displacement demand decreases, especially for groups with large Tp. For instance, the maximum mean displacement demand of seismic isolated structures with yield strength Fy= 0.02W subjected to NFGMs from Gr5 is up to 0.42 m, and decreases to 0.18 m for structures with yield strength 0.2W. However, there is no significant displacement demand change for seismic isolated structures subjected to small pulse period NFGMs (Gr1, and 2), independent of the yield strengths of the structures.

To capture the effect of decomposition NFGMs signals on the seismic isolated structures, Fig. 4.7 (b) shows the percent differences between the original ground motions and decomposed signals. It can be observed that the maximum reduction in displacements between original signal and pulse content is about 18% for Gr1 and Gr2 independent of the yield strengths. It should be noted that this reduction remains constant for all regions of post elastic periods (Td). Nonetheless, the reduction in the case of high yield strength isolated structures with small post elastic periods subjected to GMs with large Tp is considerable. For instance, the isolator displacement demand difference between mean pulse content and mean original signal for

isolated structure with F_y/w =0.2 for Gr5 reaches up to 78%. However, for this same group of NFGMs, the percent difference values decrease as the yield strength decreases.

Considering LF+Pulse component (where high-frequency components are filtered), there is no significant difference in isolator displacements between the original ground motion and LF+Pulse content for short pulse period NFGMs (Gr1 and Gr2). However, the percent difference of displacements between the original signal and LF+Pulse content increases dramatically in the situation of long velocity pulse period NFGMs with high isolator yield strength. This indicates that filtering high-frequency content does not affect significantly the structures having small strengths subjected to GMs with small Tp. Conversely, filtering high-frequency content reduces the spectral displacements considerably for the isolators with large yield strength subjected to NFGMs with large Tp.

It is noteworthy that, removing the low-frequency content, (HF+Pulse curve) has a slight effect (about 10%) on the spectral displacements for Gr1 and Gr2, other than these groups, the effects of low-frequency content on CSS are negligible.

To investigate more about the effect of decomposition of NFGMs on the behavior of seismically isolated structures, mean CDS are calculated (see Fig.4.7(a)) for very large ductility ratios ($\mu=50, 100$) since the behavior of seismic structures can be characterized by a very large ratio of maximum displacement to yield displacement. The structures are assumed to be perfectly elastoplastic ($k_r = 0$). Fig. 4.7(b) shows the percent differences between the original ground motion and decomposed contents. These figures reveal that the high-frequency content of the ground motion has a great influence on the spectra in the short period region and removing this content may cause a reduction in spectral displacements up to 20%. For the case of low-frequency content of NFGMs, the reduction in displacement demands can be as high as 30% which is more profound for larger periods of the systems.

(a)

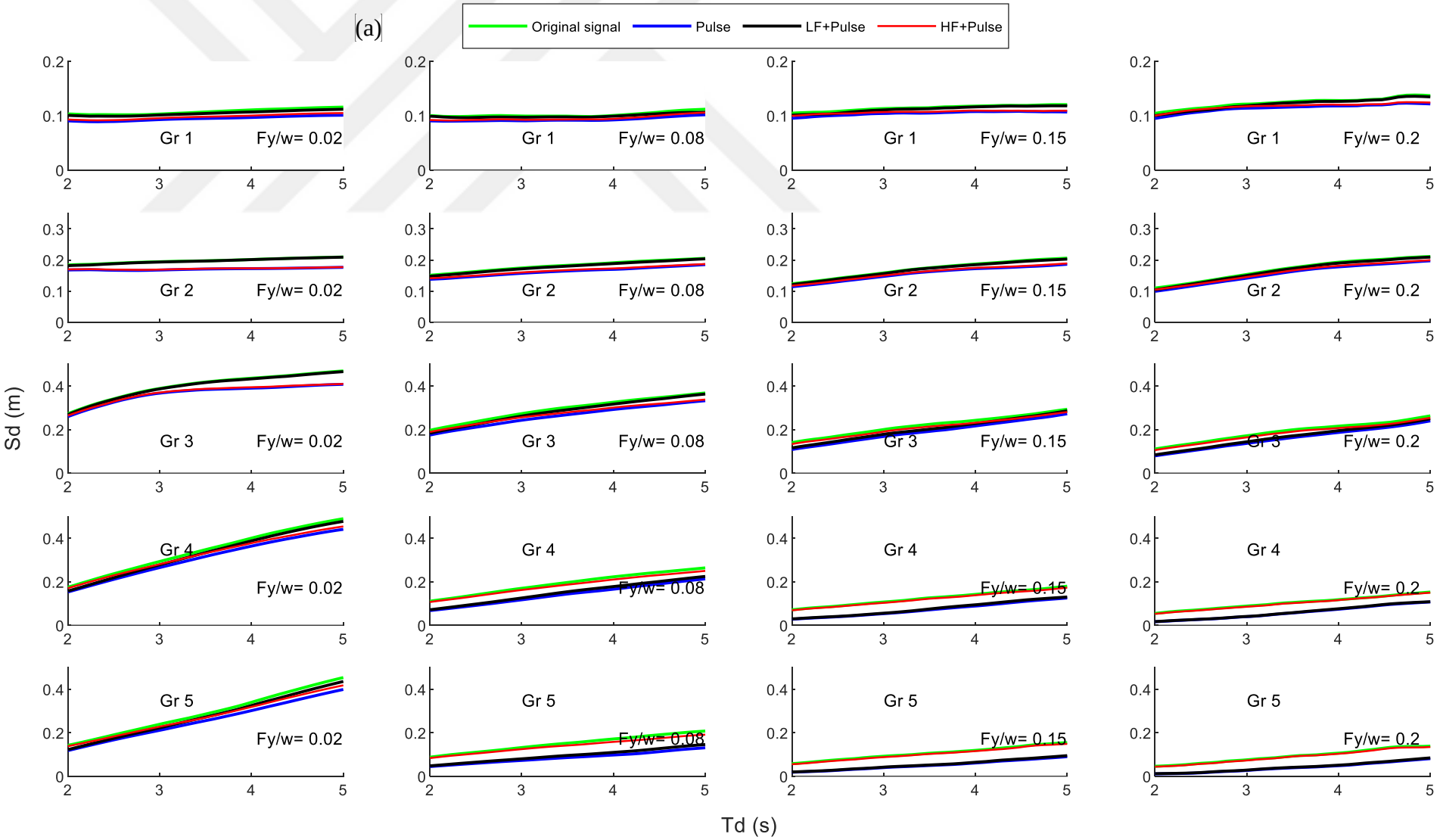
Original signal
Pulse
LF+Pulse
HF+Pulse
Gr 1 Fy/w= 0.02
Gr 1 Fy/w= 0.08
Gr 1 Fy/w= 0.15
Gr 1 Fy/w= 0.2
Gr 2 Fy/w= 0.02
Gr 2 Fy/w= 0.08
Gr 2 Fy/w= 0.15
Gr 2 Fy/w= 0.2
Gr 3 Fy/w= 0.02
Gr 3 Fy/w= 0.08
Gr 3 Fy/w= 0.15
Gr 3 Fy/w= 0.2
Gr 4 Fy/w= 0.02
Gr 4 Fy/w= 0.08
Gr 4 Fy/w= 0.15
Gr 4 Fy/w= 0.2
Gr 5 Fy/w= 0.02
Gr 5 Fy/w= 0.08
Gr 5 Fy/w= 0.15
Gr 5 Fy/w= 0.2
Sd (m)
Td (s)

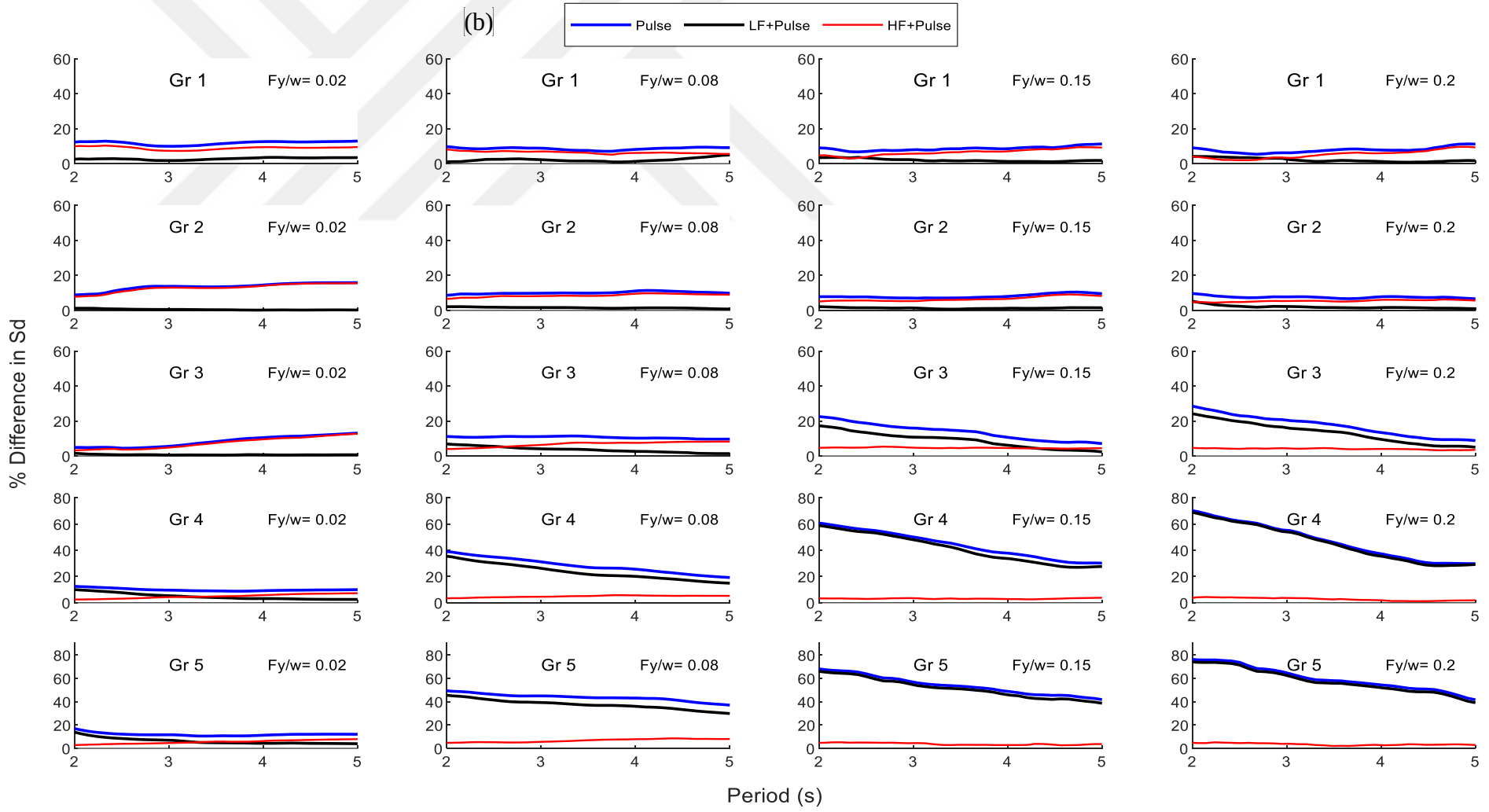

Figure 4.6 a) Mean displacement demand CSS for k_r=0.05 and for various isolator yield strengths (Fy/W=0.02, 0.08, 0.15, and 0.2)

b) Percent differences between original signal and decomposed signals

(a)

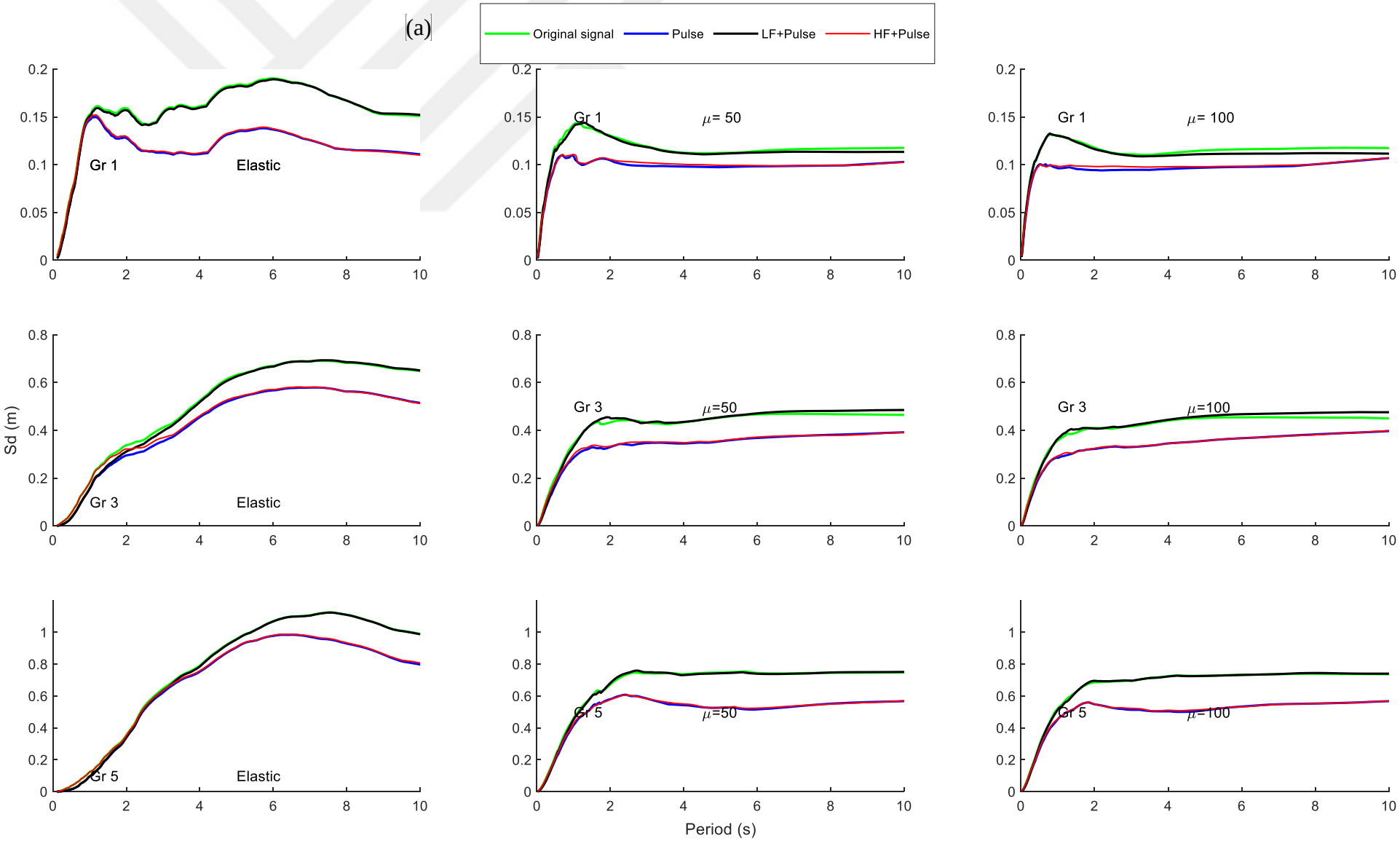
Original signal
Pulse
LF+Pulse
HF+Pulse
Gr 1
Elastic
Gr 1
μ= 50
Gr 1
μ= 100
Gr 3
Elastic
Gr 3
μ=50
Gr 3
μ=100
Gr 5
Elastic
Gr 5
μ=50
Gr 5
μ=100
Sd (m)
Period (s)

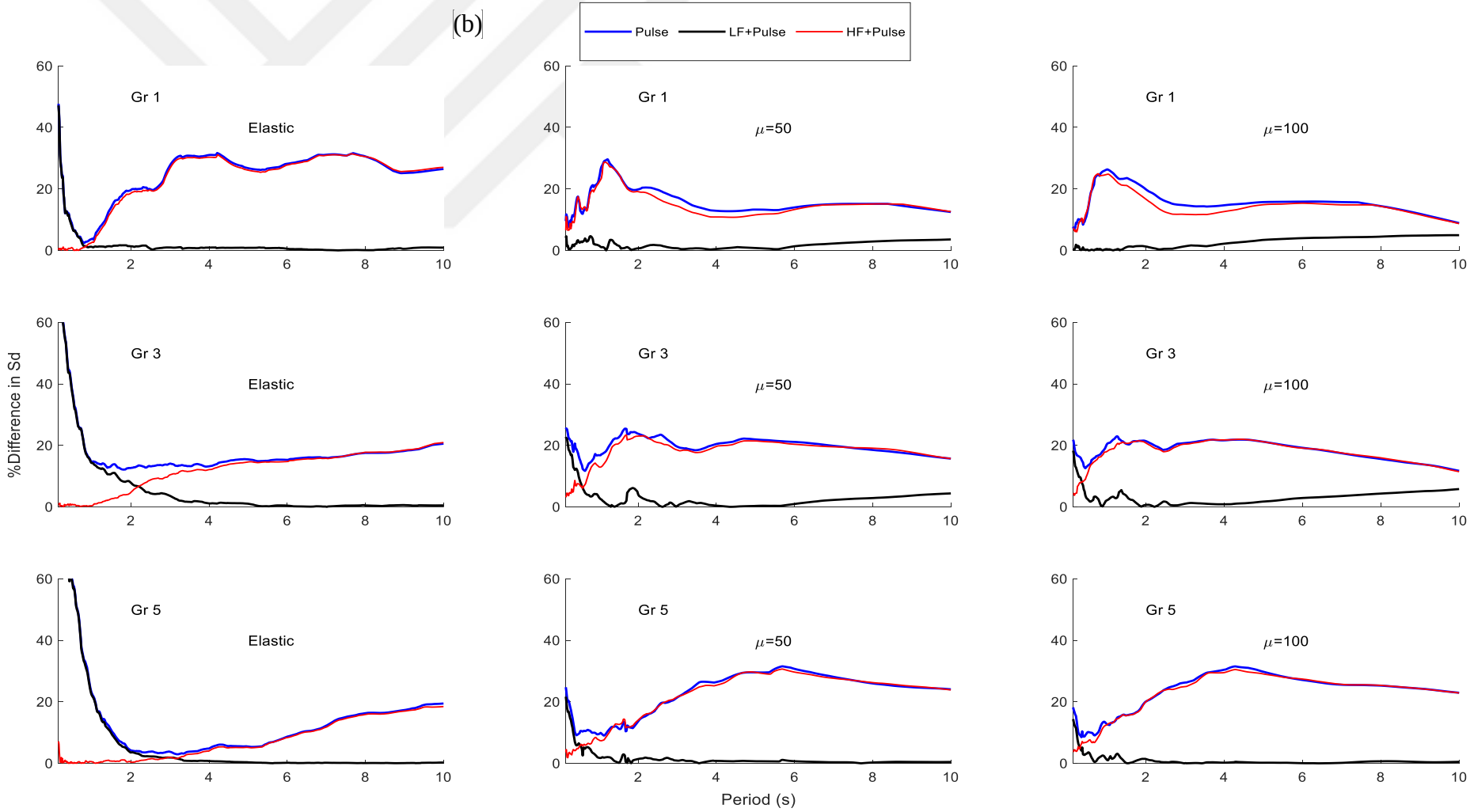

Figure 4.7 a) Mean displacement demand CDS for k_r=0 (elastic-perfectly plastic) and for various ductility ratios (μ=1 (elastic), 50, and 100), and

b) Percent differences between original signal and decomposed signals

4.4.1 Equivalent viscous damping ratio (EVDR)

This section discusses how decomposing NFGMs may affect the EVDR of an isolated structure as the post elastic stiffness period (Td) varies. For this purpose, numerous yield strengths are considered in the analyses such as, F_y/w =0.02, 0.05, 0.07, and 0.1. The analyses are conducted for a constant post elastic stiffness ratio of the bilinear SDOF system, that is k_r=0.01, and for five groups of NFGMs (Gr1 to Gr5). The spectra of EVDR are given in Fig.4.9(a) for original ground motion, pulse, HF+pulse, and LF+pulse. The figure reveals that EVDR increases as the yield strength increases for the entire range of post elastic periods. For example, mean EVDR for yield strength F_y/w =0.02 at post elastic periods Td=2 and 5s for Gr2 are ξ_e= 0.01 and 0.28 respectively, while for high isolator yield strength F_y/w =0.1 with same post elastic isolator periods these values go up to ξ_e= 0.38, and 0.51, respectively. EVDR also increases with the post elastic period almost linearly, and this increase is more pronounced for lower strengths and lower pulse periods.

Fig.4.9(b) depicts the percent differences of EVDR between the original ground motion and decomposed ones (pulse, HF+pulse, and LF+pulse). The figure shows that removing the high-frequency content or low-frequency content or both of them does not have a significant effect on mean EVDRs for groups 1 to 3. For these groups, the percent differences remain below 15%. However, for groups 4 and 5, as the high-frequency content is filtered (which is equivalent to pulse and HF+pulse content), the percent differences become more obvious and increase up to 63% for large yield strength cases.

(a)

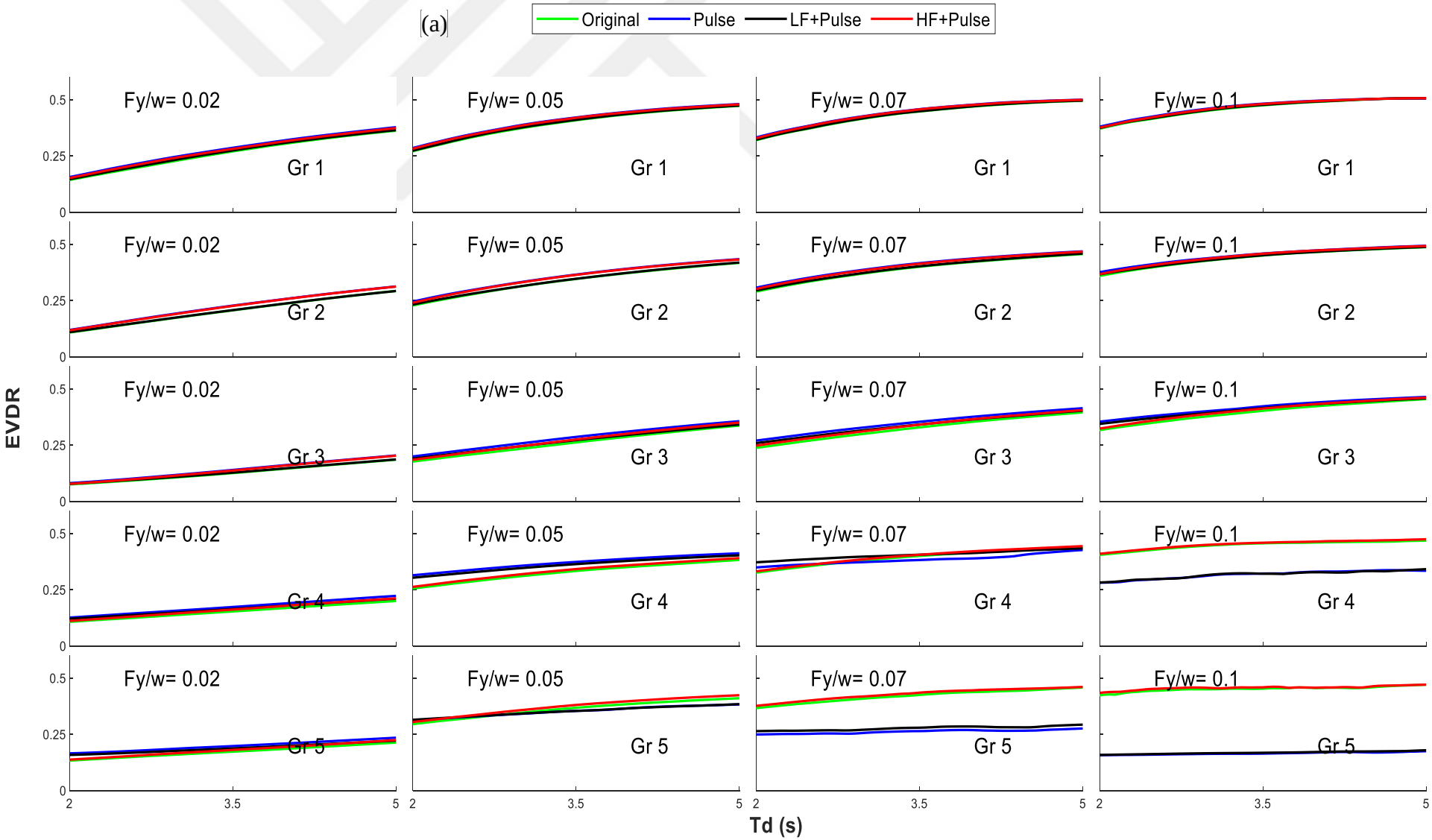
Original
Pulse
LF+Pulse
HF+Pulse
Fy/w= 0.02
Fy/w= 0.05
Fy/w= 0.07
Fy/w= 0.1
Gr 1
Gr 2
Gr 3
Gr 4
Gr 5
EVDR
Td (s)
0
0.25
0.5
2
3.5
5

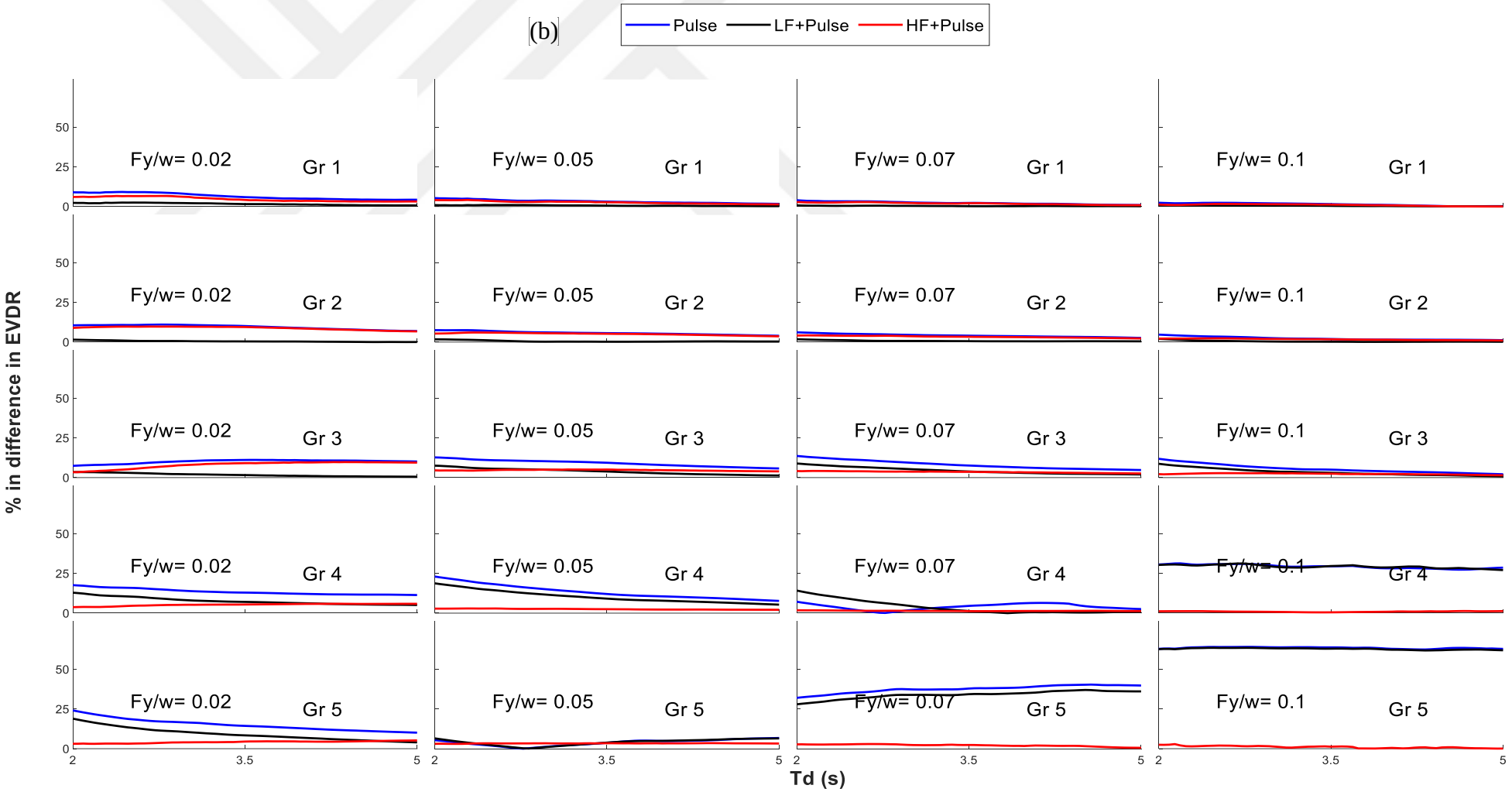

Figure 4.8 a) Mean EVDR for k_r=0.01 and for various isolator yield strengths (F_y/w =0.02, 0.05, 0.07, and 0.1)

b) Percent differences between original signal and decomposed signals

4.5 ANALYTICAL PULSE MODELS

In this section, the mean spectra of pulses obtained from EEMD analyses and analytical pulse models are compared together with the spectra of the original GMs. For this purpose, three different pulse models (Menun and Fu, 2002; Mavroeidis and Papageorgiou, 2003; He and Agrawal, 2008) are used to observe the behavior of the SDOF systems under four NFGMs with various pulse periods ranging between 1.1 s and 13 s selected from Groups 2–6 (Parkfield-02, CA 2004; Denali, Alaska,2002; Tabas, Iran 1978; Chi-Chi, Taiwan, 1999). Table 2 shows the analytical pulse model parameters for selected NFGMs.

Fig.4.10 (a) illustrates the displacement responses in terms of CDS of the original record, pulse and LF+pulse from EEMD analysis, and three analytical pulse models for different ductility ratios (μ=1 (Elastic), 2, 4, and 6). LF+pulse is taken on purpose to observe the effect of high-frequency content on the spectra. Additionally, the differences in CDS obtained from the original ground motion and pulse, LF+pulse, and analytical pulse models are shown in Fig.4.10(b) as percentages. The figures show that the ability of pulse models and pulses extracted by the EEMD method to simulate the original NFGMs varies depending on the GM, ductility ratio, and the period of SDOF systems. It can be observed from the comparisons for all curves, differences generally reduce as the period increases, and a slight reduction can be observed as the target ductility ratio increases. It is also worth noting that, incorporating the low-frequency content into the extracted pulse is observed to improve the responses. However, any of the analytical pulse models or extracted pulse by HHT could represent the original ground motion within acceptable limits at every point of the period axis. There are sudden jumps observed in Fig.4.10(a) for each curve at different periods.

Moreover, the displacement response spectra in terms of CSS for SDOF isolated systems with various yield strengths are depicted in Fig.4.11(a). The deviations of spectra from the original records are also displayed as percent differences in Fig.4.11(b). As it can be observed from the figures, the differences may go up to 100% and it is more pronounced for higher yield strengths. Except for this observation, the spectral response of analytical models and pulses extracted using the EEMD approach shows no noticeable pattern.

In general, the pulse models fail to represent the selected original signal analysis for various ductility ratios. The common point of all these models and pulses is that high-frequency contents are filtered from the NFGMs and this may result in abrupt changes in displacement

response spectra which is consistent with the findings of Yalcin and Dicleli (2020). Lastly, it should be emphasized that the low-frequency content obtained by EEMD analyses has a considerable impact on the spectral responses.

(a)

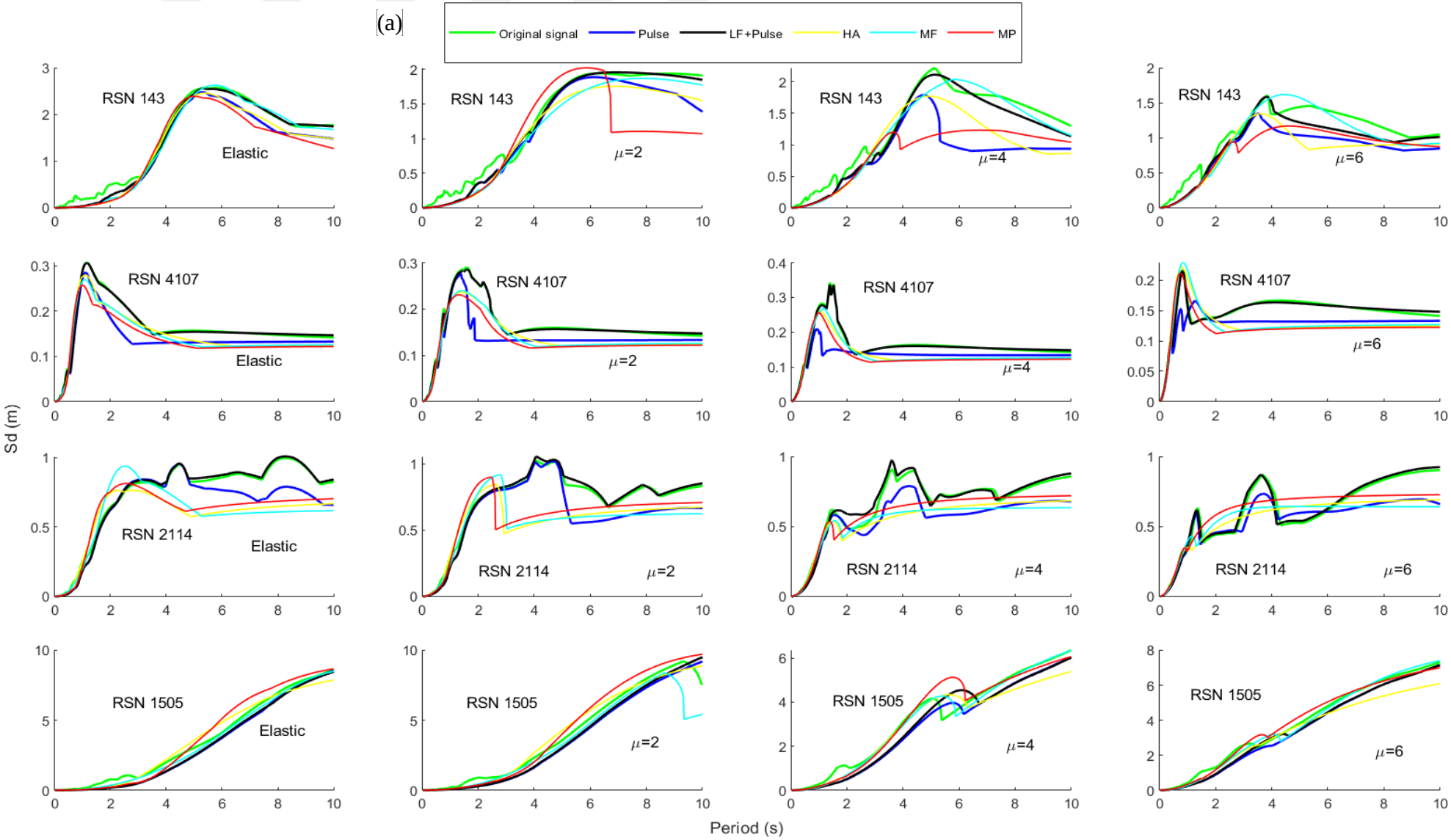
Original signal
Pulse
LF+Pulse
HA
MF
MP
RSN 143
Elastic
μ=2
μ=4
μ=6
RSN 4107
RSN 2114
RSN 1505
Sd (m)
Period (s)

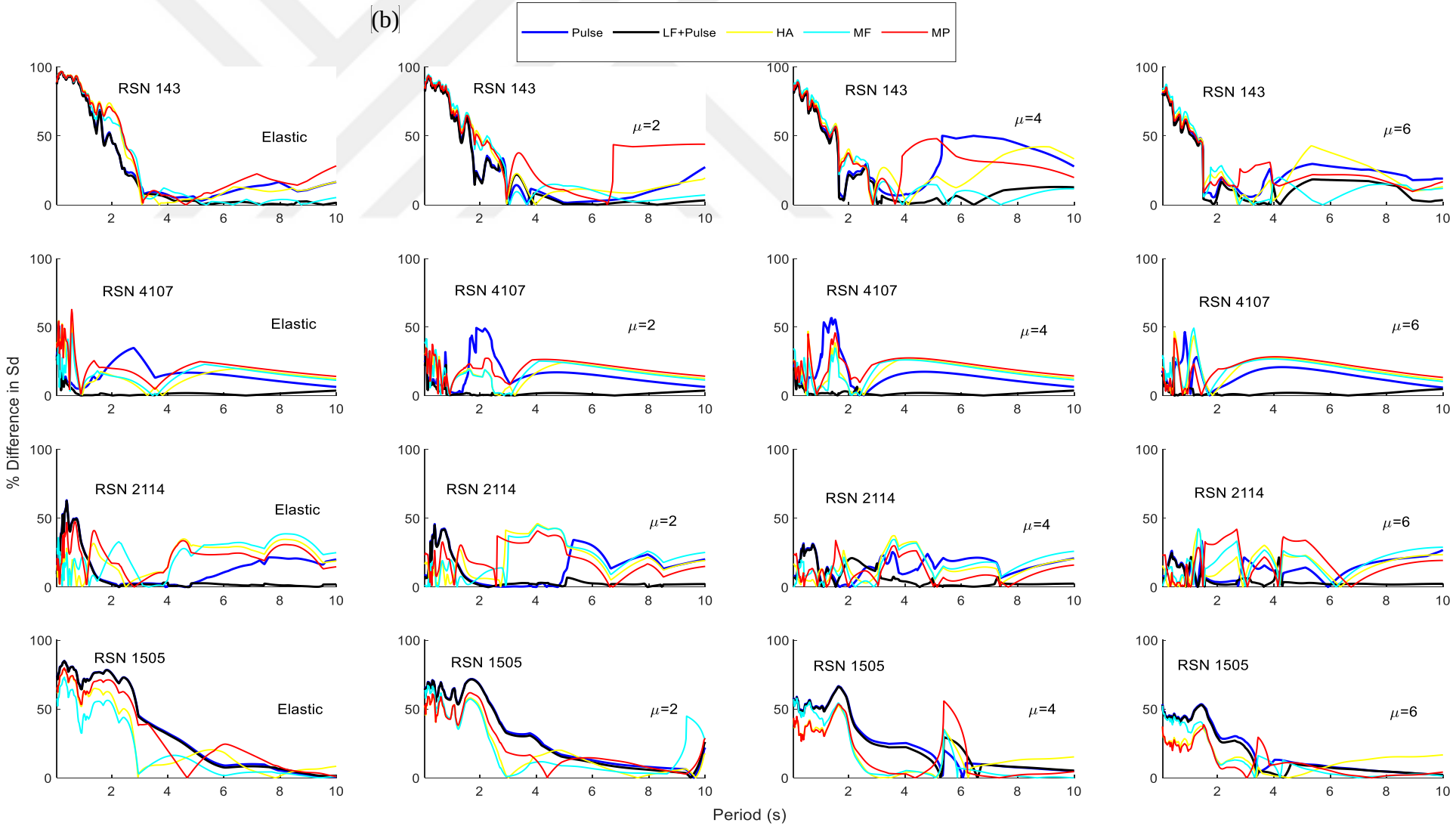

Figure 4.9 a) Displacement response of CDS for different ductility ratios (μ=1 (Elastic), 2, 4, and 6) for the original records, extracted Pulse and pulse models (HA, MF, and MP)

b) Percent differences between original records, extracted Pulse and pulse models

(a)

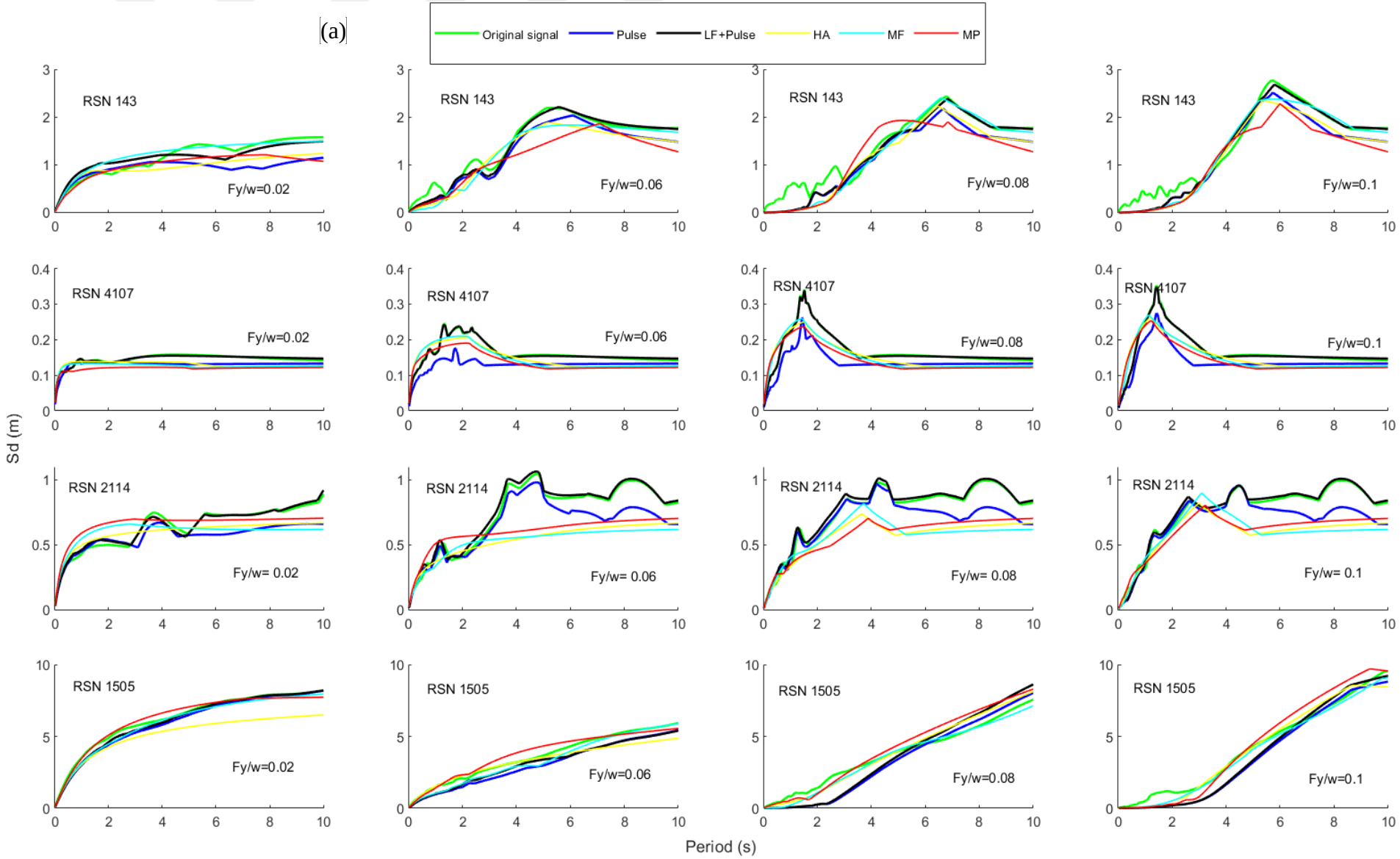
Original signal
Pulse
LF+Pulse
HA
MF
MP
RSN 143
Fy/w=0.02
RSN 143
Fy/w=0.06
RSN 143
Fy/w=0.08
RSN 143
Fy/w=0.1
RSN 4107
Fy/w=0.02
RSN 4107
Fy/w=0.06
RSN 4107
Fy/w=0.08
RSN 4107
Fy/w=0.1
RSN 2114
Fy/w= 0.02
RSN 2114
Fy/w= 0.06
RSN 2114
Fy/w= 0.08
RSN 2114
Fy/w= 0.1
RSN 1505
Fy/w=0.02
RSN 1505
Fy/w=0.06
RSN 1505
Fy/w=0.08
RSN 1505
Fy/w=0.1
Sd (m)
Period (s)

(b)

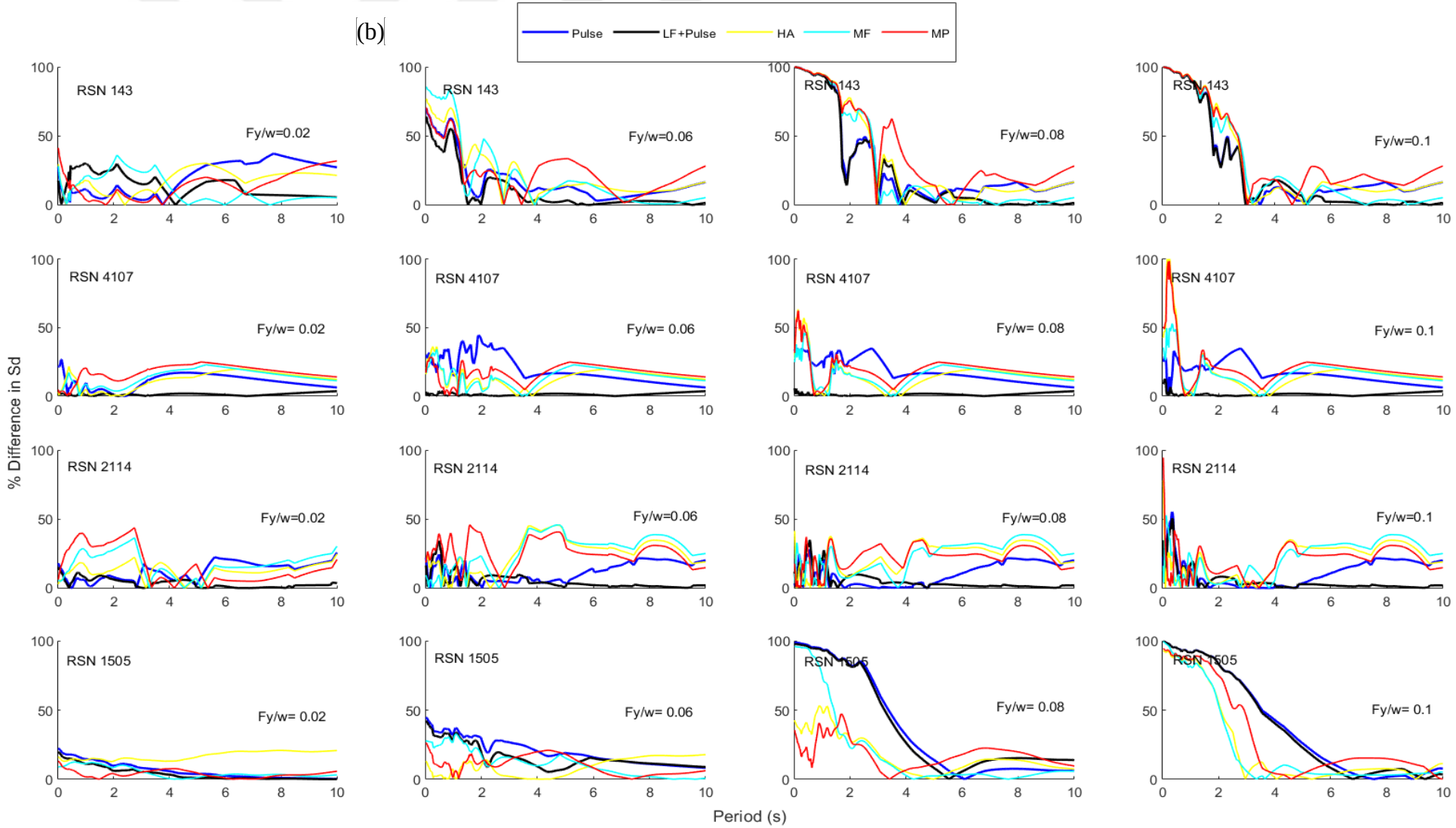

Figure 4.10 a) Displacement CSS for various yield strengths $(F_y/w = 0.02,\ 0.06,\ 0.08,\ 0.1)$ for the original records, extracted Pulse and pulse models (HA, MF, and MP)

b) Percent differences between original records, extracted Pulse and pulse models

5 CONCLUSION AND DISCUSSION

In this thesis, the effect of decomposition of the near-fault ground motions (NFGMs) on the linear and nonlinear response of the SDOF systems is investigated for 114 records to observe the effects of NFGMs. The unique characteristics of these NFGMs can cause considerable damage to the subjected structures. The selected NFGMs are classified into six groups, based on their wavelet velocity pulse periods (Tp) to monitor the effects of pulse periods. All selected records are categorized as pulse-like NFGMs with directivity effect in accordance with the criteria established by Baker (2007) based on wavelet analysis. These records are also rotated to the orientation that provides the highest amplitude value for velocity time history. Accordingly, the EEMD method (a part of HHT method) is used to decompose NFGMs into several fundamental oscillations called intrinsic mode functions (IMFs) without losing any data from the original records. IMFs represent basis functions with various frequency components. Two parameters of IMFs are used to extract velocity pulses from NFGMs: maximum energy transition and the PGV/PGA ratio.

The elastic and inelastic SDOF systems with various parameters subjected to original pulse-like NFGMs and the decomposed components (extracted pulse, pulse+high-frequency content, and pulse+low frequency content) are taken into account in this study to capture the effect of decomposition of these NFGMs. The findings of elastic analyses are shown as acceleration response spectra, whereas inelastic analyses results are shown as constant ductility (CDS) and constant strength (CSS) displacement spectra. Furthermore, the accuracy of some analytical pulse models to represent the influence of NFGMs on the response of elastic and inelastic SDOF systems is assessed. The following main conclusions may be drawn from the aforementioned investigations:

1. For the elastic systems, as the mean Tp of ground motion groups increase, the mean amplitude of elastic spectral accelerations decreases in short period regions and rises in low-frequency regions. This is anticipated because when the Tp of NFGMs increases, structures having a short period stay away from the resonant response. However long period structure's response comes close to resonance response because structure's period becomes closer to the Tp of NFGMs. When the Tp of NFGMs

coincides with the natural period of a building, it will undergo very large oscillations and suffer the greatest damage.

2. The process of removing low-frequency content from the ground motion does not have a significant effect on the elastic spectra in the short period range, however, the removal of high-frequency components has a significant impact in the short period range.
3. The percent difference of mean acceleration response of elastic systems between the pulse signal and the original signal reaches up to 75% in the short period region and linearly decreases to reach the minimum value around the regions of the mean Tp for each group. That indicates the high-frequency component has a significant effect on the acceleration response of large velocity pulse NFGMs in short period regions.
4. It is also observed that, the mean differences in elastic response spectra between original and extracted pulse component decrease in long period regions ($T \geq 2.5$), as the mean Tp of NFGMs increases.
5. Removing high-frequency content from the NFGMs has a great influence on the constant ductility response spectra (CDS) in the short period range. This influence increases as the pulse period of ground motion (equivalent to Group number) increases. On the contrary, removing low-frequency content has a minor effect for the short period region but has a great effect on long period regions. However, the effects of removing low-frequency content decrease as the Tp of NFGMs increases. The effect of the ductility ratio on CDS is negligible for NFGMs with a small Tp and somewhat significant for those with a large Tp.
6. It also could be noted that the change of post-elastic stiffness ratio in CDS does not significantly affect the behavior of displacement response demand for each group of NFGMs.
7. For constant strength response spectra (CSS), the effect of pulse content is substantial on short period region ($T \leq 2s$) as the yield strength increases for NFGMs having large velocity pulse period.
8. As in the case of CDS, post elastic stiffness ratio does not have a significant effect on CSS.
9. Similar to observations for CDS, extracting the pulse from the ground motion by removing high-frequency and low-frequency contents may reduce significantly the response values in CSS as well.

10. For seismic isolated structures, removing high-frequency content does not affect significantly the structures having small yield strengths subjected to ground motions with small Tp. Conversely, filtering high-frequency content reduces the spectral displacements considerably for the isolators with large yield strength subjected to ground motions with large Tp.
11. Additionally, the effect of decomposition of NFGMs on the inelastic response of seismic isolated structures is not affected considerably by changing the ductility ratio.
12. Removing the high-frequency content or low-frequency content or both of them from the original records does not have a significant effect on mean equivalent viscous damping ratios for groups 1 to 3. For these groups, the percent differences remain below 15%. However, for groups 4 and 5, as the high-frequency content is filtered the percent differences become more obvious and increase up to 63% for large yield strength cases.
13. Three different analytical pulse models evaluated in this study do not accurately represent NFGMs for various ductility ratios. The common point of all these models and pulses is that high-frequency contents are filtered from the NFGMs which may result in abrupt changes in displacement response spectra.
14. Furthermore, this study also reveals that, besides the high-frequency content, the low-frequency content obtained by HHT analyses has an impact on the spectral responses.

In closing, for many reasons, earthquake engineers need to extract the velocity pulses from NFGMs with forward directivity and apply these pulses instead of the original ground motion. But as it can be seen from the elastic and inelastic analyses, filtering the high-frequency contents and low-frequency contents from the NFGMs and applying only the pulse may have a significant impact on the behavior of structures and reduce the spectral displacements. When the pulse extracted from a NFGM is applied, the spectral responses may be significantly reduced in both the short period region and the long period region of the spectra. High-frequency content of the NFGMs has significant effects in the short period region of spectra, whereas low-frequency content has significant effects in the long period region.

This research focuses on the impact of record decomposition on the linear and nonlinear response spectra of SDOF systems. For further research, MDOF structures and/or alternative decomposition techniques may be studied. Moreover, the effects of the various energy contents of the NFGMs on the inelastic spectra might be investigated.

REFERENCES

Alavi, B. and Krawinkler, H. (2004) 'Behavior of moment-resisting frame structures subjected to near-fault ground motions', Earthquake Engineering and Structural Dynamics, 33(6). doi: 10.1002/eqe.369.

Aldridge, D. F. (1990) 'The Berlage wavelet', Geophysics, 55(11). doi: 10.1190/1.1442799.

Anderson, J. C. and Bertero, V. V. (1987) 'Uncertainties in establishing design earthquakes', Journal of Structural Engineering (United States), 113(8). doi: 10.1061/(ASCE)0733-9445(1987)113:8(1709).

Baker, Jack W (2007) 'Measuring bias in structural response caused by ground motion scaling', Pacific Conference on Earthquake Engineering, (056). doi: 10.1002/eqe.

Baker, Jack W. (2007) 'Quantitative classification of near-fault ground motions using wavelet analysis', Bulletin of the Seismological Society of America, 97(5). doi: 10.1785/0120060255.

Beresik, R. (2016) 'Hilbert-Huang Transform and its Application in Seismic Signal Processing', NTSP 2016 - Proceedings of the International Conference on New Trends in Signal Processing, (October 2016). doi: 10.1109/NTSP.2016.7747776.

Bertero, V. V., Mahin, S. A. and Herrera, R. A. (1978) 'Aseismic design implications of near-fault san fernando earthquake records', Earthquake Engineering & Structural Dynamics, 6(1). doi: 10.1002/eqe.4290060105.

Bozorgnia, Y., Mahin, S. A., & Brady, A. G. (1998). Vertical response of twelve structures recorded during the Northridge earthquake. Earthquake Spectra, 14 (3), 411-432.

Buckle, I. G., Constantinou, M. C., Diceli, M., & Ghasemi, H. (2006). Seismic isolation of highway bridges (No. MCEER-06-SP07).

Chang, Z. et al. (2016) 'An Improved Energy-Based Approach for Selecting Pulse-Like Ground Motions', (December 2017). doi: 10.1002/eqe.2758.

Chen, X., Wang, D. and Zhang, R. (2019) 'Identification of pulse periods in near-fault ground motions using the HHT method', Bulletin of the Seismological Society of America, 109(6), pp. 2384–2398. doi: 10.1785/0120190046.

Chopra, A. K. (2000) Dynamics of structures : theory and applications to earthquake engineering / Anil K. Chopra. 2nd ed. Upper Saddle River, NJ: Prentice Hall (Prentice-Hall international series in civil engineering and engineering mechanics).

D. Gabor, D. I. (1946) 'A Theory of Communication', Princ Literary Criticism V3, pp. 206 210. doi: 10.4324/9781315010854-28.

Dicleli, M., Buckle, I., Constantinou, M. and Ghasemi, H., 2006. Seismic Isolation of Highway Bridges (Special Report MCEER-06-SP07). Buffalo, NY: MCEER.

Dicleli, M. (2007). Supplemental elastic stiffness to reduce isolator displacements for seismic-isolated bridges in near-fault zones. Engineering Structures, 29(5), 763-775.

FEMA (2016) 'Structural Dynamics of Linear Elastic Single-Degree-of-Freedom (SDOF) Systems Equations of motion for SDOF structures', Topic 3 Notes, pp. 1–100.

Ghobarah, A. (2004), August. Response of structures to near-fault ground motion. In 13th World Conference on Earthquake Engineering (Vol. 1031).

Hall, J. F. et al. (1995) 'Near-Source Ground Motion and its Effects on Flexible Buildings', Earthquake Spectra, 11(4), pp. 569–605. doi: 10.1193/1.1585828.

He, W. and Agrawal, A. K. (2008) 'Analytical Model of Ground Motion Pulses for the Design', Journal of Structural Engineering, 134(July), pp. 1177–1188.

Housner, G. W. and Trifunac, M. D. (1967) 'Analysis of accelerograms--Parkfield earthquake', Bulletin of the Seismological Society of America, 57(6), pp. 1193–1220. Available at: http://www.bssaonline.org/cgi/content/abstract/57/6/1193.

Howard, J. K., Tracy, C. A. and Burns, R. G. (2005) 'Comparing observed and predicted directivity in near-source ground motion', Earthquake Spectra, pp. 1063–1092. doi: 10.1193/1.2044827.

Huang, N. E. et al. (1998) 'The empirical mode decomposition and the Hubert spectrum for nonlinear and non-stationary time series analysis', Proceedings of the Royal Society A: Mathematical, Physical and Engineering Sciences, 454(1971), pp. 903–995. doi: 10.1098/rspa.1998.0193.

Kalkan, E. et al. (2006) 'Effects of Fling Step and Forward Directivity on Seismic Response of', 22(2), pp. 367–390. doi: 10.1193/1.2192560.

Kardoutsou, V., Taflampas, I. and Psycharis, I. N. (2017) 'A new pulse indicator for the classification of ground motions', Bulletin of the Seismological Society of America, 107(3), pp. 1356–1364. doi: 10.1785/0120160301.

Loh, C. H., Wu, T. C. and Huang, N. E. (2001) 'Application of the empirical mode decomposition-Hilbert spectrum method to identify near-fault ground-motion characteristics and structural responses', Bulletin of the Seismological Society of America, 91(5), pp. 1339–1357. doi: 10.1785/0120000715.

MacRae, G. A., Morrow, D. V. and Roeder, C. W. (2001) 'Near-Fault Ground Motion Effects on Simple Structures', Journal of Structural Engineering, 127(9), pp. 996–1004. doi: 10.1061/(asce)0733-9445(2001)127:9(996).

Makris, N. and Chang, S.-P. (2000) 'Response of Damped Oscillators to Cycloidal Pulses', Journal of Engineering Mechanics, 126(2). doi: 10.1061/(asce)0733-9399(2000)126:2(123).

Malhotra, P. K. (1999) 'Response of buildings to near-field pulse-like ground motions', Earthquake Engineering and Structural Dynamics, 28(11), pp. 1309–1326. doi: 10.1002/(SICI)1096-9845.

Mavroeidis, G. P. and Papageorgiou, A. S. (2002) 'Near-source strong ground motion: characteristics and design issues', in Proc. of the Seventh US National Conf. on Earthquake Engineering (7NCEE), Boston, Massachusetts, p. 25.

Mavroeidis, George P. and Papageorgiou, A. S. (2003) 'A mathematical representation of near-fault ground motions', Bulletin of the Seismological Society of America, 93(3), pp. 1099–1131. doi: 10.1785/0120020100.

Menun, C. and Fu, Q. (2001) An analytical model for near-fault ground motions and the response of SDOF systems.

Mimoglou, P. (2014) 'Design-oriented simulation of near fault ground motions by a limited number of velocity pulses, forthcoming Ph. D'. dissertation, School of Civil Engineering, National Technical University of ….

Mughal, H. et al. (2005) 'Kashmir Earthquake 2005 Learning from the Shelter Response and Rural Housing Recovery'.

Mukhopadhyay, S. and Gupta, V. K. (2013) 'Directivity pulses in near-fault ground motions — I : Identification , extraction and modeling', Soil Dynamics and Earthquake Engineering, 50, pp. 1–15. doi: 10.1016/j.soildyn.2013.02.017.

Norio,et al. (2011) 'The 2011 eastern Japan great earthquake disaster: Overview and comments', International Journal of Disaster Risk Science, 2(1).

Ohsaki, Y. (2008) 'A primer on the spectral analysis of ground motions', Kajima Institute.

Reyes, B. J. C., Kalkan, E. and Survey, U. S. G. (2012) 'Should Ground-Motion Records be Rotated to Fault-Normal / Parallel or Maximum Direction for Response History Analysis of Buildings .

Rodriguez-Marek, A. (2000) Near-fault seismic site response. University of California, Berkeley.

Seber, G. A. F. and Wild, C. J. (1989) 'Nonlinear Regression John Wiley & Sons', New York.

Sehhati, R. et al. (2011) 'Effects of near-fault ground motions and equivalent pulses on multi-story structures', Engineering Structures, 33(3), pp. 767–779. doi: 10.1016/j.engstruct.2010.11.032.

Shahi, S. K. and Baker, J. W. (2014) 'An efficient algorithm to identify strong-velocity pulses in multicomponent ground motions', Bulletin of the Seismological Society of America, 104(5), pp. 2456–2466. doi: 10.1785/0120130191.

Society, S. and David, B. Y. (1974) 'Two-dimensional kinematic fault modeling of the pacoima dam strong-motion recordings of the february 9, 1971, san fernando earthquake', 64(3), pp. 555–570.

Somerville, P. G. et al. (1995) 'Accounting for near-fault rupture directivity effects in the development of design ground motions', American Society of Mechanical Engineers, Pressure Vessels and Piping Division (Publication) PVP.

Somerville, P. G. et al. (1997) ‘Modification of empirical strong ground motion attenuation relations to include the amplitude and duration effects of rupture directivity’, Seismological Research Letters, 68(1), pp. 199–222. doi: 10.1785/gssrl.68.1.199.

Somerville, P. G. (2003) ‘Magnitude scaling of the near fault rupture directivity pulse ’, 137(April 2002). doi: 10.1016/S0031-9201(03)00015-3.

Soyluk, K. and Karaca, H. (2017) ‘Near-fault and far-fault ground motion effects on cable-supported bridges’, Procedia Engineering, 199. doi: 10.1016/j.proeng.2017.09.421.

Veletsos AS, N. N. (1960) ‘Effect of inelastic behavior on the response of simple systems to earthquake motions’. Proceedings of the Second World Conference on Earthquake Engineering. doi: 895-818.

Wilfred D IWAN, CHING-TUNG HUANG and GUYADER, A. C. (2000) ‘Near Field Ground Motion.’, 2, pp. 373–378.

Wu, Z. and Huang, N. E. (2009) ‘Ensemble empirical mode decomposition: A noise-assisted data analysis method’, Advances in Adaptive Data Analysis, 1(1), pp. 1–41. doi: 10.1142/S1793536909000047.

Xia, C. (2019) ‘applied sciences Identification and Representation of Multi-Pulse Near-Fault Strong Ground Motion Using Adaptive Wavelet Transform’. doi: 10.3390/app9020259.

Xu, Z., Asce, M. and Agrawal, A. (2010) ‘Decomposition and Effects of Pulse Components in Near-Field Ground Motions’. doi: 10.1061/ASCEST.1943-541X.0000122.

Yalcin, O. F. and Dicleli, M. (2020) ‘Effect of the high frequency components of near-fault ground motions on the response of linear and nonlinear SDOF systems : A moving average filtering approach’, Soil Dynamics and Earthquake Engineering, 129, p. 105922. doi: 10.1016/j.soildyn.2019.105922.

Yang, S. et al. (2017) ‘Effect of ground motion filtering on the dynamic response of a seismically isolated bridge with and without fault crossing considerations’, Soil Dynamics and Earthquake Engineering, 92(June 2016), pp. 183–191. doi: 10.1016/j.soildyn.2016.10.001.

Zhai, C. et al. (2013) ‘Quantitative identification of near-fault pulse-like ground motions based on energy’, Bulletin of the Seismological Society of America, 103(5), pp. 2591–2603. doi: 10.1785/0120120320.

Zhai, C. et al. (2018) ‘An efficient algorithm for identifying pulse-like ground motions based on significant velocity half-cycles’, Earthquake Engineering and Structural Dynamics, 47(3), pp. 757–771. doi: 10.1002/eqe.2989.

Zhang, R. R. et al. (2003) ‘Hilbert-Huang Transform Analysis of Dynamic and Earthquake Motion Recordings’, Journal of Engineering Mechanics, 129(8), pp. 861–875. doi: 10.1061/(asce)0733-9399(2003)129:8(861).

Zhang, S. and Wang, G. (2013) ‘Effects of near-fault and far-fault ground motions on nonlinear dynamic response and seismic damage of concrete gravity dams’, Soil Dynamics and Earthquake Engineering, 53, pp. 217–229. doi: 10.1016/j.soildyn.2013.07.014.

APPENDICES